國 立 交 通 大 學

材料科學與工程學系

博 士 論 文

含三吡啶二價金屬(鋅/釕)之新型金屬錯合高分子之合成與應用

Synthesis and Application of Novel Metallo-Polymers

Containing Terpyridyl Zinc(II)/Ruthenium(II) Moieties.

研 究 生：陳益裕

指導教授：林宏洲　博士

中華民國九十六年七月

含三吡啶二價金屬(鋅/釕)之新型金屬錯合高分子之合成與應用

Synthesis and Application of Novel Metallo-Polymers Containing Terpyridyl Zinc(II)/Ruthenium(II) Moieties.

研 究 生：陳益裕   Student: Yi-Yu Chen

指導教授：林宏洲   Advisor: Prof. Hong-Cheu Lin

國立交通大學

材料科學與工程學系

博士論文

A Thesis
Submitted to Department of Materials Science and Engineering
College of Engineering
National Chiao Tung University
In Partial Fulfillment of the Requirement
For the Degree of Doctor of Philosophy of Science
In Materials Science and Engineering
July 2007
Hsinchu, Taiwan

中華民國九十六年七月

三吡啶二價金屬(鋅/釕)之新型金屬錯合高分子之合成與應用

學　生：陳益裕　　　　　　　　　　指　導　教　授：林宏洲　博士

國立交通大學材料科學與工程研究所

博士班

摘　要

本論文研究方向為探討一系列包含三吡啶(Terpyridine)二價金屬(鋅/釕)(Zinc(II)/Ruthenium(II))之錯合高分子之合成與其在光電材料的應用，並以三大方向為研究主軸。第一個部份，以炔基(ethylene)連接的莽(Flourene)單元為高分子的主鏈結構，並包含(Carbazole)或圻塄雙唑(oxadiazole)懸掛物之新型金屬錯合高分子。第二，將具有上同官能基(Me, OMe, F)的苯環單元加入至此系列金屬高分子中，並一樣藉由炔基與中心的莽以共軛的方式與其連接。最後一部份，以改變高分子中心主鏈結構(Phenothiazine)及錯合物之金屬部分做為研究的主題。在鑑定方面，藉由 ^{1}H NMR 光譜圖上的積分值可輕易的鑑定出金屬錯合高分子的主鏈結構是由上同的單體而建構(例：金屬錯合單一相高分子和金屬錯合共聚高分子)。然而，利用紫外光-可見光和螢光光譜儀，藉由改變金屬二價鋅離子的濃度，做滴定實驗亦可進一步的証明金屬錯合高分子的結構。結果發現，藉由金屬錯合的方式所形成的高分子，可提高熱穩定性(熱烈解溫度)及量子產率。以比較此系列高分子的量子產率為例，加入 OXD 可有效的提高量子產率而 CAZ 則否。再者，探討以此具有發光性質的金屬錯合高分子作為

發光層並應用於電激發光元件，發現加入具有電子傳出能力的 OXD 與電洞傳出能力的 CAZ 懸掛物的高分子上，具有提高元件效率的結果。最後，將此類型高分子以二價釕離子取代原本的鋅離子，探討其與原本以鋅為錯合金屬離子之物理及化學性質的差別，並將其應用於太陽能電池元件上。

Synthesis and Application of Novel Metallo-Polymers Containing Terpyridyl Zinc(II)/Ruthenium(II) Moieties.

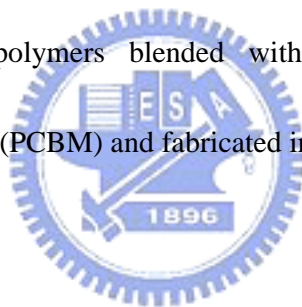Student: Yi-Yu Chen   Advisor: Dr. Hong-Cheu Lin

Department of Materials Science and Engineering National Chiao Tung University

Abstract

A series of novel terpyridyl-zinc(II) based metallo-polymers containing carbazole (CAZ) or 1,3,4-oxadiazole (OXD) pendants (attached to the C-9 position of fluorene by long alkyl spacers) were synthesized by self-assembling reactions. On the other hand, the phenylene units with various lateral substituents (Me, OMe, F) were added to such metallo-polymeric backbones structures and conjugated with central fluorene units by ethylene bridges. The integrated ratios of ^{1}H NMR spectra reveal a facile result to distinguish the well-defined main-chain metallo-polymeric structures (i.e. metallo-homopolymers and copolymers) which were constructed by different monomer ligand systems. Furthermore, UV-visible and photoluminescence (PL) spectral titration experiments were carried out to verify the metallo-polymeric structures by varying the molar ratios of zinc(II) ions to monomers. As a result, the enhancement of thermal stability (T_d) and quantum yields were introduced by the

metallo-polymerization, and their physical properties were mainly affected by the nature of the pendants. For example, in contrast to metallo-polymers containing alkyl pendants, the quantum yields were greatly enhanced by introducing OXD pendants but reduced by CAZ pendants. The electroluminescent (EL) devices with these light-emitting metallo-polymers as emitters have been investigated and EL performance were enhanced by incorporating with electron-transporting OXD and hole-transporting CAZ pedants. Finally, metallo-polymers were produced by coordination of Ruthenium(II) metal ions with two ditopic terpyridyl (tpy) receptor monomers containing central fluorene and phenothiazine units, respectively. Such polymers blended with fullerene derivative [6,6]-phenyl C_{61}-butyric acid methyl ester (PCBM) and fabricated into photovoltaic cells (PPVCs).

ACKNOWLEDGEMENTS

Table of Contents

Table Lists

Figure Lists

XII

XIV

Chapter 1

Introduction

1.1 Introduction to Supramolecular Chemistry

Supramolecular chemistry has been one of the most interesting fields in modern chemistry. In 1987, J.-M. Lehn, C. J. Pederson and D. J. Cram received the Nobel Prize for their pioneering work.[1] Self-recognition and self-assembly processes represent the basic concept of the supramolecular chemistry and the interactions involved are mainly of non-covalent nature (e.g. van der Waals, hydrogen bonding, ionic or coordinative interaction). Compared to covalent bonds, these interactions are weaker and usually reversible. Natural is the model for artificial supramolecular processes. Inter- and intramolecular non-covalent interactions are of the major importance for most biological processes such as highly selective catalytic reactions and information storage;[2,3] different non-covalent interactions are present in proteins giving them their specific structures. DNA represents one of the most famous examples, where the self-recognition and complementary base-pairs by hydrogen bonding leads to the self-assembly of the double helix. Today, many synthetic supramolecular systems are known.[1,4] The resulting compounds are expected to reveal new chemical and physical as well as biological properties. Starting from biomimetic systems, the concept was extended to "molecular machines"[5] and supramolecular polymers. [6]

1.2.1 Introduction to Supramolecular Polymers

An area of special interest in recent years is supramolecular polymer chemistry.[7] Polymers that are synthesized by non-covalent interactions, and not by conventional covalent polymerization, offer new possibilities because such interactions can be favorably influenced

by external parameters such as the temperature or mechanical stimuli causing drastic changes in the polymer properties, particularly the elasticity and solution viscosity. A large number of supramolecular polymers can be built by hydrogen bonding, [8] in some cases in combination with further interactions such as - stacking that significantly determine the structures of the polymers. Also, more exotic interactions such as dipolar aggregation have been successfully applied for the formation of highly complex polymeric dye aggregates.[9] Metal-ligand coordination provide an excellent means for the synthesis of supramolecular systems as the coordination bond is highly directional, the ligand structures can be varied in a desired manner by established organic chemistry, and the thermodynamic and kinetic stability can be fine-tuned with the appropriate ligand types and metal ions. Supramolecular systems constructed from metal-ligand bond include lattice, cyclic and filamentous motives as well as interlaced systems.[10]

1.2.2 Introduction to Coordination Polymers: Definition, Formation and Interactions

Definition

The key word *coordination polymer* (*metallo-supramolecular polymer*) is abundantly found in advanced chemistry literature. However, care most be taken because the term *coordination polymer* is defined quite differently in the organic and supramolecular chemistry communities. Inorganic chemists consider infinite one-dimensional (1D), two-dimensional (2D) and three-dimensional (3D) coordination networks as coordination polymers. These systems are in the great majority crystalline solid-state materials that fragment into molecular building blocks upon dissolution. Alternative terms for these types of compounds are *metal-organic coordination network* and *metal-organic frameworks*. [11] One highlight of recent achievements in this filed is the construction of functional porous coordination polymer.[12] In the field of supramolecular chemistry, the definition of

coordination polymer is more precise and is related to macromolecular chemistry. A coordination polymer is an entity constructed by a supramoecular approach through metal coordination and consisting of a backbone, which is held together by metal-ligand interactions. These interactions have to be strong enough to retain the polymer chain also in solution. The coordination polymers should exhibit properties that are characteristic for polymers, monomeric building blocks and/or a glassy solid state. In an outstanding review on organic/inorganic hybrid polymers, Rehahn[13] proposed a classification of different structures of coordination polymers.

Formation

The main difference between classical covalent polymers and supramolecular polymers is the dependence of the chain length [degree of polymerization (**DP**)] on the solvent and temperature dependent bonding constant (K) and related therewith, the concentration. For reversible coordination polymers, the relationship between **DP** and K is given by the following expression:[14]

$$DP \sim (K[M])^{1/2}$$

According to this relationship, high **DP** values can be achieved only at high monomer concentration ([**M**]) and with a metal-ligand coordinative bond with a large **K** value. This relationship, of course, holds true only if the complexation is a fully reversible process. For intermolecular interactions, the combination high bonding constants and reversibility is challenging because these properties are highly divergent; that is, high binding constants often hamper reversibility.[15] Therefore, a detailed investigation of both the thermodynamic and kinetic properties of the individual metal complexes is necessary when a suitable metal-ligand is being chosen. The thermodynamic properties, expressed in the individual binding constants or overall binding constant,[16] provide the information on whether the complex is stable or unstable. These expressions have to be clearly distinguished from the terms *inert* or *labile*, which describe the kinetic properties. The inertness or lability of metal

complex is determined by ligand-exchange experiments and expressed, for example, in the half-life of the complex species (Table 1).[17] When a suitable metal-ligand is being chosen for the construction of a reversible coordination polymer, the ideal combination is, therefore, a system that provides a complex of high thermodynamic stability combined with high kinetic lability. This combination ensures the formation of a high-molecular-weight coordination polymer because of the stable complex bond together with the inherent advantages of reversible (labile) noncolvant supramolecular systems, that is, error correction, the identical ligand units, and switching between the polymeric and monomeric states.

Table 1.1 Binding and Functional Properties of Selected Terpyridine (tpy) Complexes

Ion Type	Binding Constant (K_1) in Water (M^{-1})	Half-Life of $M(tpy)_2^{2+}$ in Water (min)	Magentic Properties of the $M(tpy)_2^{2+}$ Complex	Electronic Interaction with tpy Ligand
Fe^{2+}	1.3×10^7	8400	Paramagnetic	Strong
Co^{2+}	2.5×10^8	50	Paramagnetic	Medium
Ni^{2+}	5.0×10^{10}	610	Paramagnetic	Medium
Zn^{2+}	1.0×10^6	<0.1	Dimagnetic	Weak

Interactions

As discussed previously, the nature of the metal-ligand interaction has a significant effect on the mechanical properties of the resulting coordination polymer, and in this regard, the binding constant is the most important parameter. Because most applications demand a high **DP** and increase in the concentration cannot be realized in many cases because of practical limitations or insufficient solution, control of the binding strength is of paramount importance. An increase **K** value may be achieved by the combination of multiple interacting binding sites, the simplest one being the use of the chelate ligands and multivalent metal ions.

The increase in the binding constant upon application of chelating ligands is illustrated by a comparison of Zn^{2+} complexation with different types of pyridine donor ligands (Figure 1.1 and Table 1.2)[18-20]
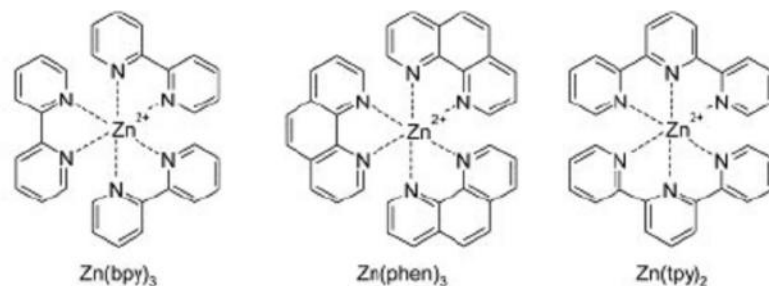
Figure 1.1 Examples of compounds with bidentate or tridetate pyridine/Zn^{2+} interactions.

Table 1.2 Binding Constants for Complexes of Zn^{2+} with Aromatic N-Donor Ligands of

Increasing Chelation

Ligand Type	K_1 $(M^{-1})^a$	β_n $(M^{-n})^a$	Solvent/Counterion
bpy^b/Zn^{2+}	2.5×10^5	2.0×10^{13} $(n = 3)$	Aqueous KNO_3
	2.0×10^5	4.2×10^{13} $(n = 3)$	0.1 M aqueous $NaNO_3$
phen^b/Zn^{2+}	2.7×10^6	1.0×10^{17} $(n = 3)$	Aqueous KNO_3
	3.5×10^6	2.5×10^{17} $(n = 3)$	0.1 M aqueous $NaNO_3$
tpy/Zn^{2+}	$>10^8$	$>10^8$ $(n = 2)$	CHl_3CN/ClO_4^-
	1.0×10^5	8.0×10^9 $(n = 2)$	CHl_3CN/ClO_4^-
	2.5×10^8	2.0×10^{14} $(n = 2)$	CHl_3CN/ClO_4^-/TBAPF

^{a} K_1 is the binding constant for the first binding event, and β_n is the overall binding constant.

^{b} Where the bpy is 2,2'-bipyridine, phen is 1,10-phenanthroline, tpy is 2,2':6',2''-terpyridines

^{c} Determined for a 4'-substituted terpyridine unit.

^{d} Determined for a 4'-substituted unit (TBAPF = 0.01M tetrabutylammonium hexafluorophosphate).

1.3 Introduction to Functional polymers and Materials Based on 2,2':6',2"-Terpyridine Metal Complexes

2,2':6',2"-Terpyridines are among the *N*-heterocycles that have very high binding affinity towards transition metal ions due to d -p * back binding of the metal to pyridine ring and the chelate effect.[21] Complexation of one or two 2,2':6',2"-terpyeidine (Figure 1.3) ligands can lead to a metal complex, and in many case bis-complexs thus formed have octahedral coordination geometries.[22] These complexes posses distinct photophyscial, electrochemical, and magnetic prorperties.[23] The complex binding can be reversed under certain conditions, e.g., varying PH, temperature, or applying even stronger competitive ligands, which makes such compounds interesting for the design of new functional materials.[5] In the search of new functional materials, metallo-supramolecular polymers, dendrimers, or micelles have been of special interest for the last few yeas, but the combination of such stable complexes with "biomolecules" such as DNA/RNA, peptides, and enzymes for labeling, intercalation, and inhibition purposes is also promising.[24] Another field which is rapidly growing due to the technical advances made is the build-up of ordered structures on a molecular scale on different kind of surfaces.[25] Here also, terpyridine complexes play an increasing role for applications such as solar-cell devices or electrode catalysis. Furthermore, such easily detectable and multifunctional entities are of great use for gaining a more fundamental understanding of self-assembly phenomena or organic or inorganic-organic hybrid materials on surfaces. Recent advances in synthesis of functionalized terpyeidine have open new possibilities for the introduction of metal complexs into polymers and onto surfaces. In particular, functionalization in the 4'-positon, by using, e.g., substitution reactions with (nowadays) commercially available 4'-chloroterpyridine[26] or 4'-hydroxyterpyridine,[27] leads to symmetrical bis-cpmplexes with ether bridged functional groups (R) which, upon complexation, do not give additional chiral products (Figure 1.2).
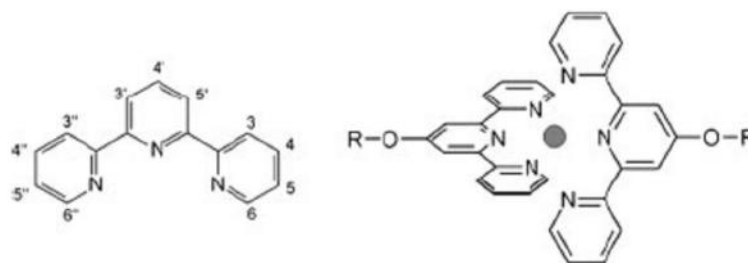
Figure 1.2 Left: unfunctionalized 2,2':6',2"-terpyeidine; right: symmetric 4'-functionalized bis-terpyridine-metal complex (charge and anions omitted).

1.3.1 Introduction to Polymeric Architectures Containing 2,2':6',2"-Terpyeidine Metal Complexes

Metallo-Polymers from Terpyridines-Fuctionalized Monodisperse Monomers

One way of classing polymers that contain terpyridine metal complexes is to distinguish between metallo-polymers built up from monodisperse or polydisperse monomers. Metallo-polymer systems, starting from monodisperse building blocks, are discussed first. In 1995, Constable presented the general concept of bis-terpyridine functionalized telechelics, which, upon addition of metal ions, should give coordination polymers (Figure 1.3).[28]
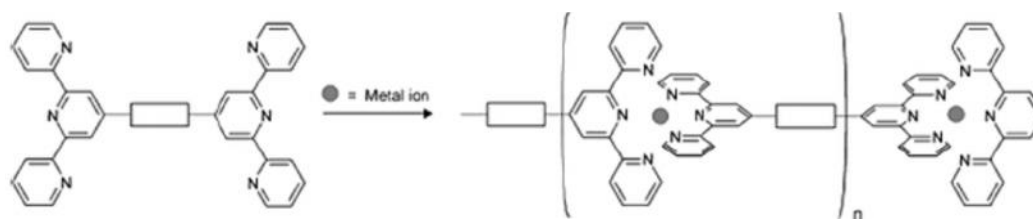
Figure 1.3 Polymeric bis-terpyridine-metal complex (charge and anions omitted).

It was mainly work by Kurth et al. and Rehahn et al. in the late 1990s that pioneered this concept,[29] using small monodiesperse di-terpyridines as monomers in order to create, for example, coordination polyelectrolyte layers. In the last few years, there have been a number of different approaches, mainly focusing on iron(II), zinc(II) and ruthenium(II) as the "metal glue" for coordination polymerization. An example of Meijer and co-workers reported the synthesis of rigid iron(II)-bis-terpyridine polymer including oligo(phenylene/vinylene) (OPV)

units (Figure 1.4).[30] Due to this rigidity, the formation of small cycles in this case is unlikely, and the DP was estimated to be 100 at applied millimolar concentration, derived from kinetic data obtained from Uv-visible titration experiment.
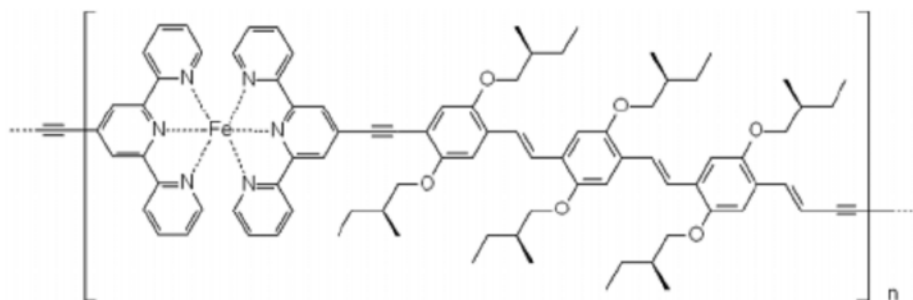
Figure 1.4 Combination of a bis-terpyridine-iron(II) complex and an oligo(phenylene vinylene) (OPV) unit.

Polydisperse System Cotaining 2,2':6',2"-Terpyridines Metal Complexes

The combination of properties of conventional polymers with those of bis-2,2';6',2"-terpyridine metal complex has become of increasing interest over the last few years. The three main approaches to chemically introducing terpyridines and their complexes into polymeric systems are: a) by functionalizing properly modified polymers with terpyridine ligands; b) by using a functionalized terpyridine as an initiator; and c) by using a terpyridine with a polymerizable group as the monomer or co-monomer (these can be classified as convergent approaches, staring from uncomplexed terpyridine). These main approaches also apply to corresponding bis-terpyridine metal complexes (a divergent approach, in which metallo-polymers are formed starting from the complex). Having a functionalized polymer with non-complexed terpyridine ligands subsequently allows different combinations upon bis-complexation with different metals, leading to a rich variety of possible new structures. For a detailed insight into these strategies, the reader should turn to recent overviews.[6,31]

The first two approaches are especially appealing for gaining access to extended polymer chains through metal complexation by a terpyridine-functionalized polymer. These

polymeric terpyridine starters can be either mono-functionalized or of telechelic nature, processing more than one terpyridine unit per chain. Having terpyridine units at both ends of each chain allow access to linearly extended chains cotaining metal "linkers". Such a system, consisting of a high molecular weight poly(enthylene oxide) polymer end-capped with terpyridines, gave upon addition of iron(II) or nickel(II) acetate an extended polymer, which was especially demonstrated through the increase in viscosity (Figure 1.5).[32]
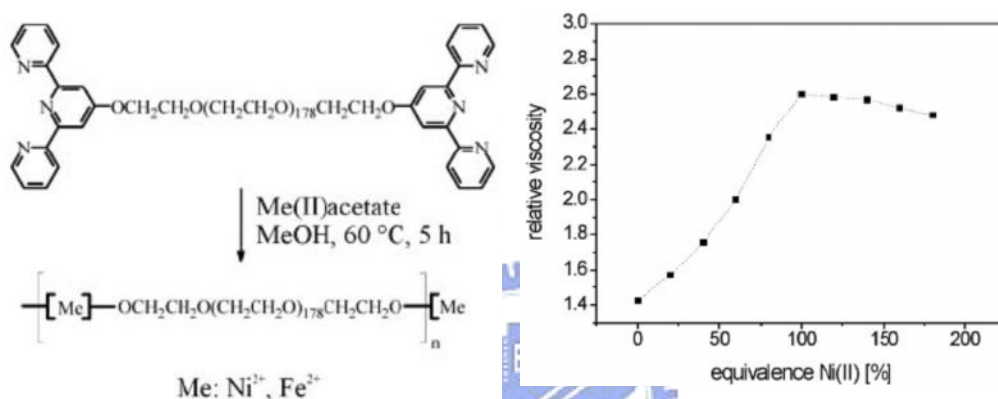
Figure 1.5 Right: synthesis of metal-linked poly(ethylene glycol)$_{180}$ (charge and anions omitted); Left: viscosity increase when adding nickel(II) acetate.

In order to investigate a variety of such polymers were synthesized using a combinatorial approach.[33] Another possibility for creating and investigating such systems is to first functionalize only one chain end with terpyridine, and than to apply directed as well as undirected coupling methods, in order to obtain AA, AB, and ABA block copolymer systems (Figure 1.6). Directed coupling can be achieved by first forming a mono-terpyridine metal complex, the most common metal for this strategy being ruthenium( ). Subsequent reduction to ruthenium(II) in the presence of a differently functionalized terpyridine leads to a heteroleptic complex. In contrast, undirected coupling use the same ligand for bis-complexation with bivalent metal salts. Looking at AA homopolymer systems, this concept was recently realized using poly(ethylene oxide) functionalized with one terpyridine, which, upon complexation with various transition metal ions, gave water soluble polymers

with double the mass of the starting polymer ligand plus the metal and counter ions.[34]
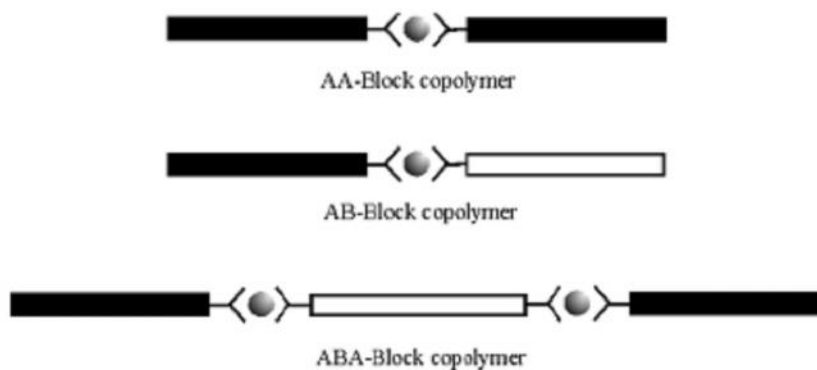
Figure 1.6 Schematic representation of AA-, AB-, and ABA-type metallo- supramolecular block copolymer systems.

Concerning AB- or ABA-type structures, their preparation requires directed coupling techniques. A well-known strategy for creating such hetero-complexes is the ruthenium( )/ruthenium(II) coupling method. First the dark brown mono-terpyridine-Ru( ) chloride in dimethylformamide (DMF) with the ligand. This is then further than reacted with a different ligand under reducing condition (ethanol/cat. N-ethyl-morpholine), resulting in the formation of the red ruthenium(II) hetero-complex. Applying this strategy to different terpyridine end-capped polymers led to the hetero-ruthenium-complex polymers (Figure 1.7).[35] Such AB-type structures combing two different polymer chains have up to now only been accessible using or controlled polymerization procedures. The same strategy has also been applied for ABA-type systems. Here, a bis-terpyridine end-capped poly(propylene oxide) telechelic was first complexed at both end with ruthenium( ) chloride and subsequently complexed symmetrically on both sides with a 4'-functionalized terpyridine.[36]
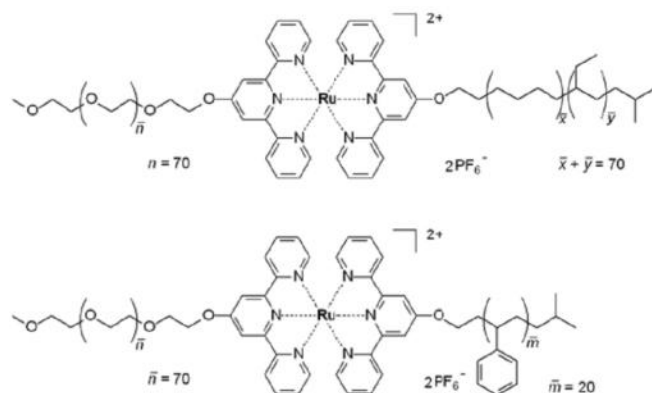
Figure 1.7 Synthesized AB-type bis-terpyridine –Ru(II) complexes combing different polymer blocks.

The third main approach for including terpyridines and their complexes in polymeric structures is to use terpyridine (complexes) functionalized with a polymerizable group as the monomer or co-monomer. As a convergent approach, this was demonstrated over 10 years ago, utilizing vinyl and acrylic groups as functional moieties for polymerization.[6] Recently, Calzia and Tew prepared a random copolymer using a methyl methacrylate-functionalized terpyridine as co-monomer (Figure 1.8).[37] Upon addition of cobalt(II) nitrate the authors observed a rise in viscosity which did not occur in the case of the homopolymer. An example for the divergent approach of polymerization bis-terpyridine complexes, which are functionalized on one side with a polymerizable group, was reported, recently.[38] Hetero bis-terpyridineu-Ru(II) complexes bearing a 4-vinyl-phenyl substituent on one of the 4'-position were copolymerized with the styrene using radical polymerization. Through possible further functionalization on the hydroxymethyl function of the ligands, new possibilities for crosslinked and grafted systems become available.
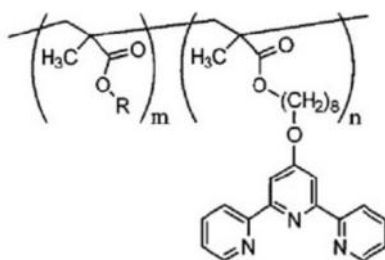
Figure 1.8 Tew's methacrylate copolymer for metal complexations.

Cho et al. used the convergent approach to produce side-chain-functionalized ruthenium(II)-complexes.[39] Here, first a conventional ABA tri-block copolymer was found by anionic polymerization to yield poly(CzMA-b-2VP-b-CzMA), with CzMA = 2-(N-carbazoly)ethyl metahacrylate, and 2VP = 2-vinylpyridine. The middle block, consisting of 0-20 2VP units, was then complexed with the mixed Ru(II)(tpy)-(dmbpy) chloride (dmbpy = 4,4'-dimethyl-2,2'-bipyridine) in order to yield the octahedral six-coordinative ruthenium(II) complexes as the grafted species (Figure 1.9)
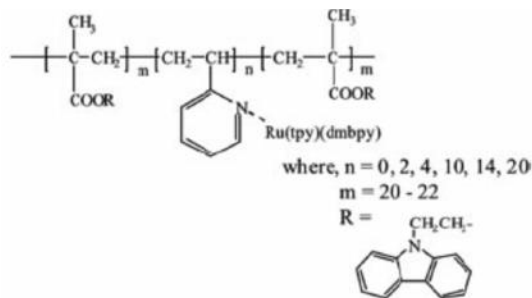
Figure 1.9 Cho's Ru-coordinated block copolymer.

1.3.2 Introduction to Surfaces Modified with 2,2':6',2''-Terpyridines Metal Complexes

Assemblies and Layers

Research concerning the modification of surface properties on a molecular level has increased since Binning and Rohrer invented scanning probe techniques STM (scanning tunneling microscopy) or AFM (atomic force microscopy) in the mid-1980s. However, there is still much to learn in terms of ordering and orientation of substances on surfaces. Metallo-supramolecular structures in particular add a whole range of possibilities, not least because of possible interactions between the complexed metal and a metal surface. Recently, there has been increasing interest in the investigation adsorbed ordered structures on surfaces containing bis-terpyridine metal complexes. For an overview on layer-by-layer self-assemblies containing terpyridine complexes, the reader is referred a review.[40] For

example, Abruña and co-workers described the synthesis of chair and dendritic multi-terpyridine molecules, which, upon complexation with iron(II) or cobalt(II) and deposition on a surface, led to well-ordered two-dimensional (2D) arrays, recently.[41] In case of terpyridine functionalized second-generation poly(amido amine) (PAMAM) starburst dendrimer, the the author states that instead of more thermodynamically stable (2D) arrays, chains stacked next to each other ("pearl necklace" formation) were found by STM investigation on highly ordered pyrolytic graphite (HOPG) (Figure 1.10).
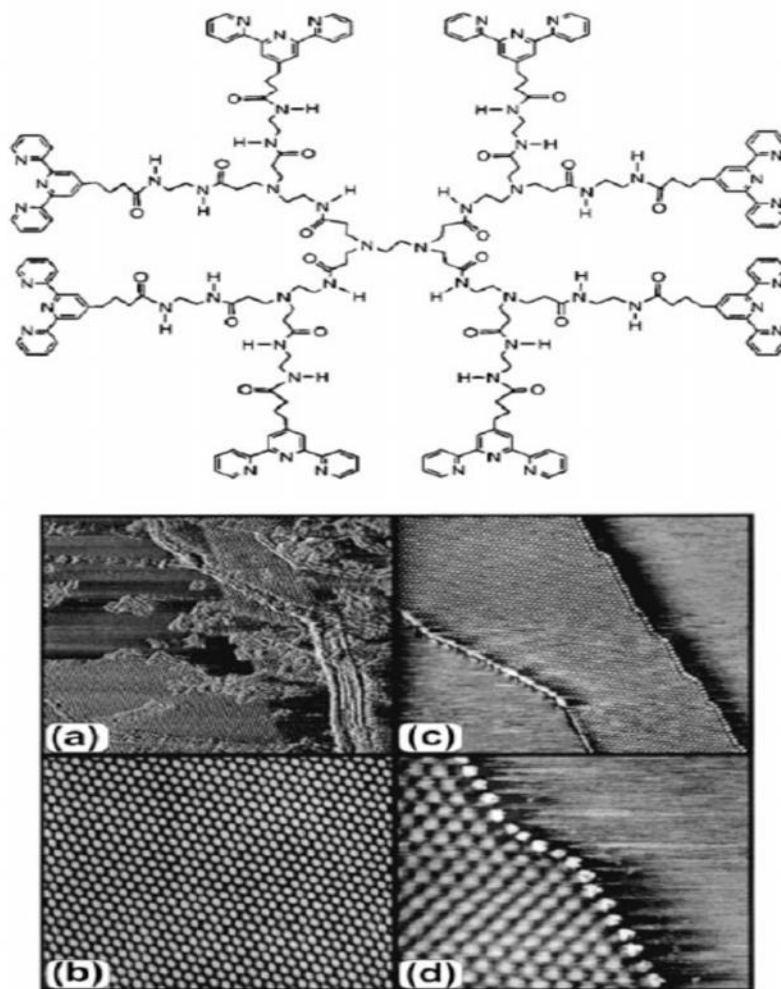
Figure 1.10 Top: structure of the terpyridine dendrimer (dend-8-tpy); bottom: unfiltered images of dend-8-tpy/Fe^{2+} on HOPG, a) 550 nm×550 nm, b) 200 nm×200 nm, c) 304 nm×304 nm, d) 69 nm×69 nm.

Photoactive Materials

Another major area of research, which includes the study of terpyridine-complex-surface interactions, is that of interfacial photophysical processes, especially systems concerning solar light to energy conversion. First example include photoelectrodes based on electropolymerized molecular ruthenium diads reported by Collin et al.[42] They described polymer films incorporating molecular diads of the type V^{2+}-[Ru(II)-(ptpy)$_2$]$^{2+}$ (V = methylviologen, ptpy = 4'-phenyl-terpyridine) (Figure 1.11, left). Thin films were prepared by anodic electropolymerization of the pyrrol groups on the ligand opposite to the ligand containing the methylviologen on an indium oxide (ITO) electrode. Upon irradiation using visible light and in the presence of triethanolamine (TEOA, irreversible electron donor), an anodic photocurrent is observed when the electrode is potentiostated to 0 V. The photoactive center is first excited by visible light upon which the charge-separated state with the methylviologen is formed. Ruthenium( ) then irreversibly oxidizes TEOA an the photocurrent is produced by electron transfer into the polymer an to the electrode. The steady-state photoresponse was moderately stable with time (loss of 19% after 30 min) in accordance with stability with modified electrode (Figure 1.12, right).
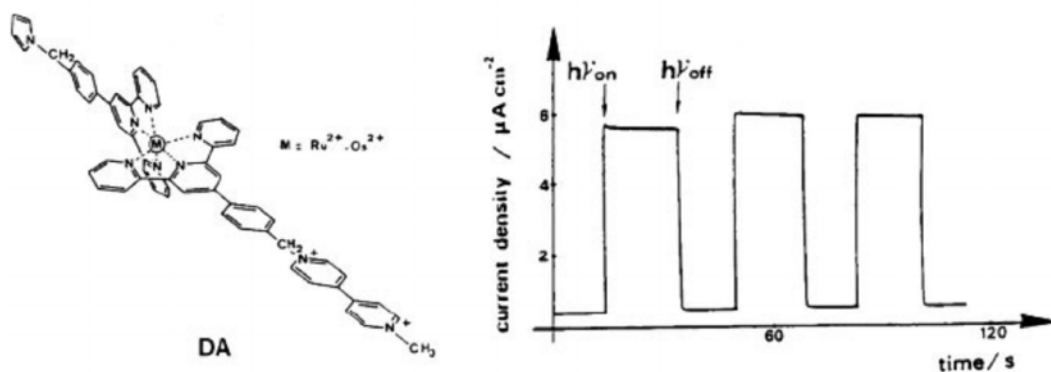
Figure 1.11 Left: donor-acceptor system DA with pyrrol (anchor), a ruthenium(II) or osmium(II) bis-terpyridine complex (photochemical center) and a methylviologen (MV^{2+}, donor); right: photocurrent response of ITO/poly-(DA) modified electrode.

Apart from solar-cell research the other photophyscially interesting example have been reported: organic light-emitting devices (OLEDs). Elliott and co-workers investigated an

electropolymerized [Ru(tpy)2]^0 film which was vapor deposited onto an AlQ/TPD/ITO (ALQ = tris(8-hydroxyquinoline) aluminum( ) complex, emissive and electron transport layer/TPD = triarylamine derivative, hole transport layer) substrate in order to create an electroluminescent device.[43] Another example of blue LED was shown very recently by Che and co-workers.[44] They used a bis-terpyridine zinc(II) polymer spin-coated on ITO with the device structure: ITO/PEDOT:PSS/zinc-terpyridine-polymer/Ca/Al. A peak maximum of 450 nm is observed in the electroluminescence spectrum with the blue EL intensity increasing with the increasing bias voltage. These examples demonstrate the versatility of terpyridine metal complex, leading to, in this case, encouraging results towards the search for stable and intense blue-light emission, which is currently of particular interest for many photo-optical application.

Finally, terpyridine-metal complexs are gaining increasing interest as a type of new functional materials. Their reversibility under certain conditions, as well as photophyscial properties led to a number of research activities combining these complexes with polymers and/or surfaces.
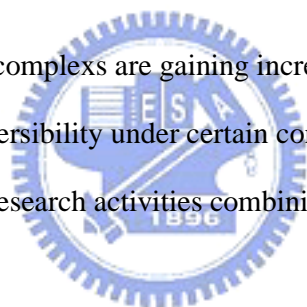
Chapter 2

Novel Light-Emitting Metallo-Homopolymers and Metallo-*alt*-copolymer Containing Terpyridyl Zinc(II) Moieties

2.1 Abstract

A series of novel terpyridyl Zn(II))-based metallo-polymers, including metallo-homopolymers and metallo-*alt*-copolymer, containing carbazole pendants attached to the C-9 position of fluorene by long alkyl spacers were constructed by self-assembled reaction. The integrated ratios of ^{1}H NMR reveal a facile result to distinguish the differences between metallo-homopolymers and copolymers. To further investigate these polymers, UV–vis and PL spectral titration experiments were also carried out by varying the molar ratios of zinc(II) ions to monomers. The photophysical properties of these polymers exhibited blue PL emissions (around 420 nm) with quantum yields of 11–23% (in DMF) and the PL results revealed that the formation of excimers were suppressed by the incorporation of carbazole pendant groups. In addition, the EL results showed green EL emissions (around 550 nm) with turn-on voltages of 6.0–6.5 V, maximum efficiencies of 0.85–1.1 cd A^{-1} (at 100 mA cm^{-2}), and maximum luminances of 1704–2819 cd/m^2 (around 15 V), correspondingly.

2.2 Introduction

Metal-ligand coordination seems to be particularly attractive in past few decades because of searching for new smart materials.[45-49] Moreover, by proper selections of metal–ligand combinations; it is possible to realize ideal conditions for self-assembly, i.e., formation of kinetically labile but nevertheless thermodynamically stable bonds. The properties of coordination polymers can be widely varied due to the availability of a multitude of ions and ligands, both having profound effects on binding strength, reversibility, and solubility.[50] Accordingly, it is not surprising that metal–ligand coordination polymers, which are processable in solutions, have gained considerable interest in recent years.

2,2′:6′,2″–Terpyridine is one of the metal–ligand combination units that have been of particular importance for construction of metallo-supramolecular polymers,[49,51] and a large number of studies have been reported on the construction of linear-rod polymers based on this terpyridyl unit.[23,52] Due to the prominent photoluminescent (PL) and electroluminescent (EL) properties, terpyridyl Zn(II) moieties were introduced to optoelectronic applications by several research groups.[49,53] During the process of light emission in the fully conjugated metallo-polymers, it is confirmed that the phenomenon of metal to ligand charge transfer (MLCT) does not occur in terpyridyl Zn(II) moieties because of the d^{10} Zn(II) species, so only intraligand charge transfer (ILCT) happens between the coordination sites and chromophores.[54] Dobrawa and Würthner have recently reported that metallo-polymers containing perylene bisimide dyes and terpyridyl Zn(II) moieties showed strong red PL emissions.[54a–b] According to Che and co-workers' report, the incorporation of terpyridyl Zn(II) moieties into different main-chain structures was proven to exhibit different emission wavelength ranging from violet to yellow colors with high PL quantum yields, and the applications of high efficient polymeric light-emitting diode (PLED) devices are plausible by using these coordination polymers.[44,55] Therefore, utilization of terpyridyl Zn(II) moieties as connecting groups to assemble suitable chromophores is an appealing strategy for the

construction of PL or EL metallo-supramolecular polymers. In this study, novel terpyridyl Zn(II)-based metallo-polymers, including metallo-homopolymers and metallo-*alternating*-copolymer (i.e., metallo-*alt*-copolymer), containing carbazole pendants attached to the C-9 position of fluorenes by long alkyl spacers were constructed by self-assembled reaction and their ^{1}H NMR, PL, and EL properties were investigated as well. More importantly, the first light emitting metallo-*alt*-copolymer built up from different ditopic ligands coordinating with Zn(II) species was developed and is surveyed in this report.

2.3 Experimental

2.3.1 Measurements.

^{1}H NMR spectra were recorded on a Varian Unity 300 MHz spectrometer using CDCl$_3$ and DMSO-d_6 solvents. Elemental analyses were performed on a HERAEUS CHN–OS RAPID elemental analyzer. Thermogravimetric analysis (TGA) was conducted on a Du Pont Thermal Analyst 2100 system with a TGA 2950 thermogravimetric analyzer at a heating rate of 10 ℃ /min under nitrogen. Melting points were determined with a Buchi SMP-20 capillary melting point apparatus. Viscosity measurements were proceeded by 10% weight of polymer solutions (in NMP) in contrast to that proceeded by monomer solutions under the same condition (with viscosity η = 6 cP) on a BROOKFILEL DV-III+ RHEOMETER system at 25 ℃ (100 rpm, Spindle number 4). UV–visible (UV–vis) absorption spectra were recorded in dilute DMF solutions (10^{-5} M) on a HP G1103A spectrophotometer, and fluorescence spectra were obtained on a Hitachi F-4500 spectrophotometer. Fluorescence quantum yields in solutions were determined relative to the integrated photoluminescence (PL) density of coumarin-1 in ethanol with a known quantum yield (ca. 5×10^{-6} M, quantum yield = 0.73). Cyclic voltammetry (CV) was performed at a scanning rate of 100 mV/s on a BAS 100 B/W electrochemical analyzer, which was equipped with a three-electrode cell. Pt wire was used as a counter electrode, and an Ag/AgCl was used as a reference electrode in the CV measurements. The CV experiments were performed by solid samples immersed into electrochemical cell containing a 0.1 M tetrabutylammonium hexafluorophosphate (Bu$_4$NPF$_6$) solutions (in DMF) at a scanning rate of 100 mV/s at room temperature under nitrogen. Polymer thin solid films were spin-coated on quartz substrates from DMF solutions with a concentration of 10 mg/mL. UV–vis and PL titration were preformed by that 1.0×10^{-5} M of monomer solutions in the solvent of CH$_3$CN/CHCl$_3$ (2/8 in vol.) was titrated with 50 µl aliquots of a 3.9×10^{-4} M of Zn(OAc)$_2$ solutions in the same solvent composition as described. The addition was done stepwisely

and the formation of Zn(II)-coordination polymers was monitored by UV-vis spectroscopy. A series of EL devices with the configuration of ITO/PEDOT: PPS/polymer/BCP(2,9-dimethyl-4,7-diphenyl-1,10-phenanthroline)/Alq$_3$(tris(8-hydroxyquinoline)aluminum)/LiF/Al were made, where BCP (i.e., 2,9-dimethyl-4,7-diphenyl-1,10-phenanthroline) or Alq$_3$ (i.e., tris(8-hydroxyquinoline)aluminum) was used as an electron transporting layer. The ITO substrates were routinely cleaned by ultrasonic treatments in detergent solutions and diluted water, followed by rinsing with acetone and then ethanol. After drying, the ITO substrates were kept in oxygen plasma for 4 min before being loaded into the vacuum chamber. The solutions (10 mg/mL) of light-emitting materials in DMF were spin-coated on glass slides precoated with indium tin oxide (ITO) having a sheet resistance of ~20 /square and an effective individual device area of 3.14 mm^2. The spin coating rate was 6000 rpm for 60 s with PEDOT: PPS, 4000 rpm for 60 s with resulting polymers, and the thicknesses of PEDOT: PPS and polymers were measured by an Alfa Step 500 Surface Profiler (Tencor). BCP and Alq$_3$ were thermally deposited at a rate of 1–2 Å/s under a pressure of ~2 ×10^{-5} Torr in an Ulvac Cryogenic deposition system. Under the same deposition systems and conditions, one layer of LiF was thermally deposited as a cathode at a rate of 0.1–0.2 Å/s, which was followed by capping with an aluminum layer.

2.3.2 Materials

Chemicals and solvents were reagent grades and purchased from Aldrich, ACROS, TCI, and Lancaster Chemical Co. Solvents were purified and dried according to standard procedures. Chromatography was performed with Merck silica gel (mesh 70–230) and basic aluminum oxide, which was deactivated with 4 wt % of water. 4 -[[(Trifuroromethyl)sulfonyl]oxy]- 2,2 :6 ,2 -terpyridines and compounds **1a** and **1b** were prepared and purified according to literature procedures.[56a–c] The synthetic routes of monomers and metallo-polymers are illustrated in Schemes 2.1–2.3.

Syntheses of Monomers. Compound 2a. To a solution of compound **1a** (13.8 g, 28 mmol) in 60 mL of THF/Et$_3$N (1/1), 3-methyl-1-butyn-3-ol (8.83 mL, 84 mmol) was added. After the solution was degassed with nitrogen for 30 min, Pd(PPh$_3$)$_2$Cl$_2$ (0.19 g, 0.28 mol), PPh$_3$ (2.9 g, 11 mol), and CuI (0.53 g, 2.8 mmol) were added. The reaction was then refluxed at 70 ºC under N$_2$ for 12 h. The solvent was removed under reduced pressure. The resulting solid was extracted with CH$_2$Cl$_2$/H$_2$O then dried over MgSO$_4$. The crude product was purified by column chromatography (silica gel, hexane/ethyl acetate = 4/1 in volume) to afford a white solid: mp 96–97 ºC. ^{1}H NMR (300 MHz, CDCl$_3$): δ 7.59 (d, J = 8.4 Hz, 2H), 7.37–7.41 (m, 4H), 2.09 (s, 2H), 1.88–1.93 (m, 4H), 1.65 (s, 12H), 1.09 (br, 16H), 0.75–0.80 (m, 6H). Yield: 82%. FABMS: m/e 498; C$_{35}$H$_{46}$O$_2$ requires m/e 498.35.

Compound 2b. The procedure is analogous to that described for **2a** to afford a white solid: mp 101–102 ºC. ^{1}H NMR (300 MHz, CDCl$_3$): δ 8.06 (d, J = 6.9 Hz, 4H), 7.57 (d, J = 7.8 Hz, 2H), 7.30–7.45 (m, 8H), 7.17–7.30 (m, 8H), 4.15 (t, J = 6.9 Hz, 4H), 2.04 (s, 2H), 1.95–1.98 (m, 4H), 1.82–1.84 (m, 4H), 1.66 (s, 12H), 1.07 (br, 12H). Yield: 78%. FABMS: m/e 817; C$_{58}$H$_{60}$N$_2$O$_2$ requires m/e 816.47.

Compound 3a. A mixture of **2a** (0.82 g, 1.63 mmol) and KOH (365 mg, 6.5 mmol) in 60 mL of 2-propanol was heated refluxed under N$_2$ with a vigorous stirring for 3 h. The solvent was then removed and crude product was purified by column chromatography (silica gel, hexane) to afford a white solid: mp 154–155 . ^{1}H NMR (300 MHz, CDCl$_3$): δ 7.63 (d, J = 8.4 Hz, 2H), 7.47–7.49 (m, 4H), 3.17 (s, 2H), 1.87–1.92 (m, 4H), 1.07 (br, 16H), 0.75–0.83 (m, 6H).Yield: 83%. FABMS: m/e 382; C$_{29}$H$_{34}$ requires m/e 382.27.

Compound 3b. The procedure is analogous to that described for **3a** to afford a white solid: mp 164–165 ºC. ^{1}H NMR (300 MHz, CDCl$_3$): δ 8.05 (d, J = 6.6 Hz, 4H), 7.87 (d, J = 7.8 Hz, 2H), 7.37–7.47 (m, 8H), 7.15–7.30 (m, 8H), 4.15 (t, J = 6.3 Hz, 4H), 3.14 (s, 2H), 1.90–1.94 (m, 4H), 1.80–1.84 (m, 4H), 1.05 (br, 12H). Yield: 80%. FABMS: m/e 700; C$_{52}$H$_{48}$N$_2$ requires m/e 700.38.

Monomer 4a. Compound **3a** (250 mg, 0.5 mmol) and 4 -[[(trifuroromethyl)sulfonyl]oxy]-2,2 :6 ,6 -terpyidine (420 g, 1.1 mmol) were dissolved in nitrogen-degassed benzene, then [Pd^0(PPh$_3$)$_4$] (70 mg, 0.06 mmol) was added and followed by nitrogen-degassed ^{i}Pr$_2$NH. The solution was then heated to 70 ℃. After complete consumption of starting materials, the solvent was evaporated and the product was purified by column chromatography (alumina, hexane/dichloromethane = 10/1 in volume) to afford a white solid: mp 206–207 ℃. ^{1}H NMR (300 MHz, CDCl$_3$): δ 8.74 (d, J = 4.8 Hz, 4H), 8.62–8.66 (m, 8H), 7.89 (t, J = 8.1 Hz, 4H), 7.74 (d, J = 8.4 Hz, 2H), 7.57–7.59 (m, 4H), 7.34–7.39 (m, 4H), 2.04 (br, 4H), 1.11 (br, 16H), 0.84 (br, 6H). Yield: 77%. FABMS: m/e 845; C$_{59}$H$_{52}$N$_6$ requires m/e 844.43. Anal. Calcd for C$_{59}$H$_{52}$N$_6$: C, 83.85; H, 6.20; N, 9.94. Found: C, 84.12; H, 6.34; N, 9.63.

Monomer 4b. The procedure is analogous to that described for **4a** to afford a white solid: mp 223–224 ℃. ^{1}H NMR (300 MHz, CDCl$_3$): δ 8.74 (d, J = 4.8 Hz, 4H), 8.63–8.67 (m, 8H), 8.04 (d, J = 7.8 Hz, 4H), 7.88 (t, J = 8.4 Hz, 4H), 7.71 (d, J = 7.8 Hz, 2H), 7.54–7.58 (m, 4H), 7.30–7.56 (m, 12H), 7.16 (t, J = 6.9 Hz, 4H), 4.19 (t, J = 7.2 Hz, 4H), 2.01 (br, 4H), 1.70 (br, 4H), 1.18 (br, 12H). Yield: 79%. FABMS: m/e 1175; C$_{83}$H$_{66}$N$_8$ requires m/e 1174.54. Anal. Calcd for C$_{83}$H$_{66}$N$_8$: C, 84.81; H, 5.66; N, 9.53. Found: C, 85.12; H, 5.89; N, 9.67.

Synthetic Procedures of Metallo-Polymers. Metallo-Homopolymer P1. To monomer **4a** (0.52 mmol) in 30 mL of NMP solution, zinc acetate (0.52 mmol) in NMP (10 mL) was added dropwisely. The resulting solution was heated at 105 ℃ under a nitrogen atmosphere. After the reaction was stirred for 24 h, excess KPF$_6$ was added into the hot solution. The resulting solution was poured into methanol and the precipitate obtained was purified by repeated precipitations using NMP and ether. The polymers were dried under vacuum at 60 ℃ for 24 h and collected as yellow solids. Yields: 82%.

Metallo-Homopolymer P2. The procedure is analogous to that described for **P1.** Yields: 80–84%.

Metallo-*alt*-copolymer P3. To zinc acetate (1.25 mmol) in 20 mL of NMP (*N*-methylpyrrolidinone) solution, monomer **4a** (0.61 mmol) in NMP (20 mL) was added dropwisely. After the reaction was stirred at room temperature for 2 h, then monomer **4b** (0.64 mmol) was also added dropwise. The resulting solution was heated to 105 ℃ under a nitrogen atmosphere. After this was stirred for 24 h, excess KPF_6 was added into the hot solution. The resulting solution was poured into methanol, and the precipitate obtained was purified by repeated precipitations using NMP and ether. The polymers were dried under vacuum at 80 ℃ for 24 h and collected as yellow solids. Yields: 79%.

2.4 Results and Discussion

2.4.1 Synthesis and Characterization.

The synthetic routes of monomers **4a-4b** and a series of metallo-polymers **P1-P3** are illustrated in scheme 2.1-2.3. According to Scheme 1, monomers **4a** (with alkyl pendants) and **4b** (with carbazole pendants) were synthesized from compounds **1a**-**1b** reacted with propargylic alcohol via the Sonogashira coupling reaction, and further deprotected by refluxing 2-propanol in a basic condition. Then, a cross-coupling reaction between **3a-3b** and 4'-[[(trifluoromethyl)sulfonyl]-oxy]-2,2':6',2''-terpyridine in the presence of a catalytic amount of Pd(0) complexes under a basic condition to obtain monomers **4a-4b**.[56d] Metallo-homopolymers **P1-P2** (see Scheme 2) were obtained by refluxing monomers **4a** and **4b** with zinc acetate at the ratio of 1:1, respectively, in NMP solutions and followed by subsequent anion exchanges, where Zn(II) species from Zn(OAc)$_2$ were used to prepare for the terpyridyl Zn(II))-based metallo-polymers.[11] The key steps in the functionalized two terpyridyl units of monomer **4a** with zinc acetate at the ratio of 1:2 to afford complex **5**. Then, complex **5** as an initiator was coordinated with monomer **4b** at the ratio of 1:1 (as a sequential-coupling method) to obtain metallo-*alt*-copolymer **P3**.

Scheme 2.1 Synthetic Routes of Monomers **4a-4b**.
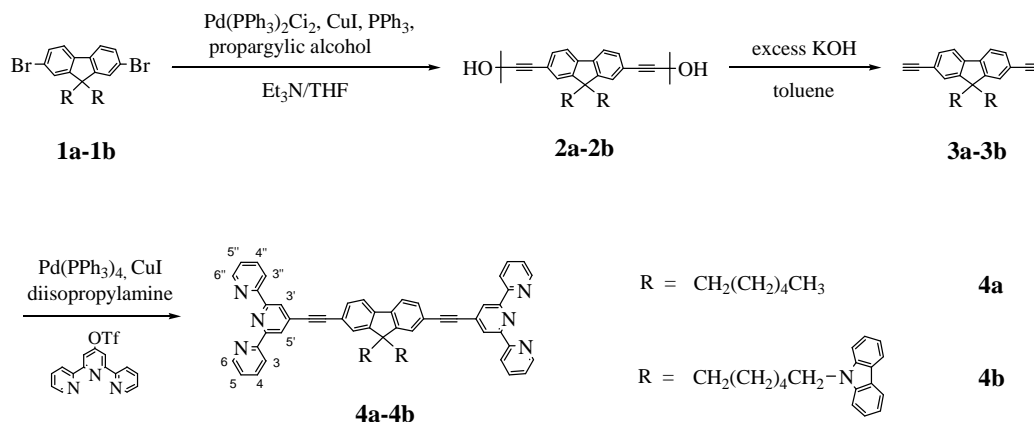
Scheme 2.2 Synthetic Routes of Metallo-Homopolymers **P1-P2**.

P1-P2

R = CH₂(CH₂)₄CH₃ **P1**

R = CH₂(CH₂)₄CH₂−N **P2**
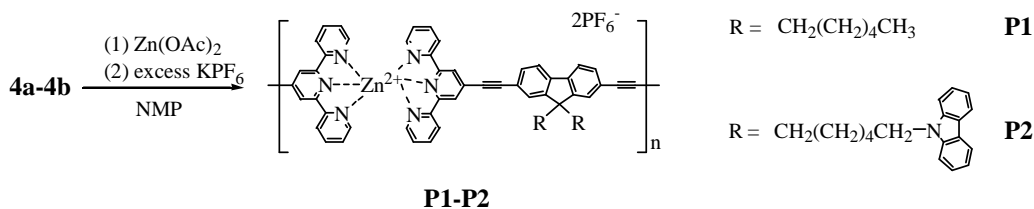
Scheme 2.3 Synthetic Route of Metallo-*Alternating*-Copolymer **P3**.

5

R₁ = CH₂(CH₂)₄CH₃

R₂ = CH₂(CH₂)₄CH₂−N

P3
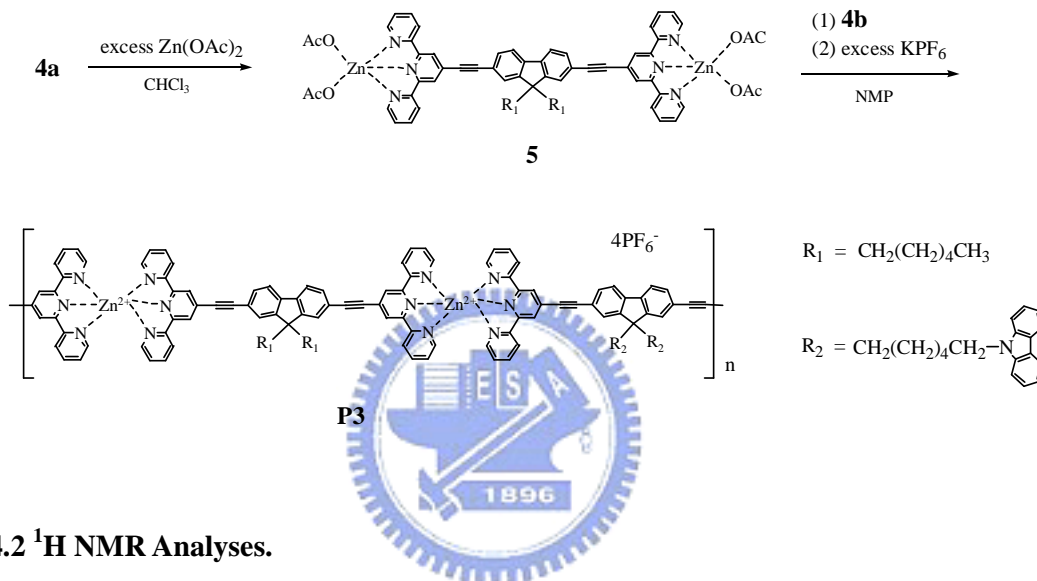
2.4.2 ¹H NMR Analyses.

¹H-NMR spectra of monomers **4a-4b**, complex **5**, and polymers **P1-P3** were recorded in DMSO-*d₆* as show in Figure 2.1. Monomers **4a** and **4b** reveal well-defined ¹H peaks for terpyridyl units. Compared with ¹H peaks in monomer **4a**, those in terpyridyl units of complex **5** show downfield shifts for (6,6"),(5,5"),(4,4"),(3',5'),(3,3")-H. Furthermore, (4,4")-H in terpyridyl units of complex **5** overlap with the ¹H peak of fluorine unit. All polymers exhibited broadening effect and dramatic shifts in ¹H peaks of terpyridyl units after coordinating with Zn²⁺ ions.[10-11a] The formation of homopolymers **P1** and **P2** is clearly indicated by the appearance of new sets of ¹H peaks and the absence of the original ¹H peaks in terpyridyl units, which belong to uncomplexed monomers **4a** and **4b**. The assignment of ¹H peaks of terpyridyl units in polymer structures are made by asterisks according to 4-chloro-terpyridine Zn²⁺ complex. In terms of ¹H peaks for carbazole pendants, there is no

obvious change in chemical shifts between monomer **4b** and polymers **P2**-**P3**. Therefore, the most up-shifted ^{1}H peaks in terpyridyl units of polymers **P2** and **P3** could be hidden under the ^{1}H peaks of carbazole pendants. To distinguish the molecular structures between metallo-homopolymer and metallo-*alt*-copolymer, the integrated ratios of the most downfield-shifted ^{1}H peaks in terpyridyl units (***A** for **P2** and ***A'** for **P3**) and the ^{1}H peaks of pendant alkyl chains (spacer -CH$_2$-) attached to carbazole units (**B** for **P2** and **B'** for **P3**) of polymers **P2**-**P3** were compared. It reveals that the integrated ratio of ***A/B** is 0.5 for homopolymer **P2** and that of ***A'/B'** is 1 for *alt*-copolymer **P3**, which suggests that the integrated ratios of polymers were consistent with the monomer amounts containing pendent carbazole units. According to these results, the amounts of ligand blocks (i.e. **P1** and **P2**: one-block ligands; **P3**: di-block ligands) can be confirmed.[57]
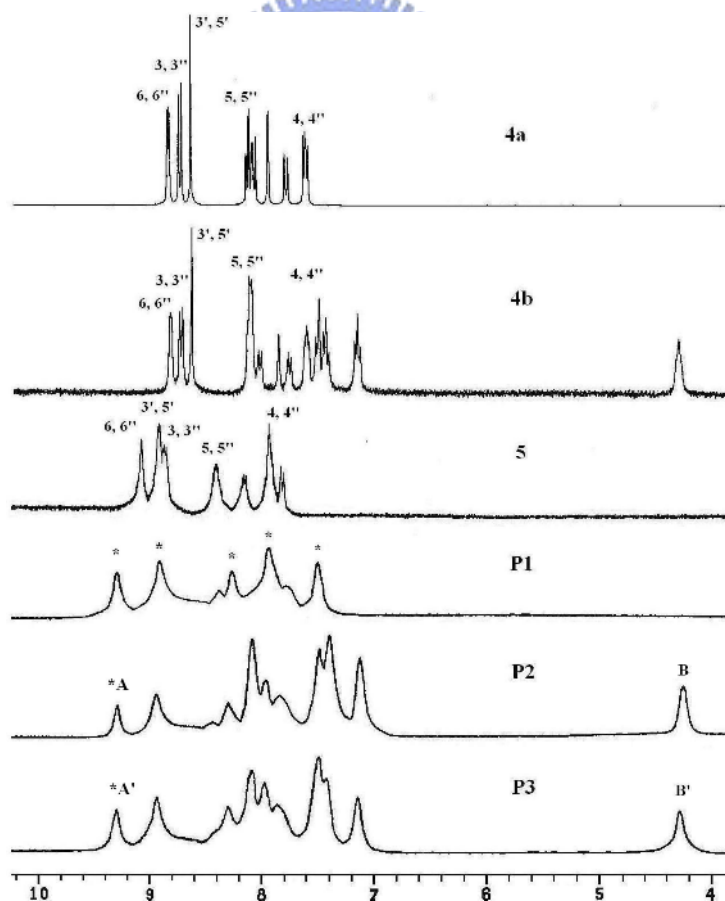
Figure 2.1 ^{1}H-NMR spectra of monomers **4a-4b**, complex **5**, and polymers **P1-P3** in DMSO-*d₆*.

2.4.3 Thermal, Electrochemical, and Viscosity Properties.

The thermal, electrochemical, and viscosity properties of polymers **P1-P3** studied by TGA, CV and rheometry, respectively, are summarized in Table 2.1

As show in Figure 2.2, the decomposition temperatures (Td) (5% weight loss measured by TGA) of metal precursor $Zn(OAc)_2$, monomers, and polymers under nitrogen were in the range of 210 , 345-351 , and 368-422 , respectively. Both of the monomers and polymers showed the same appearance of two degradation temperatures. In contrast to metal precursor $Zn(OAc)_2$ and monomers, polymers exhibited slightly enhanced thermal stability due to the increased rigidity of the main-chain structures.[55a-55b] As the alkyl pendants are attached to polymer backbones, it leads to reduced rigidity of the polymers.[48d,55b] Hence, polymers **P2** and **P3** containing bulky carbazole pendants, which further reduce the - stacking of the main-chain structures, show lower Td values than polymer **P1**. However, polymer **P3** reveals the lowest Td value, which may be caused by the reduced interchain interaction from the alternating copolymer structure and thus to decrease the rigidity of polymer **P3**. In contrast to metal precursor $Zn(OAc)_2$ and monomers, only polymers possessed 25-30% residual materials upon heating to 800 , and similar results of residual ratio in coordination polymers were reported in the literature.[55a] This result suggests that the residual materials are originated from the aggregation of polymers **P1**-**P3** due to - stacking of the fully conjugated main-chain structures. Overall, the combination of metals and ligands in the main-chain coordination polymers can enhance the thermal stability.

All polymers exhibited reversible reduction peaks at around -1.54 V in cathodic scans up to -2.5 V. These peaks are attributed to the reduction of terpyridyl-based moieties.[55,56d] The reduction potentials of these polymers are quite similar to Che's report.[55] The oxidation peaks in the anodic scans up to 1 V of these polymers were absent, because metal oxidation is extremely difficult to be observed for the d^{10} zinc( ) ion species.[58-60] The lowest unoccupied molecular level (LUMO) energy levels were estimated from reduction potentials

by the reference energy level of ferrocene (4.8 eV below the vacuum level) according to the following equation:[14] $E^{LUMO} = [-(E^{onset} - 0.45) - 4.8]$ eV. However, the oxidation potentials of all polymers were not detectable, so the highest occupied molecular level (HOMO) energy levels can be estimated by adding LUMO energy levels and optical band gaps. The optical band gaps were estimated from absorption spectra in DMF solution by extrapolating the tails of the lowest energy peaks. The optical band gaps of these polymers (**P1-P3**) were ranged from 3.13 to 3.15 eV.[53c,55] Since polymers **P1-P3** possess similar backbone structures, there are no obvious changes in the optical band gaps.

Solutions of monomers **4a**-**4b** (10 % weight ratio) in NMP with viscosity = 6 cp at 25 were used as references for determination the viscosities of polymers. In comparison with the viscosity values of monomers **4a**-**4b**, polymers **P1-P3** exhibit increased viscosity values (viscosity = 9-10 cp) by adding Zn^{2+} ions, and the relative viscosity of polymers to monomers were in the range of 1.5-1.66. The similar phenomenon was also reported by Gordaninejad et al.[61]

Table 2.1 Physical Properties of Polymers (**P1-P3**)

Polymers	$(cp)^a$	T_d $(\ )^b$	$E^{red/peak}$ $(V)^c$	E^{LUMO} $(eV)^d$	Band Gap $(eV)^e$
P1	9	422	-1.58 (r)	-2.89	3.15
P2	10	399	-1.53 (r)	-2.85	3.14
P3	10	368	-1.55 (r)	-2.88	3.15

[a] Solutions of monomers **4a** and **4b** (10 % in weight) in NMP (with viscosity = 6 cp, 25) were used as references for determination the viscosity of polymers.

[b] Decomposition temperatures (T_d) (5% weight loss) were determined by TGA with a heating rate of 20 min^{-1} under N_2 atmosphere.

[c] Reduction peak in N_2-purged DMF, r in parentheses means reversible.

[d] LUMO energy level was calculated from the measured reduction potential versus ferrocene/ferrocenium couple in DMF.

[e] Optical band gaps were estimated from the absorption spectra in solutions by extrapolating the tails of the lower energy peaks.
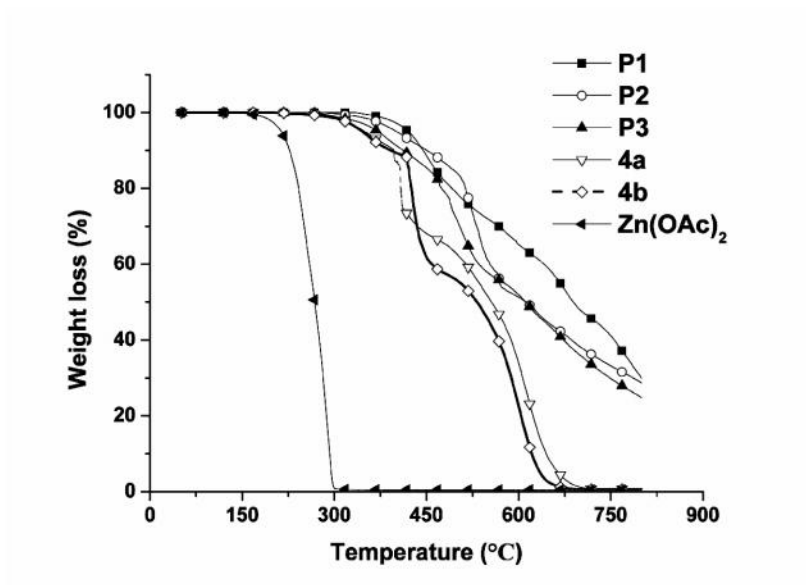
Figure 2.2 TGA thermograms of monomers **4a-4b**, Zn(OAc)$_2$, and polymers **P1-P3** upon

heating to 800   under nitrogen.

2.4.4 UV-vis and Photoluminescence Titration.

In order to further characterize homopolymers **P1-P2** and complex **5**, UV-vis titration

experiments were also carried out to confirm their supramolecular structures. Upon addition

of Zn^{2+} to monomer **4a** reaching a ratio of 1:1 (Zn^{+2}:**4a**) as shown in Figure 2.3, the spectra

revealed a shift of three other absorption bands at 357, 364, and 402 nm along with one

isosbestic point, which suggests that an equilibrium occurred between a finite number of

spectroscopically distinct species. The titration curves (Figure 2.3, inset) showed a linear

increase and a sharp end point at the ratio of 1:1 (Zn^{+2}:**4a**), indicating the formation of

metallo-polymers.
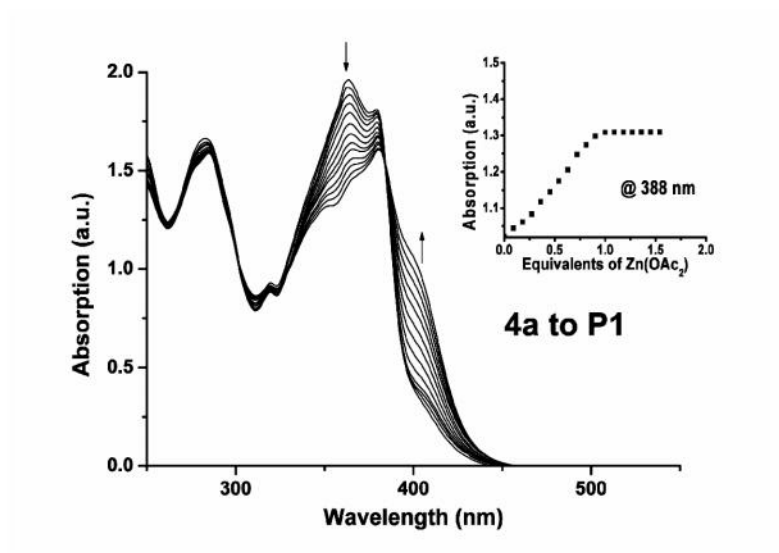
Figure 2.3 UV-vis spectra acquired (in the process of **4a** to **P1**) upon the titration of monomer **4a** in $CH_3CN/CHCl_3$ (2/8 in vol.) with $Zn(OAc)_2$. The spectra are shown at selected Zn^{+2}:**4a** ratios ranging from 0 to 1. The inset shows the normalized absorption at 388 nm as a function of Zn^{+2}:**4a** ratio.

Beyond this point (Figure 2.4), the subsequent addition of Zn^{2+} induced new peaks at 275, 349, and 388 nm as well as new isosbestic points to form, which points out that another new equilibration arose between a different set of spectroscopically distinct species. Thus, as the ratio of Zn^{2+} to monomer **4a** is above 1:1, depolymerization driven by the formation of chain-terminating complex **5** will occur.[54a,62] Figure 2.5 depicts that upon addition of Zn^{2+} to monomer **4b** to reach a ratio of 1:1 (Zn^{+2}:**4b**), and the insets spectra also revealed the same results as Figure 2.3.
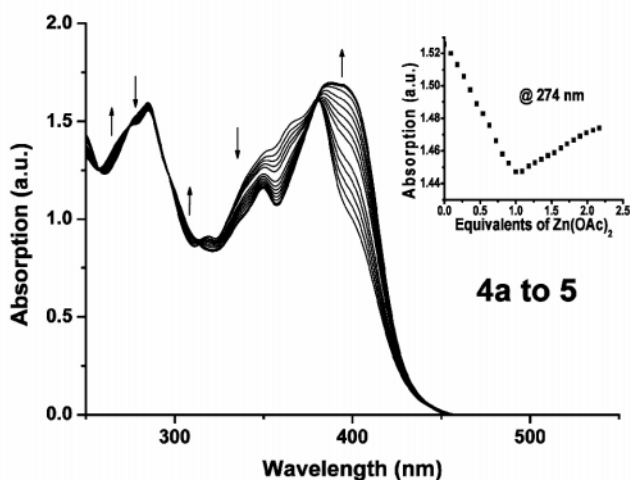
Figure 2.4 UV-vis spectra acquired (in the process of **4a** to **5**) upon the titration of monomer **4a** in CH$_3$CN/CHCl$_3$ (2/8 in vol.) with Zn(OAc)$_2$. The spectra are shown at selected Zn^{+2}:**4a** ratios ranging from 1 to 2. The insert shows the normalized absorption at 274 nm as a function of Zn^{+2}:**4a** ratio.
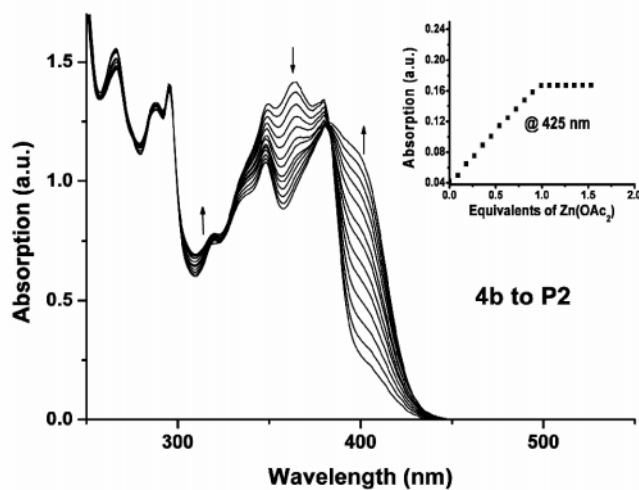
Figure 2.5 UV-vis spectra acquired (in the process of **4b** to **P2**) upon the titration of monomer **4b** in CH$_3$CN/CHCl$_3$ (2/8 in vol.) with Zn(OAc)$_2$. The spectra are shown at selected Zn^{+2}:**4b** ratios ranging from 0 to 1. The insert shows the normalized absorption at 425 nm as a function of Zn^{+2}:**4b** ratio.

All polymers displayed a shoulder near the lowest energy absorption (around $_{Abs}$ = 400 nm) which corresponds to a charge transfer occurring between the electron-rich central fluorenyl components and the electron-deficient metal-coordinated terpyridyl moieties.[62] The

complexation also can be followed by a photoluminescence (PL) titration experiment to further investigate PL properties of homopolymers **P1** and **P2**. In Figure 2.6, monomer **4a** showed two emission bands around 399 and 418 nm. As the ratio of Zn^{+2}: **4a** reached 1:1, a new emission band at 457 nm was induced. The PL quantum yields of medium complexes (the ratio of Zn^{+2}: **4a** gradually approaching 1:1 in inserts of Figure 2.6) were marginally enhanced and followed by increasing the molar ratio of Zn^{+2} ions.
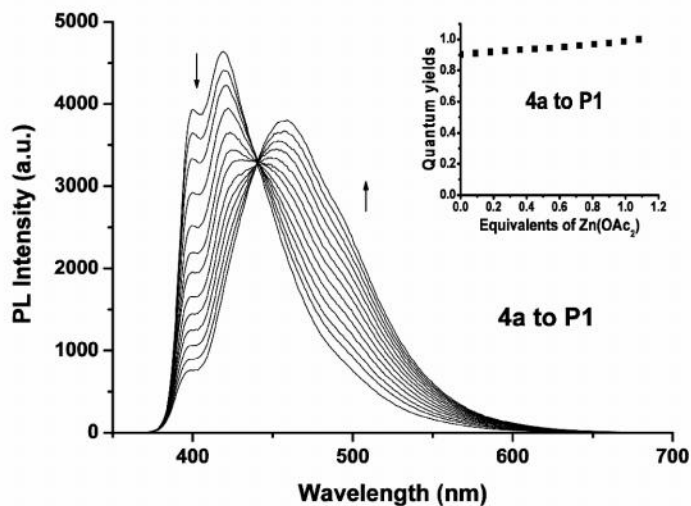
Figure 2.6 PL spectra acquired (in the process of **4a** to **P1**) upon the titration of monomer **4a** in $CH_3CN/CHCl_3$ (2/8 in vol.) with $Zn(OAc)_2$. The spectra are shown at selected Zn^{+2}:**4a** ratios ranging from 0 to 1. The insert shows the quantum yields as a function of Zn^{+2}:**4a** ratio.

Monomer **4b** also showed the same emission band as **4a** (shown in Figure 2.7). As an end point of titration was reached, polymer **P2** displayed a significant decrease in PL quantum yield of medium complexes (the ratio of Zn^{+2}: **4b** gradually approaching 1:1 in inserts of Figure 2.7) and a new weak emission band was observed at 558 nm. Due to different pendent groups attached to monomer ligands **4a** (with alkyl pendants) and **4b** (with carbazole pendants), metallo-polymer **P1** exhibited a little higher PL quantum yield than its corresponding monomer **4a**, but metallo-polymer **P2** displayed a much lower PL quantum yield than its corresponding monomer **4b**. Therefore, the PL quantum yields of

metallo-polymers can be sufficiently controlled by attaching different pendent groups to monomer ligands.
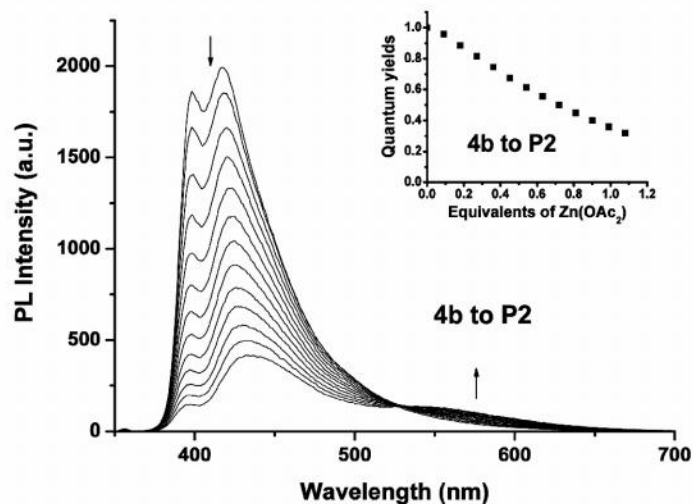
Figure 2.7 PL spectra acquired (in the process of **4b** to **P2**) upon the titration of monomer **4b** in $CH_3CN/CHCl_3$ (2/8 in vol.) with $Zn(OAc)_2$. The spectra are shown at selected Zn^{+2}:**4b** ratios ranging from 0 to 1. The insert shows the quantum yields as a function of Zn^{+2}:**4b** ratio.

2.4.5 Photophysical Properties.

The photophysical characteristics of polymers **P1-P3** were measured by UV-vis absorption and PL spectra in both dilute DMF (*N,N*-dimethylformamide) solutions and solid films, and their photophysical properties are summarized in Table 2.2.

Table 2.2 Photophysical Properties of Polymers (**P1-P3**)

Polymer	$\lambda_{Abs,sol}$ (nm)^a	$\lambda_{max,PL,sol}$/ $\Phi_{PL,sol}$ (nm)^{a,b,c}	$\lambda_{Abs,film}$ (nm)	$\lambda_{max,PL,film}$ (nm)
P1	285, 319, 365, 376	418/0.23	289, 338, 353, 400	513
P2	288, 293, 320, 348, 362, 377	420/0.11	289, 295, 335, 399	457 (547)
P3	286, 293, 319, 362, 376	418/0.18	289, 298, 337, 399	459 (527)

^{a} Concentration of 1×10^{-6} M in DMF.

^{b} Coumarin-1 in ethanol (ca. 5×10^{-6} M, quantum yield = 0.73) used as a reference for determination the quantum yields of PL in solutions. The PL quantum yields (in solutions) of monomers **4a** and **4b** are 0.20 and 0.25, respectively.

^{c} PL emission shoulders are shown in the parentheses.

In Figure 2.8, similar absorption features were observed in DMF solutions of polymers **P1-P3**, where the values of λ_{Abs} are around 285, 319, 360, and 378 nm. Interestingly, polymers **P2** and **P3** showed an additional absorption band at λ_{Abs} = 294 nm, which is associated with carbazole moieties. PL emissions of all polymers are assigned to intra-ligand (π^*-π) fluorescence. They showed purple-blue colors in DMF solutions, where the values of $\lambda_{max,PL}$ were around 420 nm, and the quantum yields (Φ) were 23 %, 11 %, and 18 % for polymers **P1**, **P2**, and **P3**, respectively (see Table 2.2). Since polymer **P1** (with alkyl pendants) has a higher quantum yield than its monomer **4a** (Φ = 0.20) and polymer **P2** (with carbazole pendants) has a lower quantum yield than its monomer **4b** (Φ = 0.25), it is reasonable to observe that metallo-*alt*-copolymer **P3** has a medium quantum yield value (Φ = 0.18) between **P1** (Φ = 0.23) and **P2** (Φ = 0.11). These trends fit well to their quantum yield changes of PL titration experiments (as shown in the inserts of Figures 2.6-2.7). Hence, carbazole pendants are detrimental to the PL quantum yields of metallo-polymers. However, for monomer ligands, **4b** with carbazole pendants (Φ = 0.25) has a higher PL quantum yield than **4a** with alkyl pendants (Φ = 0.20), so it did not have the same effect on the PL quantum yields of the monomers.
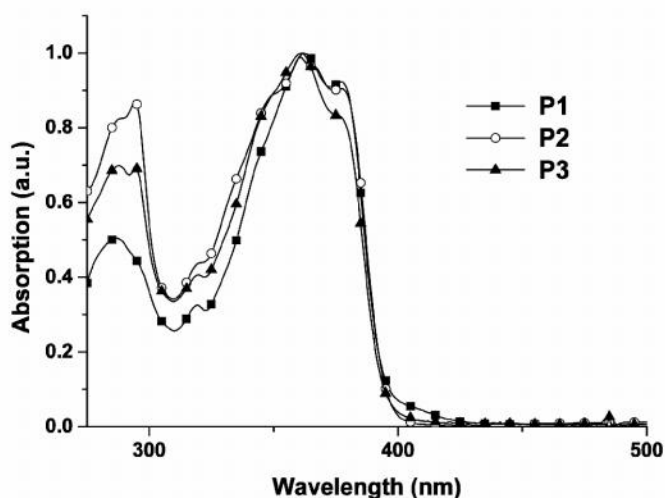
Figure 2.8 UV-vis spectra of metallo-polymers **P1-P3** in DMF solutions.

Moreover, solid films of these polymers emitted blue to green lights with values of $_{max,PL}$ ranging at 456-514 nm (Figure 2.9). From PL emissions of polymer films, polymer **P1** showed the largest Stokes shift (ca. 98 nm), which was attributed to the excimer formation resulting from - stacking of aromatic interaction in the solid state.[62-64] On the other hand, both polymers **P2** and **P3** showed weaker excimer emission bands (around 513 nm) than polymer **P1**, which indicate that the incorporation of carbazole pedants attached to the C-9 position of fluorene by long alkyl spacers can suppress the excimer formation.
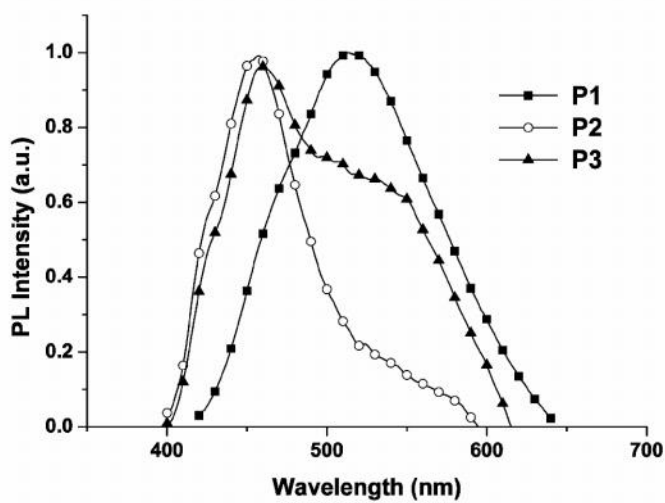
Figure 2.9 PL spectra of metallo-polymers **P1-P3** in solid films.

2.4.6 Electroluminescence Properties.

Polymers **P1-P3** were fabricated into four-layer PLED devices, respectively, with a configuration of ITO/PEDOT:PSS(40-50 nm)/polymer (**P1-P3**) (50-60 nm)/BCP(10 nm)/Alq$_3$(30 nm)/LiF(1 nm)/Al(150 nm) using standard procedures of spin-coating and vacuum deposition methods, where polymers **P1-P3** were used as the emission layer and PEDOT: PSS as the hole transporter. Besides, either BCP or ALQ was used as an electron transporter.[63c] The EL properties are listed in Table 2.3.

Table 2.3 Electroluminescence (EL) Properties of PLED Devices[a] Containing an Emitting

Layer of Polymer (**P1-P3**)

Polymers	max,EL (nm)	V_{on} (V)[b]	Max.Luminescence (cd/m^2) (V)	Power Efficiency (cd /A^{-1})[c]	CIE Coordinates (x and y)
P1	551	6.0	1704 (14.5)	0.85	(0.41, 0.52)
P2	549	6.5	2819 (15)	1.11	(0.41, 0.53)
P3	550	6.0	2640(15)	1.10	(0.41, 0.52)

[a] Device structure: ITO/PEDOT:PSS/polymer(**P1-P3**)/BCP/ Alq$_3$/LiF/Al, where the polymer (**P1-P3**) is an
emitting layer.

[b] V_{on} is the turn-on voltage.　[c] Power efficiencies were obtained at 100 mA/cm^2.

At a bias voltage of 10 V, all PLED devices showed green emissions with max,EL around 550 (as shown in Figure 2.10) and its EL intensity was enhanced by increasing the bias voltage. The turn-on voltage of these PLED devices were about 6.0 V, and their maximum efficiencies and luminances were 0.85-1.1 cd A^{-1} (at 100 mA cm^{-2}) and 1704-2640 cd m^{-2} (at around 15 V), respectively. Comparing the results of the maximum efficiency and luminance for each device, we can conclude that the incorporation of hole-transporting carbazole units into polymers as pendants will improve the EL performance of the PLED devices.[65,66] It is worthy noting that the EL spectra of these devices did not resemble their corresponding PL spectra in solid films. This is presumably due to the EL and PL emissions originating from different excited states and/or ground states.[55,63c] Figure 2.11 depicts the current

density-voltage-luminance (I-L-V) characteristic curves of polymers **P1-P3**, and similar turn-on voltages for both of the current density and luminance illustrated that a matched balance of both injection and transportation in charges was achieved.[67]
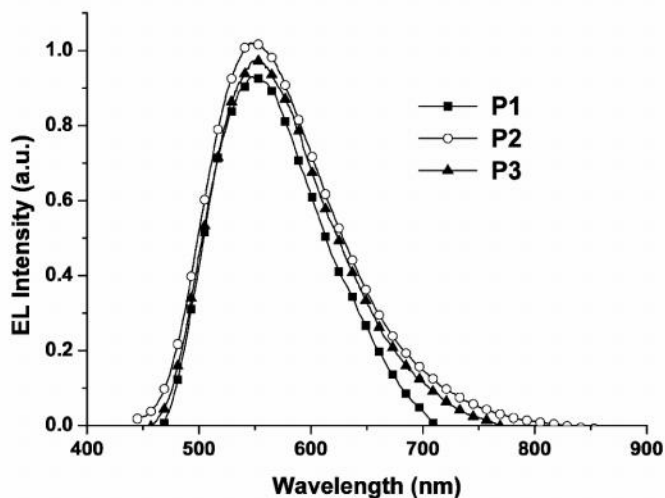
Figure 2.10 EL spectra of PLED devices with the configuration of ITO/PEDOT:PSS/polymer (**P1-P3**)/BCP/Alq$_3$ /LiF /Al
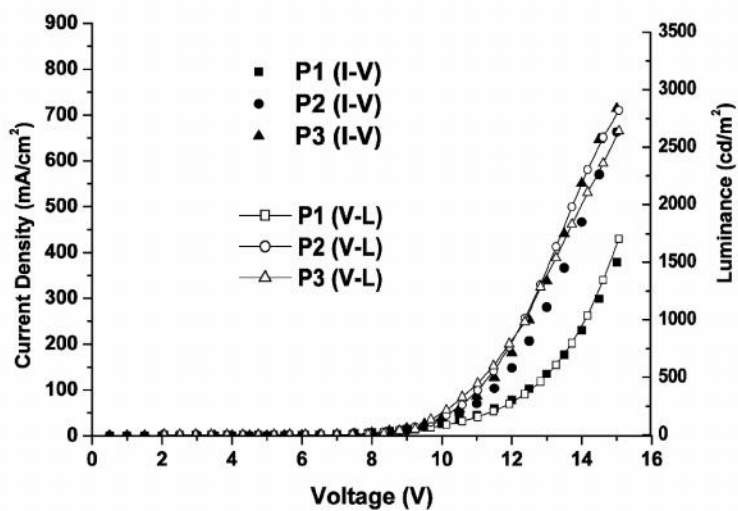
Figure 2.11 Current-voltage-–luminance (I-V-L) characteristics of PLED devices with the configuration of ITO/PEDOT:PSS/polymer (**P1-P3**)/BCP/Alq$_3$/LiF/Al.

2.5 Conclusion

In summary, a logical synthetic protocol for the synthesis of back-to-back bis-terpyridyl-based monomers is presented and novel metallo-supramolecular polymers, including metallo-homopolymers and metallo-*alternating*-copolymer were developed with proper stoichiometric ratios of monomer ligands and ions by self-assembled reactions. Furthermore, the photophysical and electroluminescent properties are greatly affected by the nature of the pendent groups of the coordination polymers. The incorporation of carbazole pendants into polymer side-chains reveals that the formation of excimers was suppressed and both PL and EL properties were enhanced. With finely tuned structures incorporating with coordination chemistry, metallo-polymers can provide a new entry to the development of polymeric materials for PLEDs.

Chapter 3

Synthesis and Characterization of Light-Emitting Main-Chain Metallo-Polymers Containing Bis-terpyridyl Ligands with Various Lateral Substituents

3.1 Abstract

A series of conjugated monomers (**5a-5d**) with various lateral substituents were symmetrically synthesized by the Sonogashira coupling reaction, in which central aromatic units (i.e., 9,9-dipropylfluorenes) were linked to 2,2':6',2''-terpyridyl (tpy) units via phenylene/ethynylene fragments. These light-emitting monomers were further reacted with zinc(II) ions and subsequently anion exchanged to produce supramolecular main-chain metallo-polymers (**6a-6d**). The formation of polymers **6a-6d** was confirmed by the increased viscosities (up to 1.5-1.83 times) relative to those of their analogous monomers. The results of ^{1}H NMR titration and UV-vis spectral titration revealed a detailed complexation process of metallo-polymers by varying the molar ratios of zinc(II) ions to monomers. After coordination with zinc(II) ions, the luminescent and thermal properties of the polymers were enhanced by the formation of metallo-supramolecular structures in contrast to their monomer counterparts. PLED devices employing these metallo-polymers as emitters gave yellow to orange electroluminescence (EL) emissions with turn-on voltages around 6 V. The maximum power efficiency, external quantum yield, and brightness of the PLED device containing polymer **6c** were 0.33 cd A^{-1} (at 14 V), 1.02%, and 931 cd m^{-2} (at 14 V), respectively.

3.2 Introduction

Many different coordination polymers with bipyridyl or terpyridyl backbones have been investigated over last few decades while searching for new smart materials.[68-79] Especially, the interest regarding 2,2':6',2"-terpyridyl (tpy) units has increased, because tpy units have very high bonding affinities towards transition metal ions due to the chelating effect and d p * back bonding of metals to the pyridyl rings.[80] Upon addition of proper metal ions, metallo-polymers can be built from the bifunctional monomers containing bis-tpy moieties. The general concept of functionalized bis-tpy telechelics to give coordination metallo-polymers was presented in 1995.[13] It was proven that metallo-polymers generated by complexation of two tpy units with transition metal ions gave octahedral coordination geometries,[22] and possessed distinct photophysical, electrochemical, and magnetic properties.[23]

Using zinc(II) ions as templates to assemble organic building blocks into polymer chains through complexation of tpy units is an appealing strategy for the construction of photoluminescent (PL) or electroluminescent (EL) metallo-polymers with well-defined structures.[55,81-83] Lately, Dobrawa and Würthner reported that metallo-polymers containing perylene bisimide dyes bearing (tpy)zinc(II) moieties showed high quantum yields and strong red emissions in PL.[54b] According to Che and co-workers' report, the incorporations of (tpy)zinc(II) moieties into different main-chain structures exhibited different emission colors ranging from violet to yellow with high PL quantum yields and EL performance.[55a] Moreover, the well-defined light-emitting metallo-*alt*-copolymer containing terpyridyl zinc(II) moieties has been reported by us recently.[55a,84]

It is confirmed that the phenomenon of metal to ligand charge transfer (MLCT) does not occur in (tpy)zinc(II) complexes due to the d^{10} zinc(II) species, so only intraligand charge transfer (ILCT) happens between (tpy)zinc(II) coordination sites and chromophores even in fully conjugated metallo-polymers.[54] Therefore, the incorporation of (tpy)zinc(II) moieties

into the metallo-polymers with fine-tuned chromophores can provide good quantum yields[54b,55a] and thermal stabilities[55a], and thus to have the potential to become high-performance emissive or host materials in PLED applications.

Herein, the syntheses of conjugated bis-tpy monomers containing identical chelating functions, which were linked to 9,9-dipropylfluorene units via phenylene/ethynylene fragments, and self-assembled processes of bis-tpy monomers with zinc(II) ions to afford (tpy)zinc(II) metallo-polymers are presented. In addition, the PL, thermal, electrochemical, and EL properties will be reported as well.

3.3 Experiment

3.3.1 Measurements

^{1}H NMR spectra were recorded on a Varian unity 300M Hz spectrometer using CDCl$_3$ solvents. Elemental analyses were performed on a HERAEUS CHN-OS RAPID elemental analyzer. Transition temperatures were determined by differential scanning calorimetry (Perkin Elmer Pyris 7) at a heating and cooling rate of 10 °C/min. Thermogravimetric analysis (TGA) was conducted on a Du Pont Thermal Analyst 2100 system with a TGA 2950 thermogravimetric analyzer at a heating rate of 20°C/min under nitrogen. Viscosity measurements were proceeded by comparing polymer solutions (10 % weight ratio in NMP) with the corresponding monomer solutions in the same condition (with viscosity = 6 cp) on a BROOKFILEL DV-Ⅲ+ RHEOMETER system at 25 °C (100 RPM, Spindle number: 4). UV-visible (UV-vis) titration experiments were preformed by that 1.0×10^{-5} M monomer solutions in the solvent of CH$_3$CN/CHCl$_3$ (2/8 in vol.) were titrated with 50 µl aliquots of 3.9×10^{-4} M Zn(OAc)$_2$ solutions in the solvent with the same composition. UV-vis absorption spectra were recorded in dilute DMF solutions (10^{-5} M) on a HP G1103A spectrophotometer, and fluorescence spectra were obtained on a Hitachi F-4500 spectrophotometer. Fluorescence quantum yields in solutions were determined relative to the integrated photoluminescence (PL) density of quinine sulfate in 1 N sulfuric acid with a known quantum yield (ca. 5×10^{-5} M, quantum yield = 0.55) in solutions. Cyclic voltammetry (CV) was performed at a scanning rate of 100 mV/s on a BAS 100 B/W electrochemical analyzer, which was equipped with a three-electrode cell. Pt wire was used as a counter electrode, and an Ag/AgCl electrode was used as a reference electrode in the CV measurements. The polymer thin films were cast onto a Pt disc as a working electrode with ferrocene as a standard in acetonitrile, and 0.1 M tetrabutylammonium hexafluorophosphate (TBAPF$_6$) was used as a supporting electrolyte. Polymer thin films were spin-coated on a quartz substrate from DMF solutions with a concentration of 10 mg/ml. A series of double-layer EL

devices with the configuration of ITO/PEDOT:PPS/Polymer/LiF/Al were made. The solutions (10 mg/ml) of light-emitting materials in DMF were spin-coated on glass slides precoated with indium tin oxide (ITO) having sheet resistances of ~20 /square and an effective device area of 3.14 mm^2. The ITO glasses were routinely cleaned by ultrasonic treatment in detergent solutions and diluted water, followed by through rinsing in acetone and then ethanol. After drying, the ITO glasses were kept in oxygen plasma for 4 min before being loaded into the vacuum chamber. The spin coating rate was 6000 rpm for 60 s with PEDOT:PPS, 3000 rpm for 60 s with polymers, and the thicknesses of polymers were about 47-70 nm. One thin layer of LiF (1 nm) was deposited thermally as a cathode at a rate of 0.1-0.2 Å/s under a pressure of ~2x10^{-5} torr in an Ulvac Cryogenic deposition system, which was capped with 150 nm of aluminum. The current-voltage-luminescence properties were measured in ambient conditions with a Keithley 2400 Source meter and a Newport 1835C Optical meter equipped with an 818ST silicon photodiode.
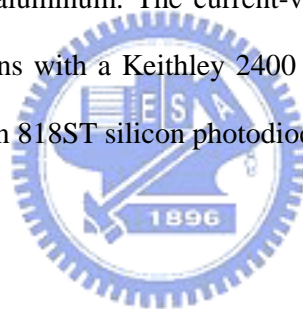
3.3.2 Materials

Chemicals and solvents were reagent grades and purchased from Aldrich, ACROS, TCI, and Lancaster Chemical Co. Solvents were purified and dried according to standard procedures. Chromatography was performed with Merck silica gel (mesh 70-230) and basic alumina oxide, which was deactivated with 4 wt% of water. The synthetic routes of bis-2,2':6',2''-terpyridyl monomers (**5a-5d**) and metallo-polymers (**6a-6d**) are illustrated in Scheme 3.1.

2,7-Diethynyl-9,9-dipropylfluorene (1). Compound **1**[85] and starting materials **2a-2d**, i.e., 1,4-dibromo-2,5-dimethoxybenzene,[86] 1-bromo-4-iodo-2,5-disubstitutentbenzene,[87] and 4'[[(trifluoromethyl)sulfonyl]oxy]-2,2':6',6''-terpyridines,[56b] were prepared and purified according to the literature procedures. Triethylamine and diisopropylamine were dried over suitable reagents and freshly distilled under nitrogen before using Schlenk tube

techniques.[56b]

1-Bromo-4(3-hydroxy-3-methylbutynyl)benzene (2a). To a solution of 1-bromo-4-iodobenzene (8 g, 28 mmol) in 60 mL of THF/Et$_3$N (2/1), 3-methyl-1-butyn-3-ol (2.76 ml, 27 mmol) was added. After the solution was degassed with nitrogen for 30 min, Pd(PPh$_3$)$_2$Cl$_2$ (0.19 g, 0.28 mol), PPh$_3$ (2.9 g, 11 mol), and CuI (0.53 g, 2.8 mol) were added. The reaction was then refluxed at 70 under N$_2$ for 12 h. The solvent was removed under reduced pressure. The resulting solid was extracted with CH$_2$Cl$_2$/H$_2$O then dried over MgSO$_4$. The crude product was purified by column chromatography (silica gel, hexane/ethyl acetate = 4/1) to afford a white solid (4.65 g). ^{1}H NMR (300 MHz, CDCl$_3$): 7.44 (d, $J = 7.5$ Hz, 2H), 7.28 (d, $J = 7.2$ Hz, 2H), 2.03 (s, 1H), 1.61 (s, 6H). Yield: 75%. FABMS: m/e 238; C$_{11}$H$_{11}$BrO requires m/e 238.10.

1-Bromo-2,5-dimethyl-4(3-hydroxy-3-methylbutynyl)benzene (2b). The procedure is analogous to that described for **(2a)**. Yield: 78%. ^{1}H NMR (300 MHz, CDCl$_3$): 7.37 (s, 1H), 7.24 (s, 1H), 2.49 (s, 3H), 2.38 (s, 3H), 2.04 (s, 1H), 1.63 (s, 6H). FABMS: m/e 266; C$_{13}$H$_{15}$BrO requires m/e 266.15.

1-Bromo-2,5-dimethoxyl-4(3-hydroxy-3-methylbutynyl)benzene (2c). The procedure is analogous to that described for **(2a)**. Yield: 74%. ^{1}H NMR (300 MHz, CDCl$_3$): 7.06 (s, 1H), 6.91 (s, 1H), 3.84 (s, 3H), 3.82 (s, 3H), 2.67 (s, 1H), 1.64 (s, 6H). FABMS: m/e 298; C$_{13}$H$_{15}$BrO$_3$ requires m/e 298.15.

1-Bromo-2,5-difluoro -4(3-hydroxy-3-methylbutynyl)benzene (2d). The procedure is analogous to that described for **(2a)**. Yield: 67%. ^{1}H NMR (300 MHz, CDCl$_3$): 7.27 (dd, $J_1 = 5.7$ Hz, $J_2 = 5.7$ Hz, 1H), 7.13 (dd, $J_1 = 6$ Hz, $J_2 = 6$ Hz, 1H), 2.10 (s, 1H), 1.60 (s, 6H). FABMS: m/e 274; C$_{11}$H$_9$BrF$_2$O requires m/e 273.98.

2,7-Bis[(3-hydroxy-3-methylbutynyl)-phenylethynyl]-9,9-dipropylfluorene (3a). A mixture of 2,7-diethynyl-9,9-dipropylfluorene (0.71 g, 2.38 mmol) and **(2a)** (1.31 g, 5.9 mmol) was dissolved in 60 mL of Et$_3$N/THF. After the solution was degassed with N$_2$ for 30

min, Pd(PPh$_3$)$_2$Cl$_2$ (20 mg, 0.024 mol), PPh$_3$ (250 g, 0.95 mmol), and CuI (47 mg, 0.24 mmol) were added with mechanical stirring. The reaction was then refluxed at 80 under N$_2$ over 24 h. The solvent was removed under reduced pressure. The resulting solid was extracted with CH$_2$Cl$_2$/H$_2$O then dried over MgSO$_4$. The crude product was purified by column chromatography (silica gel, hexane/dichloromethane = 4/1) to afford a yellow solid (1.1 g). ^{1}H NMR (300 MHz, CDCl$_3$): 7.70 (d, J = 8.1 Hz, 2H), 7.51-7.56 (m, 8H), 7.42-7.45 (m, 4H), 2.05 (s, 2H), 1.99 (br, 4H), 1.65 (s, 12H), 0.69 (br, 10H). Yield: 79%. FABMS: m/e 615; C$_{45}$H$_{42}$O$_2$ requires m/e 614.81.

2,7-Bis[(3-hydroxy-3-methylbutynyl)-2,5-dimethy-phenylethynyl]-9,9-dipropyl fluorene (3b). The procedure is analogous to that described for **(3a)**. ^{1}H NMR (300 MHz, CDCl$_3$): 7.66 (d, J = 7.8 Hz, 2H), 7.52-7.48 (m, 4H), 7.37 (s, 2H), 7.28 (s, 2H), 2.49 (s, 6H), 2.38 (s, 6H), 2.03 (s, 2H), 1.98 (br, 4H), 1.65 (s, 12H), 0.69 (br, 10H). Yield: 78%. FABMS: m/e 671; C$_{49}$H$_{50}$O$_2$ requires m/e 670.92.

2,7-Bis[(3-hydroxy-3-methylbutynyl)-2,5-dimethoxy-phenylethynyl]-9,9-dipropyl fluorene (3c). The procedure is analogous to that described for **(3a)**. ^{1}H NMR (300 MHz, CDCl$_3$): 7.66 (d, J = 8.4 Hz, 2H), 7.56-7.54 (m, 4H), 7.04 (s, 2H), 6.94 (s, 2H), 3.92 (s, 6H), 3.87 (s, 6H), 2.13 (s, 2H), 1.96 (br, 4H), 1.66 (s, 12H), 0.69 (br, 10H). Yield: 82%. FABMS: m/e 735; C$_{49}$H$_{50}$O$_6$ requires m/e 734.92.

2,7-Bis[(3-hydroxy-3-methylbutynyl)-2,5-difluoro-phenylethynyl]-9,9-dipropyl fluorene (3d). The procedure is analogous to that described for **(3a)**. ^{1}H NMR (300 MHz, CDCl$_3$): 7.69 (d, J = 8.1 Hz, 2H), 7.56-7.53 (m, 4H), 7.24 (dd, J_1 = 8.7, J_2 = 6 Hz, 2H), 7.16 (dd, J_1 = 8.7, J_2 = 6 Hz, 2H), 2.09 (s, 2H), 1.98 (br, 4H), 1.64 (s, 12H), 0.68 (br, 10H). Yield: 75%. FABMS: m/e 687; C$_{45}$H$_{38}$F$_4$O$_2$ requires m/e 686.78.

2,7-Bis(phenylethynyl)-9,9-dipropylfluorene (4a). A mixture of **(3a)** (1 g, 1.63 mmol) and KOH (365 mg, 6.5 mmol) in 60 mL of toluene was refluxed under N$_2$ with a vigorous stirring for 3 h. The solvent was then removed and crude product was purified by column

chromatography (silica gel, hexane) to afford a white solid (6.1g). ^{1}H NMR (300 MHz, CDCl$_3$): 7.69 (d, J = 8.1 Hz, 2H), 7.56-7.49 (m, 12H), 3.20 (s, 2H), 1.99 (br, 4H), 0.69 (br, 10H). Yield: 76%. FABMS: m/e 499; C$_{39}$H$_{30}$ requires m/e 498.66.

2,7-Bis(2,5-dimethy-phenylethynyl)-9,9-dipropylfluorene (4b). The procedure is analogous to that described for **(4a)**. ^{1}H NMR (300 MHz, CDCl$_3$): 7.67 (d, J = 7.8.Hz, 2H), 7.53-7.49 (m, 4H), 7.39 (s, 2H), 7.35 (s, 2H), 3.34(s, 2H), 2.49 (s, 6H), 2.42 (s, 6H), 1.98 (br, 4H), 0.69 (br, 10H). Yield: 78%. FABMS: m/e 555; C$_{43}$H$_{38}$ requires m/e 554.76.

2,7-Bis(2,5-dimethoxy-phenylethynyl)-9,9-dipropylfluorene (4c). The procedure is analogous to that described for **(4a)**. ^{1}H NMR (300 MHz, CDCl$_3$): 7.67 (d, J = 8.4 Hz, 2H), 7.57-7.53 (m, 4H), 7.07 (s, 2H), 7.02 (s, 2H), 3.92 (s, 12H), 3.42 (s, 2H), 1.97 (br, 4H), 0.67 (br, 10H). Yield: 76%. FABMS: m/e 619; C$_{43}$H$_{38}$O$_4$ requires m/e 618.76.

2,7-bis(2,5-difluoro-phenylethynyl)-9,9-dipropylfluorene (4d). The procedure is analogous to that described for **(4a)**. ^{1}H NMR (300 MHz, CDCl$_3$): 7.79 (d, J = 87.5 Hz, 2H), 7.56-7.53 (m, 4H), 7.19-7.27 (m, 4H), 3.42 (s, 2H), 2.01 (br, 4H), 0.67 (br, 10H). Yield: 72%. FABMS: m/e 571; C$_{39}$H$_{26}$F$_4$ requires m/e 570.62.

Monomer 5a. Compound **4a** (250 mg, 0.5 mmol) and 4'-[[(trifluoromethyl)sulfonyl]oxy]-2,2':6',6''-terpyridine (420 g, 1.1 mmol) were dissolved in nitrogen-degassed benzene, then [Pd^0(PPh$_3$)$_4$] (70 mg, 0.06 mmol) was added and followed by nitrogen-degassed ^{i}Pr$_2$NH. The solution was then heated to 70 . After complete consumption of starting materials, the solvent was evaporated and the product was purified by column chromatography (alumina, hexane/dichloromethane = 10/1) to afford a yellow solid (393 mg). ^{1}H NMR (300 MHz, CDCl$_3$): 8.73 (d, J = 5.4 Hz, 4H), 8.59-8.65 (m, 8H), 7.89 (t, J = 7.2 Hz, 4H), 7.69 (d, J=7.5 Hz, 2H), 7.56-7.58 (m, 12H), 7.35-7.38 (m, 4H), 2.00 (br, 4H), 0.70 (br, 10H). Yield: 82%. FABMS: m/e 961; C$_{69}$H$_{48}$N$_6$ requires m/e 960.39. Anal. Calcd for C$_{69}$H$_{48}$N$_6$: C, 86.22; H, 5.03; N, 8.74. Found: C, 85.89; H, 4.99; N, 8.30.

Monomer 5b. The procedure is analogous to that described for monomer **5a**. ^{1}H NMR (300 MHz, CDCl$_3$): 8.76 (d, J = 5.4 Hz, 4H), 8.58-8.67 (m, 8H), 7.91 (t, J = 8.1 Hz, 4H), 7.69 (d, J=7.8 Hz, 2H), 7.53-7.56 (m, 4H), 7.45 (s, 4H), 7.37-7.41 (m, 4H), 2.55 (s, 12H), 2.01 (br, 4H), 0.71 (br, 10H). Yield: 74%. FABMS: m/e 1018; C$_{73}$H$_{56}$N$_6$ requires m/e 1017.27. Anal. Calcd for C$_{73}$H$_{56}$N$_6$: C, 86.19; H, 5.55; N, 8.26. Found: C, 85.77; H, 5.12; N, 8.12.

Monomer 5c. The procedure is analogous to that described for monomer **5a**. ^{1}H NMR (300 MHz, CDCl$_3$): 8.73 (d, J = 5.4 Hz, 4H), 8.62-8.65 (m, 8H), 7.88 (t, J = 7.5 Hz, 4H), 7.69 (d, J = 8.4 Hz, 2H), 7.56-7.59 (m, 4H), 7.34-7.38 (m, 4H), 7.10 (s, 4H), 3.97(s, 6H), 3.96 (s, 6H), 1.99 (br, 4H), 0.69 (br, 10H). Yield: 89%. FABMS: m/e 1082; C$_{73}$H$_{56}$N$_6$O$_4$ requires m/e 1081.26. Anal. Calcd for C$_{73}$H$_{56}$N$_6$O$_4$: C, 81.09; H, 5.22; N, 7.77. Found: C, 81.34; H, 5.23; N, 7.56.

Monomer 5d. The procedure is analogous to that described for monomer **5a**. ^{1}H NMR (300 MHz, CDCl$_3$): 8.73 (d, J = 4.8 Hz, 4H), 8.61-8.64 (m, 8H), 7.88 (t, J = 7.2 Hz, 4H), 7.69 (d, J = 7.8 Hz, 2H), 7.56-7.59 (m, 4H), 7.35-7.39 (m, 4H), 7.27-7.33 (m, 4H), 2.01 (br, 4H), 0.71 (br, 10H). Yield: 72%. FABMS: m/e 1034; C$_{69}$H$_{44}$F$_4$N$_6$ requires m/e 1033.12. Anal. Calcd for C$_{69}$H$_{44}$F$_4$N$_6$: C, 80.22; H, 4.29; N, 8.13. Found: C, 79.80; H, 4.16; N, 8.34.

Polymer 6a. To monomer **5a** (500 mg, 0.52 mmol) in 30 ml of N-methylpyrrolidinone (NMP) solution, zinc acetate (114.16 mg, 0.52 mmol) in NMP (10 ml), was added dropwise. The resulting solution was heated at 105   under a nitrogen atmosphere. After stirring for 24 h, excess KPF$_6$ was added into the hot solution. The resulting solution was poured into methanol and the precipitate obtained was purified by washing with acetone. The polymers were dried under vacuum at 40   for 24 h and collected as yellow solids. Yields: 77 to 82%.

Polymers 6b- 6d. The procedure is analogous to that described for polymer **6a**. Yields: 76 to 88%.

3.4 Result and Discussion

3.4.1 Synthesis and Characterization

The synthetic routes of the monomers (**5a-5d**) and metallo-polymers (**6a-6d**) are demonstrated in Scheme 3.1.

Scheme 3.1 Synthetic Routes of Monomers (**5a-5d**) and Polymers (**6a-6d**)
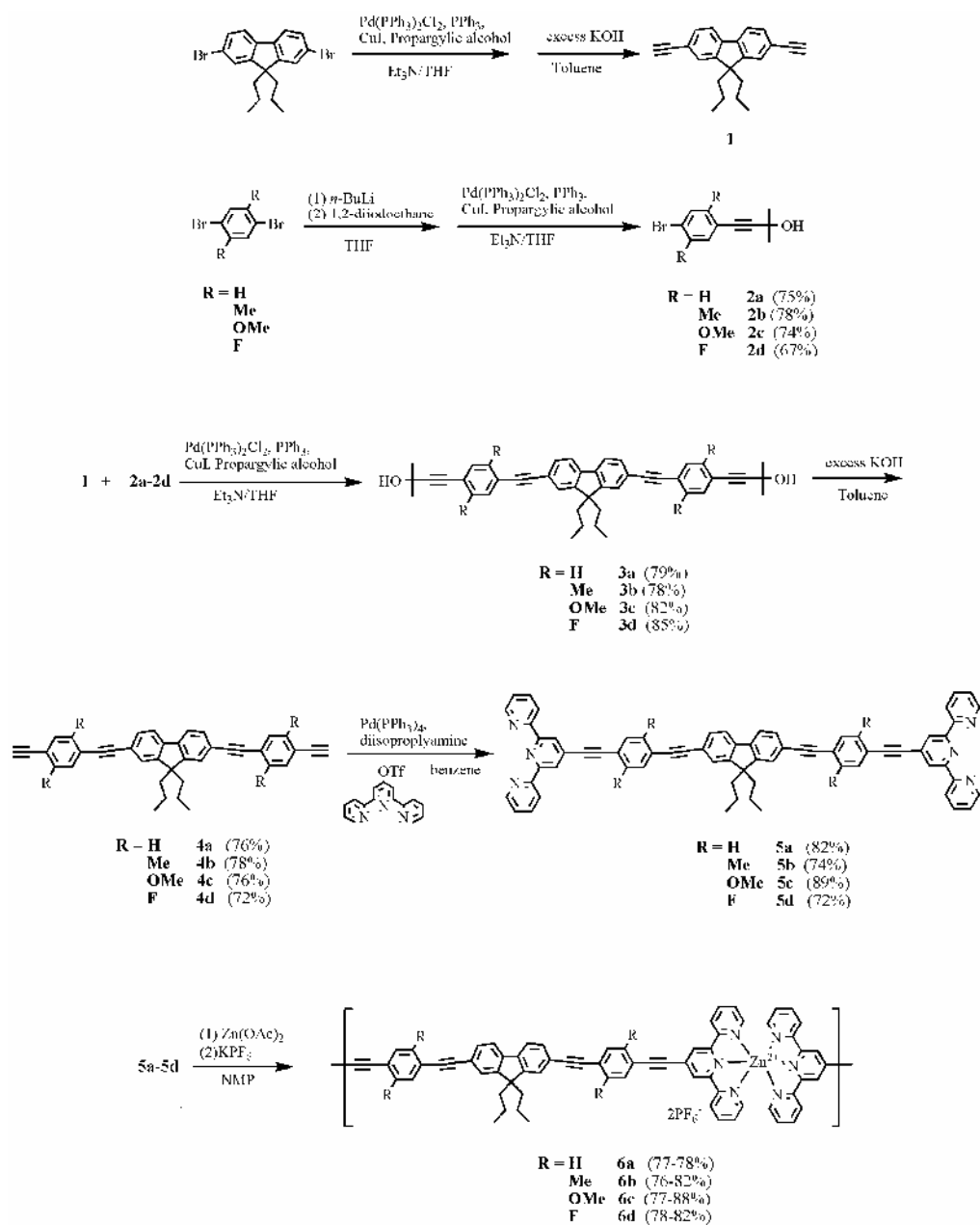
Compound **1** was synthesized by the reaction of 2,7-dibromo-9,9-dipropylfluorene with propargylic alcohol via the Sonogashira coupling reaction, and further deprotection by

refluxing toluene in a basic condition. To obtain a series of compounds **2a-2d** in good yields**,** it is necessary to convert bromine substitutents into iodine substitutents by metal–halogen exchange before proceeding the Pd catalyzed alkyne-aryl-coupling reaction selectively. Various combinations of compounds **3a-3d** allow the conjunction of compound **1** with compounds **2a-2d** in similar coupling reactions followed by deprotection under a basic condition, which led to compounds **4a-4d** bearing acetylene groups. To access a family of monomers, the monomer ligands **5a-5d** were prepared in 75% overall yields by cross-coupling reactions between **4a-4d** and 4'-[[(trifluoromethyl)sulfonyl]-oxy]-2,2':6',2''-terpyridine (tpy-OTf) in the presence of catalytic amounts of Pd(0) complexes under a basic condition.[56d] In fact, monomers **5a-5d** were readily prepared by Pd(0)-promoted reactions using appropriate solvents (benzene and toluene) and reaction time, which could produce the required products in excellent yields. Finally, meatllo-polymers **6a-6d** were synthesized by refluxing with zinc acetate in NMP solutions and followed by subsequent anion exchange. Yields of all polymers were up to 77-88% after repeated washing with acetone. In contrast to other polymerization methods, such as the Wittig or Heck coupling reaction, the present procedure does not need any catalyst.[88,89] The `reactive modulation` of zinc( ) ions and the stability of six-coordinate bis(tpy)zinc(II) moieties allow the self-assembled reaction to take place under mild conditions.

All pure monomers (**5a-5d**) are soluble in most chlorinated solvents and isolated as yellow powders, which were also characterized by ^{1}H NMR, mass spectrometry, UV-vis spectrometry, and elemental analysis. Compared with the monomers, the metallo-polymers (**6a-6d**) have less solubility due to the rigid linear cores of the polymers, which depends on the lateral sizes of substitutents attached to the phenylene rings, i.e., solubility: OMe (**6c**) > Me (**6b**) > F (**6d**) > H (**6a**). Moreover, these polymers are only soluble in some polar solvents, for instance DMSO, DMAc, and DMF.

3.4.2 ^{1}H NMR Titration

In order to confirm the formation of these metallo-polymers, ^{1}H NMR titration is an important tool for the analysis of self-assembled processes where the stoichiometries of the metal ions and monomer ligands need to be carefully controlled in a ratio of 1:1. The studies of ^{1}H NMR titration in Figure 3.1 were carried out by varying the molar ratios of zinc(II) ions to monomer **5c** in deuterated dimethylsulfoxide (DMSO-d_6). The addition of zinc(II) ions to monomer **5c** resulted in a number of dramatic shifts in ^{1}H signals around the aromatic regions. The ^{1}H signals of free monomer **5c** around 8.8 ~ 8.0 and 7.6 ppm belonged to tpy rings, and those (two peaks) around 7.4 ppm belong to *p*-dimethoxyphenylene rings. It is worthy noting that the ^{1}H signals of fluorene units are around 7.95 and 7.7 ppm. As the molar ratio of **5c**/Zn^{2+} = 1/0.2, these ^{1}H signals started to change and new signals around 8.9, 8.3, and 7.8 ppm became noted. When the ratio of **5c**/Zn^{2+} reaches 1/0.7, all signals belonging to tpy rings in free monomer **5c** were not observed, and the signals (two peaks around 7.4 ppm) of *p*-dimethoxyphenylene rings also altered to a single peak (except for that of the central fluorene rings). These phenomena originated from the electron-delocalized happened between zinc(II)-tpy complexs and central chromophore (fluorenyl/ethynylene/phenylene) components which induced the new ^{1}H signals raised in terpyridine units and the signals (two peaks around 7.4 ppm) of *p*-dimethoxyphenylene broaden and merged into a single peak. Furthermore, the conjugated distance between the tpy rings and the central fluorene rings (separated by a phenylene unit and two ethynylene bridges) which are long enough to avoid the influence of the coordination processes. Until the ratio of **5c**/Zn^{2+} reached 1/1, all variations in ^{1}H signals became saturated, and the solution remained clear and no precipitation or further aggregation was observed. Even after increasing the ratio of **5c**/Zn^{2+} up to 1/1.2, no further shifts and changes of ^{1}H signals were detected in the ^{1}H NMR spectrum. Therefore, the alteration of ^{1}H signals during NMR titration was attributed to the coordination process among the metal ions and tpy units.[54b]

Based on these data, the formation of all coordination polymers (**6a-6d**) containing monomers (**5a-5d**) can be concluded. Dobrawa, Würthner, and Che showed that the polymer formation can be controlled by the exact stoichiometric ratios of the metal ions to the monomer ligands.[54b,55a,84] Exceeding the stoichiometric ratio of **5c**/Zn^{2+} over 1/1.2, the tpy units and zinc(II) ions will be in an over-coordinated situation to cause incomplete polymer chains, which will not be further discussed in this study.
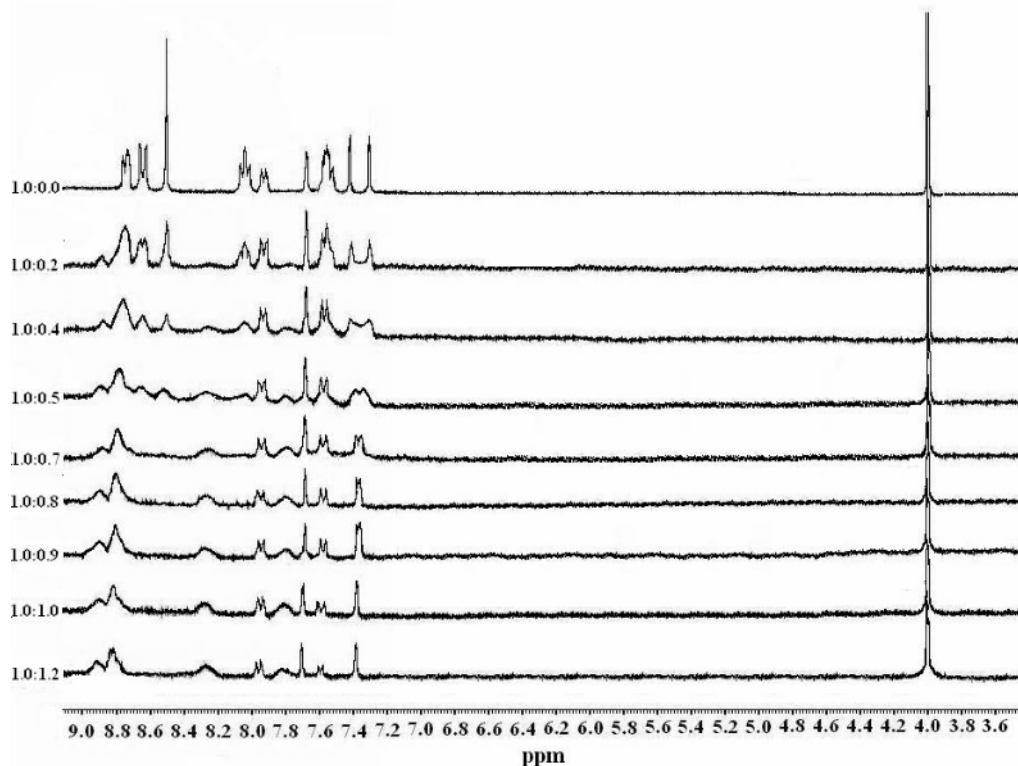
Figure 3.1 ^{1}H NMR spectra with different ratios (**5c:Zn^{2+}**) of monomer (**5c**) to metal ions (**Zn^{2+}**) in DMSO (5 mM) from free **5c** (top, **5c:Zn^{2+}** = 1:0) to polymer **6c** (next to bottom, **5c:Zn^{2+}** = 1:1).

3.4.3 UV-visible Titration

To further characterize metallo-polymers **6a-6d**, they were also confirmed by UV-vis titration experiments. Upon addition of Zn^{2+} to monomer **5c** reaching a ratio of 1:1 (Zn^{+2}:**5c**) as shown in Figure 3.2, the spectra revealed a shift of three other absorption bands at 284, 317, 343, and 405 nm along with one isosbestic point, which suggests that an equilibrium

occurred between a finite number of spectroscopically distinct species.
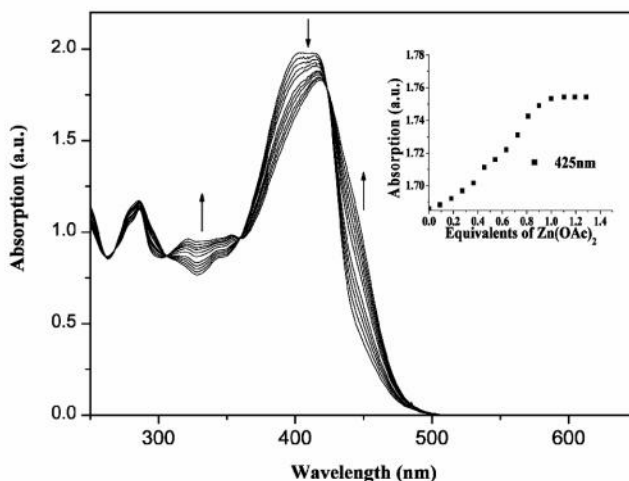
Figure 3.2 UV-vis spectra acquired upon the titration of monomer **5c** in CH$_3$CN/CHCl$_3$ (2/8 in vol.) with Zn(OAc)$_2$. The spectra are shown at selected Zn^{+2} : **5c** ratios ranging from 0 to 1. The inset shows the normalized absorption at 425 nm as a function of Zn^{+2} : **5c** ratio.

The titration curves (Figure 3.2, insets) showed a linear increase and a sharp end point at the ratio of 1:1 (Zn^{+2}:**5c**), indicating the formation of metallo-polymers. Furthermore, polymer **6c** displayed a shoulder in the lowest energy absorption at λ_{Abs} = 450 nm, which corresponded to a charge transfer occurring within the monomers between the electron rich central chromophore (fluorenyl/ethynylene/phenylene) components and the metal-coordinated (electron-deficient) terpyridyl moieties.[62]

3.4.4 Thermal Properties

The thermal properties of the monomers (**5a-5d**) and polymers (**6a-6d**) were studied by thermogravimetric analysis (TGA) and differential scanning calorimetry (DSC), as summarized in Table 3.1.

Table 3.1 Thermal Properties of Monomers (**5a-5d**) and Polymers (**6a-6d**)

Compound	$T_d{}^a$ ( )	$T_m/T_c{}^b$ ( )	$T_g{}^b$ ( )
5a	297	232/--	145
5b	311	254/--	149
5c	320	276/--	157
5d	351	294/145	197
6a	325	-- /-- ^{c}	-- ^{c}
6b	342	-- /-- ^{c}	-- ^{c}
6c	375	--/-- ^{c}	-- ^{c}
6d	410	--/-- ^{c}	-- ^{c}

^{a} T_d was determined by TGA with heating rates of 20 min^{-1} under N_2 atmosphere.

^{b} T_m (melting temperature), T_c (crystallization temperature) and T_g (glass transition temperature) were determined by DCS with heating/cooling rates of 10 under N_2 atmosphere.

^{c} The transition temperatures of T_m, T_c, and T_g in polymers were not found in DSC scans.

The decomposition temperatures (T_d) (5% weight loss measured by TGA) of the monomers under a nitrogen atmosphere ranged from 297 to 351 , and those of polymers ranged from 325 to 410 . The glass transition temperatures of the monomers were characterized by DSC. For instance, monomer **5c** obviously possesses T_g (~157) during the first cooling and second heating cycles. All monomers show high glass transition temperatures ($T_g >$ 145), which were affected by different lateral substituents (with different polarities and sizes) attached to the central conjugated structures. According to the glass transition temperatures of the monomers: **5d** (F) > **5c** (OMe) > **5b** (Me) > **5a** (H), it seems that the polarity effect (of the lateral substituents) is more influential than the size effect (of the lateral substituents) on the T_g values of the monomers. In addition, similar trends (i.e., the dipole moment effects of the lateral substituents) also occurred in the melting temperatures (T_m) and the decomposition temperatures (T_d) for both monomers and polymers, i.e. **5d** > **5c** > **5b** > **5a** and **6d** > **6c** > **6b** > **6a**. In general, the result of high T_g values in monomers can be attributed to the rigid and linear conformation of monomers. In comparison with monomers, the increases of the decomposition temperatures (T_d) of metallo-polymers **6a-6d** in Table 1 were observed and similar results in coordination polymers were reported in the literature.[78,81]

Owing to the coordination, it was found that 25-30 wt% of the residual materials were left upon heating polymers to 800   . Similar to another report,[63c] no phase transitions were observed in the DSC measurements of polymers **6a-6d**. However, as described in the elevation of decomposition temperatures (T_d) of polymers in contrast to monomers, the glass transition temperatures (T_g) of coordination polymers should be higher than those of monomeric counterparts.

3.4.5 Viscosity and Electrochemical Properties

The viscosity and electrochemical properties of the polymers (**6a-6d**) were studied by rheometer and cyclic voltammetry (CV), as summarized in Table 3.2. By adding Zn^{2+} ions into monomer solutions, the formation of metallo-polymers **6a-6d** was confirmed by the enhancement of the viscosities (up to 1.5-1.83 times) relative to those of their analogous monomers. Similar results have also been reported by Gordaninejad's group.[61]

To determine the energy band structures of PLED materials, it is necessary to measure the energy levels of the highest occupied molecular orbital (HOMO) and the lowest unoccupied molecular orbital (LUMO) of all light-emitting metallo-polymers **6a-6d**, which were carried out by cyclic voltammetry (CV) to investigate the oxidox/redox behavior of the polymer thin films and their electrochemical properties are summarized in Table 3.2.

Table 3.2 Electrochemical and Viscosity Properties of Polymers (**6a-6d**)

Polymers	η^a (cp)	$E_{1/2}$ (red)^b (V)	E_{onset} (red) (V)	LUMO^c (V)	Band Gap^d (V)
6a	9	-1.12(r), -2.13, -2.51, -2.64	-0.98	-3.32	3.00
6b	10	-1.13(r), -2.18, -2.57, -2.72	-0.95	-3.35	2.88
6c	11	-1.14(r), -2.26, -2.61, -2.82	-0.89	-3.41	2.78
6d	10	-1.18(r), -2.13, -2.39, -2.64	-0.99	-3.31	2.95

^{a} Monomers **5a**-**5d** dissolved in NMP (by 10 % weight ratio with viscosity η = 6 cp at 25 ℃) were used as a reference to determine the viscosities of the polymers.

^{b} Half-wave potential in N_2-purged acetonitrile, r in parentheses indicates a reversible process.

^{c} LUMO level was calculated from the measured reduction potential versus ferrocene/ ferrocenium couple in acetonitrile.

^{d} The optical band gaps were estimated from the absorption spectra in solid films by extrapolating the tails of the lower energy peaks.

All metallo-polymers (**6a-6d**) exhibit quasi-reversible reduction wave at $E_{1/2}$ value of -1.12 to -1.18 V in cathodic scans up to -3 V. The reduction waves of polymers **6a-6c** (in Figure 3.3) were attributed to the reduction of tpy units in metal complexes.[83] Other reduction processes take place at more negative potentials, but they are not well defined. The absence of oxidation process in these polymers was expected, because metal oxidation is extremely difficult to be observed for the d^{10} zinc(Ⅱ) ion species (the anodic sacns up to 1 V).[55a,59b] The LUMO levels estimated here are based on the reference energy level of ferrocene (4.8 eV below the vacuum level) according to the following equation:[56a] $E^{LUMO} = [-(E^{onset} - 0.50) - 4.8]$ eV. The optical band gaps were estimated from absorption spectra in solid films by extrapolating the tails of the lowest energy peaks. Moreover, the band gaps of polymers **6a** (3.0 eV) and **6d** (2.95 eV) were quite similar, and their films both showed green photoluminescence. Polymer **6c** had the smallest band gap (2.78 eV) and gave a yellow emission. [27,47]
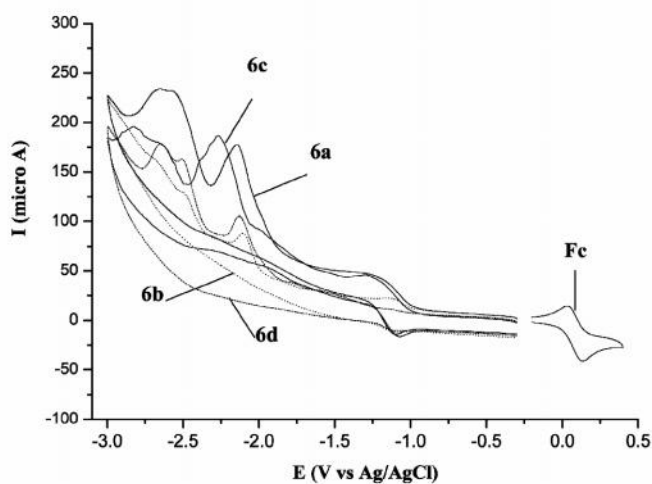
Figure 3.3 Cyclic voltammetry (CV) measurements of polymers **6a**-**6d** during the reduction processes.

3.4.6 Photophyscial Properties

In order to further investigate the photophyscial properties, the UV-vis absorption and PL spectra of the monomers (**5a-5d)** and polymers (**6a-6d)** in both solutions (DMF as solvent) and solid films were measured and summarized in Table 3.3.

Table 3.3 Photophyscial Properties of Monomers (**5a-5d)** and Polymers (**6a-6d**)

Compound	$\lambda_{max,Abs.,sol}$[a,b] (nm)	$\lambda_{max,PL,sol}/\Phi_{PL,sol}$[a,b,c] (nm)	$\lambda_{max,Abs.,film}$[d] (nm)	$\lambda_{max,PL,film}/\Phi_{PL,film}$[d,e] (nm)
5a	285,319,375	417(432)/0.27	286,318,374	495/-- [f]
5b	284,321,381	421(436)/0.18	285,322,380	507/-- [f]
5c	285,342,402(415)	440(460)/0.29	286,343,404	530/- - [f]
5d	284,322,382	444/0.21	285,321,383	494/-- [f]
6a	283,316,362	435/0.38	284,316,364	545/0.35
6b	283,321,371	421(438)/0.31	283,322,372	559/0.26
6c	284,340,397	440(461)/0.41	283,341,396	570/0.37
6d	283,320,370	449/0.33	283,318,369	528/0.32

[a] Concentration of 1×10^{-5} M in DMF.

[b] The absorption and PL emission shoulders are shown in the parentheses.

[c] Quinine sulfate in 0.1 N of sulfuric acid used as a reference to determine the quantum yields (Φ_{PL}) of PL in solutions.

It is noted that similar absorption patterns between 270 and 500 nm were observed in these monomers and polymers with various lateral substitutions. In general, three major absorption peaks were observed in the absorption spectra for all compounds (in solutions and solid films), where the shorter absorption peaks around 283 to 342 nm belong to the tpy units and the central fluorene/phenylene cores, and the longest absorption peak belongs to their charge-transfer (CT) transition states. For the longest absorption peaks, the values of λ_{max} have the order of **c** (OMe) > **b** (Me) > **a** (H) because the electron-donating (ED) effect, with the exception of **6d** (F) on account of the electron-withdrawing (EW) effect. When strong ED (OMe) group was laterally attached to the conjugated core, the CT transition state was progressively shifted toward lower energy. However, monomer **5d** (with lateral F units) did not exhibit an obvious blue shift of absorption (λ_{max} = 382 nm in solutions, as shown in Table 3.3) in the CT transition state, that could be attributed to a weak electron-withdrawing effect. In addition, all polymers showed no significant changes in the absorption transition bands.

All monomers and polymers exhibit intensive violet to blue PL emissions (λ_{max} = 417 to 449 nm) in DMF solutions (shown in Table 3.3). The aggregation effect of monomers (**5a-5d**) and polymers (**6a-6d**) can be compared by the PL spectra in the solid states from Table 3.3. In contrast to $\lambda_{max,PL}$ values in solutions, polymers have Stokes shifts (red shifts) of $\lambda_{max,PL}$ values (ca. red shifts of 130 nm) in solid films than analogous monomers (ca. red shifts of 80 nm), except for monomer **5d** and polymer **6d**. This suggests that the metallo-supramolecular structures of polymers have stronger aggregation than the monomers in solid films. However, smaller red shifts of $\lambda_{max,PL}$ values in lateral F substituted monomer **5d** and polymer **6d**, for instance a red shift of 50 nm in monomer **5d** and a red shift of 79 nm in polymer **6d**, which

caused the shortest emission wavelength of PL in the solid films of monomer **5d** and polymer **6d** compared with their analogues in solutions, respectively. Importantly, the quantum yields of the coordination polymers (in both solutions and solid films) are higher than those of their analogous monomer ligands. Therefore, the particular metal ions, i.e. zinc(II), of these coordination polymers serving to increase electron delocalization on the polymer backbones induce the enhancement and red shifts of PL emissions in solid films.

In Figure 3.4, monomers **5a-5c** show a shoulder in their PL spectra (in solutions), except monomer **5d**. Whereas, monomer **5d** exhibits only one emission band and its full width at half-maximum (fwhm) value is broader than the others. The observed behavior is consistent with the difference of ED and EW effect in influencing the energy and transition dipole of the potential CT transitions localized on the monomers. Comparing the structures of monomers **5a-5c**, the sizes of their lateral subutitutents are in the order of **5c** (OMe) > **5b** (Me) > **5a** (H), so the intensities of their shoulders follow the order of **5c** < **5b** < **5a**. Furthermore, monomer **5c** and polymer **6c** (OMe) in solutions exhibited the smallest full width at half-maximum (fwhm) values in the PL emission spectra (see Figures 3.4 and 3.5). This indicates that the excimer emissions in PL solutions might be reduced by increasing the size of lateral substituents, so the phenomenon of excimer emission (in solutions) was minimized by increasing the steric hindrance, e.g. monomer **5c** and polymer **6c**. However, this is not true for the solid film of polymer **6c** in Figure 3.5, because a strong aggregation effect (i.e. a large red-shifted $_{max,PL}$ value of 130 nm obtained by changing from the solution state to the solid state) still occurred in the solid state of polymer **6c**, which is also confirmed by the increase of the fwhm values in PL emissions of polymer **6c** in solid films (Figure 3.5) compared with that of polymer **6c** in solutions (see Figures 3.4 and 3.5). Thus, the polymers (**6a-6d**) emitted green to yellow fluorescence ($_{max}$ = 528 to 570 nm) in solid films, and these PL emissions showed large Stokes shifts, which were also attributed to excimer formation or aggregation in the solid films.[62,81] Here, we can find that even polymer **6c** possesses more

bulky lateral substitutents (OMe) in the phenelyene rings; whereas, there is no significant influence on reduced aggregation of the polymer chains and suppression of the excimer formation in polymer **6c**. As a result, the lateral substitutents of -OMe in the phenylene rings are not bulky enough to have substantial effects on the reduction of aggregation from rigid conjugated cores in the polymers.
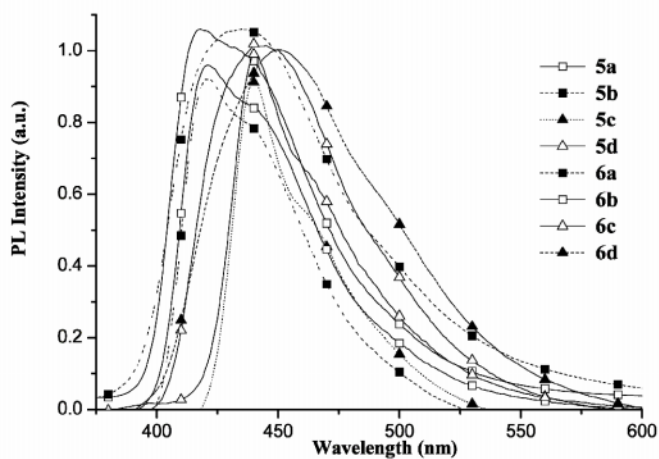
Figure 3.4 Normalized PL spectra of monomers and polymers in DMF solutions.
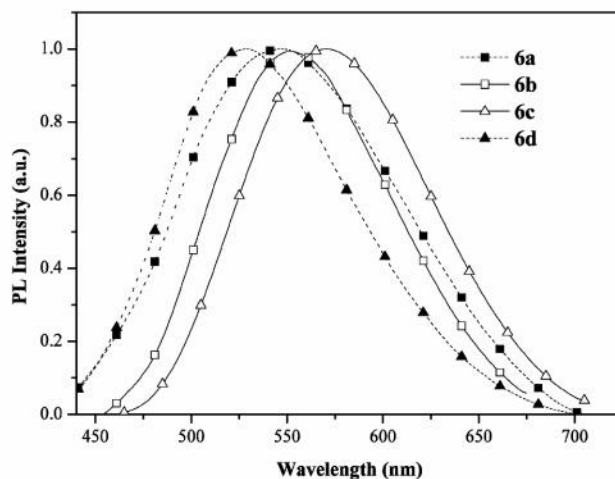
Figure 3.5 Normalized PL spectra of polymers in solid films.

Interestingly, the PL spectra of these monomers and polymers show poor mirror symmetry with the lowest energy absorption transition, and in fact, the UV-vis and PL spectra are quite different from each other (in shape). For example, Figure 3.6 shows the UV-vis and PL spectra of polymer **6c** (in solutions).[82]
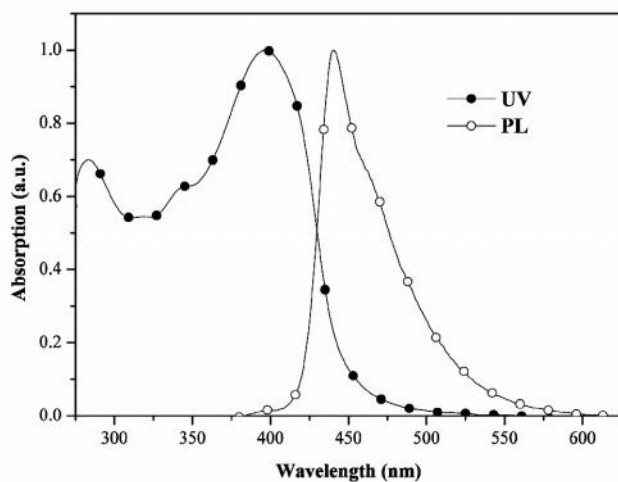
Figure 3.6 Normalized UV-vis and PL spectra of polymer **6c** in DMF solutions.

Most importantly, the metallo-polymers exhibit higher PL quantum yields than the corresponding monomers (as shown in Table 3.3, i.e., $_{f,sol}$ = 0.18-0.29 for monomers in DMF and $_{f,sol}$ = 0.31-0.41 for polymers in DMF; $_{f,film} \sim 0$ for monomer films and $_{f,film}$ = 0.26-0.37 for polymer films). Due to the poor film quality of monomers, the quantum yields of the monomers in solid films were not measured in the PL experiments. Therefore, luminescent bis-tpy units upon coordination to zinc( ) ions (possibly serving to increase electron delocalization on the polymer backbones) induce the enhancements and red shifts of PL emissions in solid films, which were also reported in recent publications.[55a]

3.4.7 Electroluminescence Properties

The CV results show that both HOMO and LUMO energy levels of the metallo-polymers do not match the work functions of indium-tin oxide (ITO) anode and Al cathode. Therefore, we

choose PEDOT and LiF/Al as the hole transporting layer and cathode, respectively, to overcome these large energy barriers. The electroluminescence (EL) properties of these polymers were investigated, except polymer **6a** due to its poor solubility. The other polymers (**6b-6d**) were used as emitting layers in a double-layer light-emitting devices with configuration of ITO/PEDOT:PSS/Polymer/LiF/Al. The function of LiF/Al as a cathode is because that the electron injection capability from a high work-function cathode can be significantly improved by inserting polar or ionic species between a metal electrode and a light-emitting layer.[55b] The electroluminescence properties of PLED devices (device structure: ITO/PEDOT:PPS/Polymer(**6b-6d**)/LiF/Al) with good external quantum yields between 0.36 and 1.02 and maximum brightnesses between 323 and 931 cd/m^2 (at 14 V) are listed in Table 3.4.

The emission colors of these devices (at a bias voltage around 10 V) were yellow to orange in Commission Internationale de l'Eclairage (CIE) coordinates, and the emission intensity was augmented by increasing bias voltages. The turn-on voltages of all devices were approximately 6 V, and the best power efficiency and brightness (in polymer **6c**) were 0.33 cd A^{-1} and 931 cd m^{-2} (at 14 V), respectively. The current density-voltage-brightness characteristic curves of polymer **6c** in the PLED device (device structure: ITO/PEDOT:PPS/Polymer(**6c**)/LiF/Al) are shown in Figure 3.7, and similar turn-on voltages for both of the current density and brightness illustrate that a matched balance of both injection and transportation in charges was achieved.[90] Compared with the corresponding PL spectra of solid films in Figure 3.5 and Table 3.3, polymers **6c** and **6d** (excluding **6b**) both showed red shifted emissions of $_{max}$ in EL spectra and polymer **6d** exhibited a broader EL emission peak (see Figure 3.8 and Table 3.4). The different EL and PL emissions of polymers **6c** and **6d** may originate from different excited state or/and ground states.[63c] The broader EL spectra of polymer **6d** may be due to the recombination of excitons at wide interfaces of the emission layer and the hole-transporting layer in the PLED devices.[90]
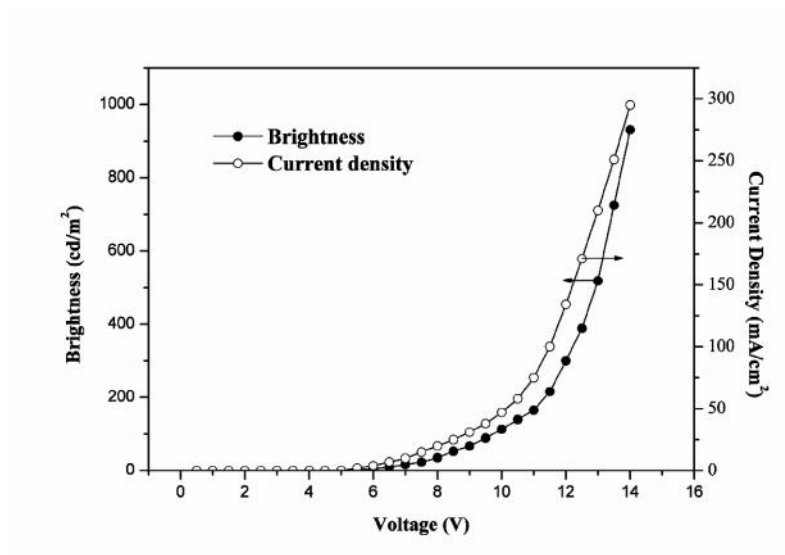
Figure 3.7 Current-voltage-brightness characteristics of the PLED device with the configuration of ITO/PEDOT:PSS/**6c**/LiF/Al.
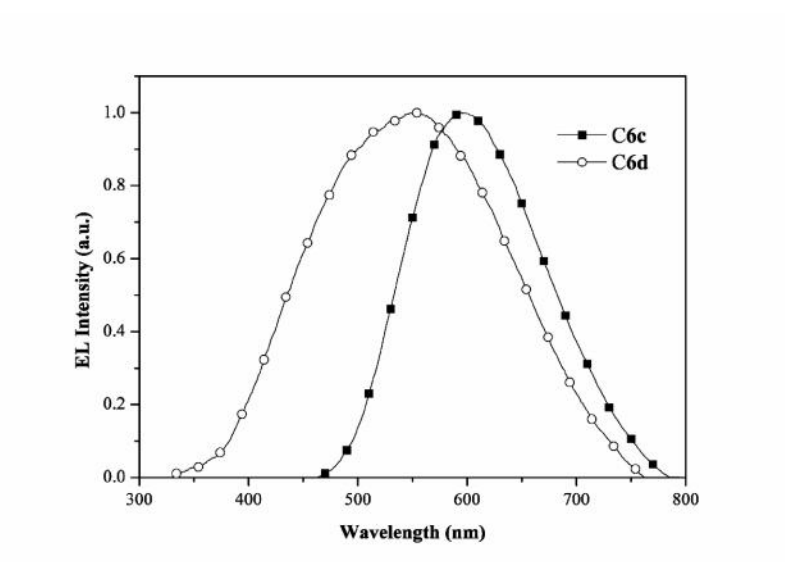
Figure 3.8 Normalized EL spectra of the PLED devices with the configurations of ITO/PEDOTPSS/(**6c** or **6d**)/LiF/Al.

3.5 Conclusion

In summary, a series of bis-tpyzinc(II)-based supramolecular polymers were obtained by self-assembled process. The formation of polymers **6a-6d** was confirmed by the increased viscosities (up to 1.5-1.83 times) relative to those of their analogous monomers. Besides, the experiments of ^{1}H-NMR and UV-vis titration over the ratio of Zn^{2+}/monomer = 1/1 confirmed the exact stoichiometric ratio of these metallo-supramolecular polymers. Various lateral substituents, such as methoxy (OMe), methyl (Me), and fluorine (F) units, were attached to the conjugated bis-tpy ligands, and thus to control the thermal properties and energy band gaps of the resulting metallo-polymers. Compared with the monomer counterparts, the film quality and the quantum yields of PL and EL were enhanced by the metallo-supramolecular design via introducing zinc(II) ions. These metallo-polymers gave green to yellow PL emissions (with good PL quantum yields) in solid films, and showed yellow to orange EL emissions. In general, the incorporation of lateral substituents into metallo-polymers reveals that the thermal and photophysical properties can be easily adjusted. Hence, with finely tuned structures integrated with coordination chemistry, metallo-polymers can provide a new protocol for the development of novel PLED materials.

Chapter 4

Metallo-homopolymer and metallo-copolymers containing light-emitting poly(fluorene/ethynylene/(terpyridyl)zinc(II)) backbones and 1,3,4-oxadiazole (OXD) pendants

4.1 Abstract

A series of novel metallo-polymers containing light-emitting poly(fluorene/ethynylene/(terpyridyl)zinc(II)) backbones and electron-transporting 1,3,4-oxadiazole (OXD) pendants (attached to the C-9 position of fluorene by long alkyl spacers) were synthesized by self-assembled reactions. The integrated ratios of ^{1}H NMR spectra reveal a facile result to distinguish the well-defined main-chain metallo-polymeric structures which were constructed by different monomer ligand systems (i.e. single, double, and triple monomer ligands with various pendants). Furthermore, UV-visible and photoluminescence (PL) spectral titration experiments were carried out to verify the metallo-polymeric structures by varying the molar ratios of zinc(II) ions to monomers. As a result, the enhancement of thermal stability (T_d) and quantum yields were introduced by the metallo-polymerization, and their physical properties were mainly affected by the nature of the pendants. The photophysical properties of these metallo-polymers exhibited blue PL emissions (around 418 nm) with quantum yields of 34-53 % (in DMF). In contrast to metallo-polymers containing alkyl pendants, the quantum yields were greatly enhanced by introducing 1,3,4-OXD pendants but reduced by carbazole (CAZ) pendants. Moreover, electroluminescent (EL) devices with these light-emitting metallo-polymers as emitters showed green EL emissions (around 550 nm) with turn-on voltages of 6.0-6.5 V, maximum efficiencies of 1.05-1.35 cd A^{-1} (at 100 mA cm^{-2}), and maximum luminances of 2313-3550

cd/m^2 (around 15 V), respectively.

4.2 Introduction

Recently, the use of transition or rare earth metal complexes to build up polymeric light-emitting diode (PLED) devices has attracted much attention because of the enhancement in EL efficiency.[28,48b,91-92] Chan and co-workers demonstrated that the construction of conjugated polymers made of ruthenium bipyridyl complexes can enhance the light-emitting performance by utilizing energy transfer from the triplet excited state.[55,93] A whole set of coordination polymers consisting of ditopic electro- and photo-active terpyridyl ligands complexed with zinc ions were recently published by Che et al.[44] These coordination polymers exhibit different emission wavelengths ranging from violet to yellow colors with high PL quantum yields, and these polymers were successfully applied to PLED devices. Hence, tuning electroluminescent (EL) properties could be achieved through the incorporation of different transition metal complexes into polymer main-chains.[49,76-77,94] Moreover, it is confirmed that the phenomenon of intraligand charge transfer (ILCT) happens between terpyridine/zinc(II) complexes and chromophores even in fully conjugated metallo-polymers, due to the d^{10} zinc(II) species.[44,84,94] Therefore, the incorporation of terpyridine/zinc(II) moieties into the metallo-polymers with fine-tuned chromophores can provide good quantum yields and thermal stabilities, and thus to have the potential to become high-performance emissive or host materials in PLED applications.[53c,78,79]

However, some important and fundamental challenges remain to solve, including the maximization of luminescence and power efficiency, the designs and syntheses of new materials for purer colors, and the modes of addressing devices for full-color displays with optimized resolutions. A major factor responsible for poor device performance is that the charge injection and transportation in emissive materials are generally unbalanced. This imbalance arises because the energy barrier between the indium tin oxide (ITO) anode and the highest-occupied molecular orbital (HOMO) level of an emissive material is different from that between the metal cathode and its lowest-unoccupied molecular orbital (LUMO)

level.[95] In previous studies, molecular and polymeric 1,3,4-oxadiazole (OXD) derivatives are one of the most widely studied classes of electron injection and/or hole-blocking materials, mainly because of their electron deficiencies, high photoluminescence quantum yields, and chemical stabilities.[95-99] Therefore, the introduction of electron-deficient OXD groups into the C-9 position of the fluorene units increase the electron affinities of resulting polymers and lead to more balanced charge injection and transporting properties as well as better recombination behavior.[65,67]

In this context, various electron- and hole-transporting substituents, i.e. 1,3,4-oxadiazole (OXD) and carbazole (CAZ) pendants, were incorporated into poly(fluorene/ethynylene/(terpyridyl)zinc(II))-based metallo-copolymers (as shown in Figure 4.1). In addition, the ^{1}H-NMR, thermal, photophysical, and electrochemical properties were investigated as well. Furthermore, the PLED applications of metallo-copolymers as emitters in multilayer EL devices with two different hetero-junction configurations of ITO/PEDOT:PSS/Polymer/TPBI[2,2',2''-(1,3,5-benzenetriyl)tris[1-phenyl-1H-benzimidazole]/LiF/Al and ITO/PEDOT:PSS/Polymer/BCP(2,9-dimethyl-4,7-diphenyl-1,10-phenanthroline)/ALQ(tris(8-hydroxyquinoline)aluminium)/LiF/Al were studied.

4.3 Experiment

4.3.1 Measurements

^{1}H NMR spectra were recorded on a Varian Unity 300 MHz spectrometer using CDCl$_3$ and DMSO-d_6 solvents. Elemental analyses were performed on a HERAEUS CHN-OS RAPID elemental analyzer. Phase transition temperatures were determined by differential scanning calorimetry (DSC, Model: Perkin Elmer Diamond) with a heating and cooling rate of 10 °C/min. Thermogravimetric analysis (TGA) was conducted on a Du Pont Thermal Analyst 2100 system with a TGA 2950 thermogravimetric analyzer with a heating rate of 10 °C/min under nitrogen. Melting points were determined by a Buchi SMP-20 capillary melting point apparatus. Viscosity measurements were proceeded by 10 % weight of polymer solutions (in NMP) in contrast to those proceeded by the same condition of monomer solutions (with viscosity $=$ 6 cp) on a BROOKFILEL DV-III+ RHEOMETER system (100 RPM, Spindle number: 4) at 25 . UV-visible (UV-vis) absorption spectra were recorded in dilute DMF solutions (10^{-5} M) on a HP G1103A spectrophotometer, and fluorescence spectra were obtained on a Hitachi F-4500 spectrophotometer. Fluorescence quantum yields were determined by comparing the integrated photoluminescence (PL) intensity of coumarin-1 in ethanol with a known quantum yield (ca. 5 x 10^{-6} M, quantum yield = 0.73). Cyclic voltammetry (CV) was performed at a scanning rate of 100 mV/s on a BAS 100 B/W electrochemical analyzer, which was equipped with a three-electrode cell. Pt wire was used as a counter electrode, and an Ag/AgCl electrode was used as a reference in the CV measurements. The CV experiments were performed by solid samples immersed into electrochemical cell containing 0.1 M tetrabutylammonium hexafluorophosphate (Bu$_4$NPF$_6$) solutions (in DMF) with a scanning rate of 100 mV/s at room temperature under nitrogen. UV-vis and PL titrations were preformed by that 1.0 x 10^{-5} M of monomer solutions in the solvent of CH$_3$CN/CHCl$_3$ (2/8 in vol.) were titrated with 50 µl aliquots of 3.9 x 10^{-4} M of Zn(OAc)$_2$ solutions in the same solvent composition as described. The addition was done

stepwisely and the formation of Zn(II)-coordination polymers was monitored by UV-vis spectroscopy. Polymer thin solid films in UV-vis and PL measurements were spin-coated on quartz substrates from DMF solutions with a concentration of 10 mg/ml.   A series of EL devices with two device configurations of ITO/PEDOT:PPS/Polymer/TPBI(2,2',2"-(1,3,5-benzenetriyl)tris[1-phenyl-1H-benzimidazole])//LiF/Al and ITO/PEDOT:PPS/Polymer/BCP(2,9-dimethyl-4,7-diphenyl-1,10-phenanthroline)/AlQ(tris(8-hydroxyquinoline)aluminium)/LiF/Al were made, where TPBI and AlQ were used as electron transporting layers, and BCP was used as a hole-blocking layer collocated to AlQ. ITO substrates were routinely cleaned by ultrasonic treatments in detergent solutions and diluted water, followed by rinsing with acetone and then ethanol. After drying, ITO substrates were kept in oxygen plasma for 4 min before being loaded into the vacuum chamber. The solutions (10 mg/ml) of light-emitting materials in DMF were spin-coated on glass slides precoated with indium tin oxide (ITO) having a sheet resistance of ~20   /square and an effective individual device area of 3.14 mm^2. The spin coating rate was 6000 rpm for 60 s with PEDOT: PPS, 4000 rpm for 60 s with resulting polymers, and the thicknesses of PEDOT: PPS and polymers were measured with an Alfa Step 500 Surface Profiler (Tencor). TPBI, BCP, and AlQ were thermally deposited at a rate of 1-2 Å/s under a pressure of ~2x10^{-5} torr in an Ulvac Cryogenic deposition system. Under the same deposition conditions and systems, one layer of LiF was thermally deposited as a cathode at a rate of 0.1-0.2 Å/s, which was followed by capping with aluminum.

4.3.2 Materials

Chemicals and solvents were reagent grades and purchased from Aldrich, ACROS, TCI, and Lancaster Chemical Co. Solvents were purified and dried according to standard procedures. Chromatography was performed with Merck silica gel (mesh 70-230) and basic aluminum oxide, which was deactivated with 4 wt% of water.

4'-[[(Trifuroromethyl)sulfonyl]oxy]-2,2':6',6"-terpyridines and compounds **1a**, **4b** (**M2**), and **4c** (**M3**) were prepared and purified according to literature procedures.[56,84,94] The synthetic routes of monomer **4a-4c** (**M1-M3**) and metallo-polymers **P1-P4** are illustrated in Schemes 4.1-4.2.

Compound (2a). To a solution of compoumd (**1a**) (28 mmol) in 60 mL of THF/Et$_3$N (1/1), 3-methyl-1-butyn-3-ol (84 mmol) was added. After the solution was degassed with nitrogen for 30 min, Pd(PPh$_3$)$_2$Cl$_2$ (0.28 mol), PPh$_3$ (11 mol), and CuI (2.8 mmol) were added. The reaction was then refluxed at 70   under N$_2$ for 12 h. The solvent was removed under reduced pressure. The resulting solid was extracted with CH$_2$Cl$_2$/H$_2$O then dried over MgSO$_4$. The crude product was purified by column chromatography (silica gel, hexane/ethyl acetate = 4/1) to afford a white solid. mp 76-77   . ^{1}H NMR (300 MHz, CDCl$_3$):   8.01-8.05 (m, 8H), 7.60 (d, J = 7.8 Hz, 2H), 7.39-7.42 (m, 4H), 7.32 (d, J = 8.4 Hz, 4H), 6.94 (d, J = 9 Hz, 4H), 3.90 (t, J = 6.3 Hz, 4H), 2.44 (s, 6H), 2.04 (s, 2H), 1.95 (br, 4H), 1.59-1.66 (m, 16H), 1.13-1.18 (m, 12H). Yield: 77%. FABMS: *m/e* 996; C$_{65}$H$_{66}$N$_4$O$_6$ requires *m/e* 998.50.

Compound (3a). A mixture of (**2a**) (1.63 mmol) and KOH (6.5 mmol) in 60 mL of 2-propanol was heated refluxed under N$_2$ with a vigorous stirring for 3 h. The solvent was then removed and crude product was purified by column chromatography (silica gel, hexane) to afford a white solid. mp 82-83   . ^{1}H NMR (300 MHz, CDCl$_3$):   7.99-8.04 (m, 8H), 7.64 (d, J = 7.8 Hz, 2H), 7.47-7.50 (m, 4H), 7.32 (d, J = 8.4 Hz, 4H), 6.95 (d, J = 9 Hz, 4H), 3.91 (t, J = 6.3 Hz, 4H), 3.16 (s, 2H), 2.44 (s, 6H), 1.97 (br, 4H), 1.59-1.66 (m, 4H), 1.13-1.20 (m, 12H). Yield: 77%. FABMS: *m/e* 882; C$_{59}$H$_{54}$N$_4$O$_4$ requires *m/e* 882.41.

Monomer   4a   (M1).   Compound   (**3a**)   (0.5   mmol)   and 4'-[[(trifuroromethyl)sulfonyl]oxy]-2,2':6',6"-terpyidine (1.1 mmol) were dissolved in nitrogen-degassed benzene, then [Pd^0(PPh$_3$)$_4$] (70 mg, 0.06 mmol) was added and followed by nitrogen-degassed ^{i}Pr$_2$NH. The solution was then heated to 70   . After complete consumption of starting materials, the solvent was evaporated and the product was purified

by column chromatography (alumina, hexane/dichloromethane = 10/1 in vol.) to afford a white solid. mp 115-116   . ^{1}H NMR (300 MHz, CDCl$_3$):   8.7 (d, J = 5.1 Hz, 4H), 8.60-8.64 (m, 8H), 7.93-7.97 (m, 8H), 7.86 (t, J = 7.8 Hz, 4H), 7.75 (d, J = 8.7 Hz, 2H), 7.58-7.61 (m, 4H), 7.33-7.37 (m, 4H), 7.30 (d, J = 8.1 Hz, 4H), 6.93 (d, J = 8.7 Hz, 4H), 3.92 (t, J = 6.6 Hz, 4H), 2.43(s, 6H), 2.08 (br, 4H), 1.64 (br, 4H), 1.22 (br, 12H). Yield: 75%. FABMS: m/e 1343; C$_{89}$H$_{72}$N$_{10}$O$_4$ requires m/e 1344.57. Anal. Calcd for C$_{89}$H$_{72}$N$_{10}$O$_4$: C, 79.44; H, 5.39; N, 10.42; O, 4.76. Found: C, 80.15; H, 5.77; N, 10.22; O, 4.41.

Metallo-homopolymer P1. To monomer **4a** (**M1**) (0.52 mmol) in 30 ml of NMP solution, zinc acetate (0.52 mmol) in NMP (10 ml) was added dropwisely. The resulting solution was heated at 105   under nitrogen atmosphere. After stirring for 24 h, excess KPF$_6$ was added into the hot solution. The resulting solution was poured into methanol and the precipitate obtained was purified by repeated precipitations using NMP and ether. The polymers were dried under vacuum at 60   for 24 h and collected as a yellow solid. Yields: 78-82 %.

Metallo-*alt*-copolymer P2. To zinc acetate (1.25 mmol) in 20 ml of NMP (*N*-methylpyrrolidinone) solution, monomer **4b** (**M2**) (0.61 mmol) in NMP (20 ml) was added dropwisely. After stirring at r.t. for 2 hr, then monomer **4a** (**M1**) (0.64 mmol) was also added dropwisely. The resulting solution was heated at 105   under a nitrogen atmosphere. After stirring for 24 h, excess KPF$_6$ was added into the hot solution. The resulting solution was poured into methanol and the precipitate obtained was purified by repeated precipitations using NMP and ether. The polymers were dried under vacuum at 80   for 24 h and collected as a yellow solid. Yields: 74-80 %.

Metallo-*alt*-copolymer P3. The procedure is analogous to that described for **P2.** Yields: 80-84 %.

Metallo-copolymer P4. To zinc acetate (0.92 mmol) in 20 ml of NMP (*N*-methylpyrrolidinone) solution, monomer **4b** (**M2**) (0.45 mmol) in NMP (20 ml) was added dropwisely. After stirring at r.t. for 2 hr, then mixture monomers **4a** (**M1**) and **4c** (**M3**)

(0.42 mmol, **4a** (**M1**):**4c** (**M3**) = 1:1) was also added dropwisely. The resulting solution was heated at 105 under nitrogen atmosphere. After stirring for 24 h, excess KPF_6 was added into the hot solution. The resulting solution was poured into methanol and the precipitate obtained was purified by repeated precipitations using NMP and ether. The polymer was dried under vacuum at 80 for 24 h and collected as a yellow solid. Yields: 80 %.

4.4 Result and Discussion

4.4.1 Synthesis and Characterization

The synthetic routes of monomers **4a,** metallo-homopolymer **P1** and metallo-copolymers **P2-P4** are illustrated in Schemes 4.1-4.2.

Scheme 4.1 Synthetic Routes of Monomers **4a-4c** (**M1-M3**)
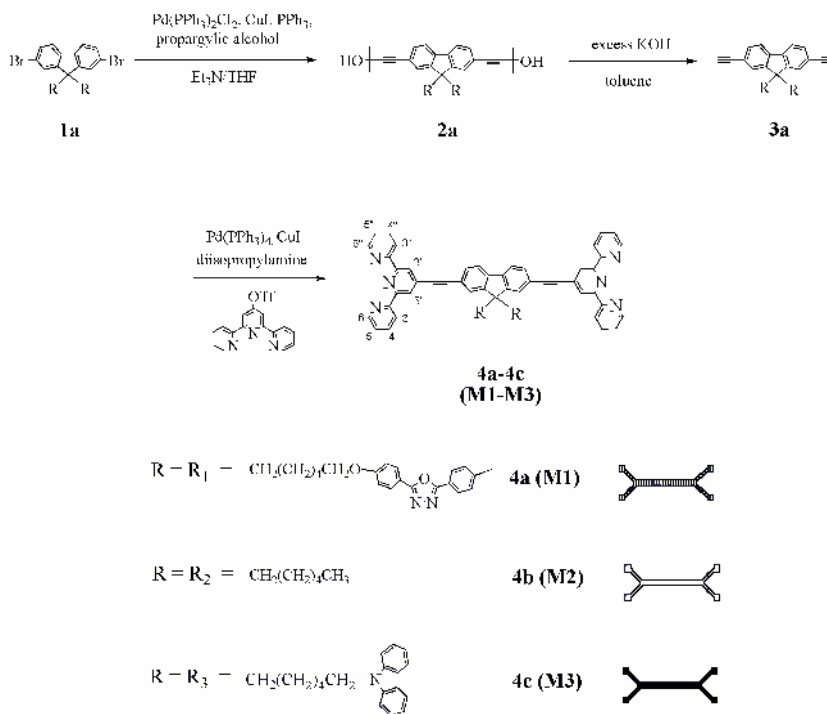
Metallo-homopolymer **P1** was obtained by refluxing monomer **4a** (**M1**) with Zn(OAc)$_2$ at a ratio of 1:1 in NMP solution and followed by subsequent anion exchange.[84,94] The key steps in the syntheses of metallo-*alt*-copolymers were first to functionalize two end terpyridyl units of monomers **4b** (**M2**) and **4c** (**M3**) with Zn(OAc)$_2$ at the ratio of 1:2 to afford complexes **5b** and **5c**, respectively. Then, complexes **5b** and **5c** as initiators were coordinated with monomer **4a** (**M1**) (see Scheme 4.2) at the ratio of 1:1 (as a sequential-coupling method), respectively, to obtain metallo-*alt*-copolymers **P2** and **P3**.[84]

Scheme 4.2 Synthetic Routes of Metallo-polymer P1-P4
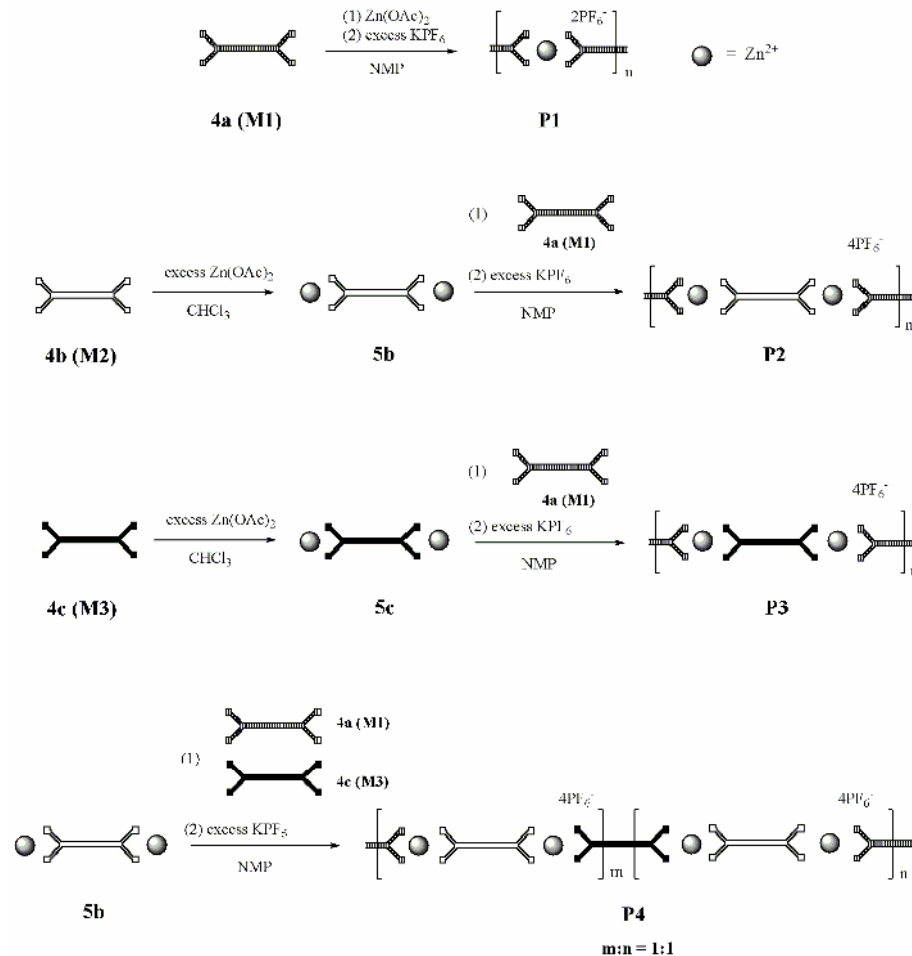
Moreover, metallo-copolymer **P4** was obtained by reacting the mixture of monomers **4a** (**M1**) and **4c** (**M3**) (at the ratio of 1:1) with complex **5b** (monomer mixture: complex **5b** = 1:1). In contrast to other polymerization methods, i.e. the Witting or Heck coupling reactions, there are three points worthy to be noted: First, the reactive liability of zinc( ) ions and the stability of six-coordinate bis-terpyridine zinc(II) moieties allow self-assembled reactions to take place under refluxing conditions.[28,44,48] Second, the present procedure does not need any catalysts. Third, the chemical structures of metallo-copolymers can be controlled by proper stoichiometries of metals and monomers.[84,94]

4.4.2 Structural Characterization of ^{1}H NMR.

^{1}H-NMR spectra of monomers **4a**-**4c** (**M1**-**M3**), complexes **5b**-**5c,** and metallo-polymers **P1**-**P4** were recorded in DMSO-d_6 as shown in Figure 4.1 Compared with ^{1}H peaks of monomers **4b** (**M2**) and **4c** (**M3**) in our previous study,[84] those in terpyridyl units of complexes **5b** and **5c** show the same downfield shift effect in proton peaks of (6,6")-, (5,5")-, (4,4")-, (3',5')-, and (3,3")-H. Furthermore, proton peaks of (4,4")-H in terpyridyl units of complexes **5b** and **5c** overlap with ^{1}H peaks of fluorene units. It appears that the formation of complexes **5b**-**5c** can be respectively proven by the disappearance of original ^{1}H peaks in terpyridyl units of monomers **4a**-**4b** (**M1**-**M2**) in the mixture of zinc ions and monomers at the ratio of 2:1.[84] The formation of homopolymer **P1** is clearly indicated by the appearance of a new set of ^{1}H peaks and the absence of the original ^{1}H peaks in terpyridyl units, which belong to the uncomplexed monomer **4a** (**M1**).
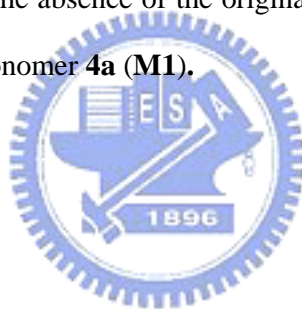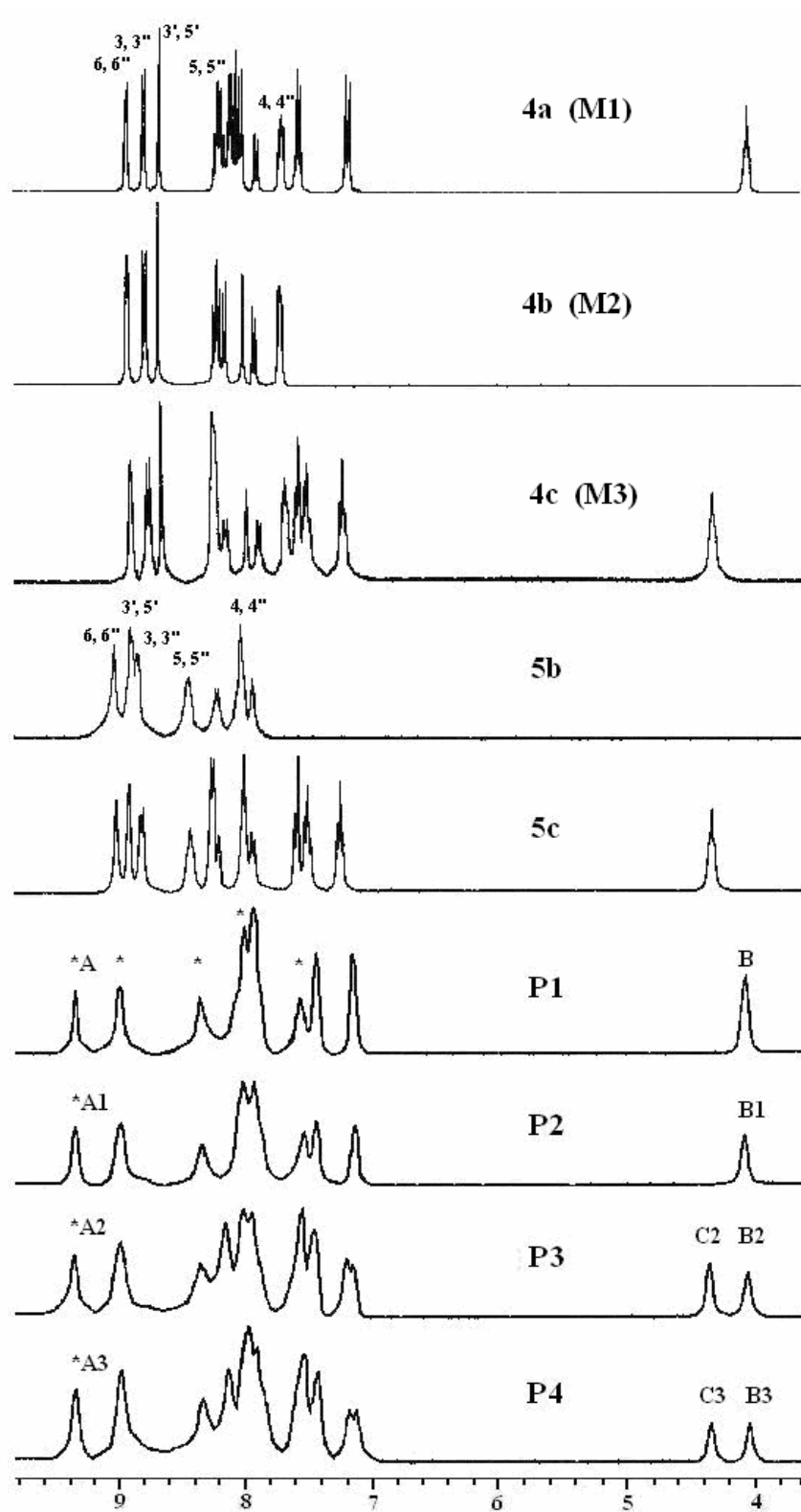
Figure 4.1 ^{1}H-NMR spectra of monomers **4a-4c (M1-M3)**, complexes **5a-5b**, and metallo-polymers **P1-P4** in DMSO-d_6.

(The assignments of ^{1}H peaks of the terpyridyl units for all polymers are made by asterisks with respect to 4-chloro-terpyridine Zn^{2+} complexes). In terms of ^{1}H peaks of 1,3,4-OXD and carbazole (CAZ) pendants, there are no obvious changes in chemical shifts among monomers **4a** (**M1**), **4c** (**M3**) and polymers **P3**, **P4**. Therefore, the most up-shifted ^{1}H peaks in the terpyridyl units of polymers **P3** and **P4** could be overlapped with the ^{1}H peaks of these pendants. To distinguish the structural differences among these main-chain metallo-polymers **P1**-**P4**, it is feasible to compare the relative integrated ratios of the ^{1}H peaks. As a result, the integrated ratios of the ^{1}H peaks in the terpyridyl units (***A** for **P1, *A1** for **P2, *A2** for **P3,** and ***A3** for **P4**) and the ^{1}H peaks of the alkyl chains (spacer $-CH_2-$) attached to 1,3,4-OXD (**B** for **P1**, **B1** for **P2, B2** for **P3,** and **B3** for **P4**) and CAZ units (**C2** for **P3** and **C3** for **P4**) of these polymers are compared. It reveals that the relative integrated ratios are ***A/B** = 0.5, ***A1/B1** = 1, ***A2/B2** = 1, and ***A3/B3** = 2 for metallo-polymers **P1**, **P2**, **P3,** and **P4**, respectively, which suggests that the integrated ratios of polymers were consistent with the monomer amounts containing pendent 1,3,4-OXD units.[84] In contrast to the relative integrated ratio of **B2/C2** (=1.1) in polymer **P3,** that of **B3/C3** was 1 for polymer **P4**. According to these results, the input ratios (molecular ratios) of monomers for polymerization were very similar to the output ratios (the relative integrated ratios of ^{1}H-NMR) of the metallo-polymers. Consequently, the amounts of monomer ligands incorporated in the monomer ligand-based metallo-polymers (i.e., **P1**: single monomer ligand system; **P2** and **P3**: double monomer ligand systems; **P4**: triple monomer ligand system) can be confirmed by ^{1}H-NMR.[54,57]

4.4.3 Thermal and Viscosity Properties

The thermal and viscosity properties of monomers **4a**-**4c** (**M1**-**M3**) and metallo-polymers **P1**-**P4** were studied by thermogravimetric analysis (TGA) and rheometry as summarized in Table 4.1.

<p align="center">**Table 4.1** Physcial Properties of Metallo-Polymers (**P1-P4**)</p>

Polymer	T_d ( )[a]	(cp)[b,c]	$E^{red/peak}$ (V)[d]	E^{LUMO} (eV)[e]	E^{HOMO} (eV)[f]	Band Gap (eV)[g]
P1	355	11	-1.54(r)	-3.10	-6.26	3.16
P2	389	10	-1.54(r)	-3.04	-6.20	3.16
P3	366	10	-1.54(r)	-2.88	-6.03	3.15
P4	356	9	-1.55(r)	-2.87	-6.02	3.15

[a] The decomposition temperatures (T_d) (5% weight loss) were determined by TGA with heating rates of 20 ℃ min^{-1} under N_2 atmosphere. The T_d values were 221   for **4a** (**M1**), 351   for **4b** (**M2**), and 354   for **4c** (**M3**), respectively.

[b] The viscosities of metallo-polymers (10 % in weight) in NMP solutions at 25   (100 RPM, Spindle number: 4) were determined by rheometer system.

[c] Solutions of monomers **4a**-**4c** (**M1-M3**) (10 % in weight) in NMP (with viscosities   = 6-7 cp, 25   ) were used as references to determine the viscosities of metallo-polymers.

[c] Reduction peaks in N_2-purged DMF, r in parentheses means reversible.

[d] LUMO energy levels were calculated from the measured reduction potentials versus the ferrocene/ferrocenium couple in DMF solutions.

[e] Optical band gaps were estimated from the absorption spectra in solutions by extrapolating the tails of the lower energy peaks.

The decomposition temperatures (T_d) (5% weight loss measured by TGA) of monomers under nitrogen atmosphere were ranged from 221 to 351   , and those of polymers were ranged from 355 to 389   . In contrast to monomers, polymers exhibited slightly enhanced thermal stability due to the increased rigidity of the main-chain structures.[55] As the bulky OXD and CAZ pendants are attached to the backbones of the metallo-polymers, it leads to reduced rigidity of the polymers.[31-32] Hence, compared with polymers **P1, P3,** and **P4** containing more bulky OXD and CAZ pendants, **P2** shows the highest T_d value among these metallo-polymers due to its higher molar ratio of less bulky alkyl pendants. This behavior was also confirmed by that the T_d value (422   ) of metallo-homopolymer containing **M2** (with alkyl pendants) is larger than that (399   ) of metallo-homopolymer containing **M3** (with CAZ pendants) in our previous report,[84] and both T_d values are larger than that (355   as shown in Table 1) of metallo-homopolymer **P1** containing **M1** (with OXD pendants).

Moreover, the same trend of the pendent size effect on the Tg values were also observed in the monomers, i.e., **4b** (**M2** with alkyl pendant) = 103   > **4c** (**M3** with CAZ pendant) = 92   > **4a** (**M1** with OXD pendant) = 67   , so molecular structures with larger pendant groups have lower Tg values. This obviously indicates that the presence of OXD and CAZ pendants in these metallo-polymers suppresses the crystallinity (and chain aggregation) of the polymers effectively. Similar results were also observed in poly(fluorene)-based copolymers containing various 1,3,4-oxadiazole dendritic pendants.[67a]

To further investigate these polymers, molecular weight should be reported, however, these polymers showed the poor solubility in THF, CH$_3$Cl, and alcoholic solvents. Therefore, the relative viscosities of polymer to monomer were carried out to support the polymers structures. Solutions of monomers **4a**-**4b** (**M1**-**M2**) (10 % weight ratio) in NMP with viscosities   = 6-7 cp at 25   were used as references to determine the viscosities of regarding polymers. In comparison with the viscosities of monomers **4a**-**4c** (**M1**-**M3**), those of metallo-polymers **P1-P4** exhibit increased viscosities (= 9-11 cp) by adding Zn^{2+} ions, and the ratios of relatively increased viscosities of polymers to those of monomers were in the range of 1.50-1.66. Similar phenomena were also reported in our previous study.[84]

4.4.4 Electrochemical Properties

The electrochemical behaviors of polymers were studied by cyclic voltammetry (CV), and the electrochemical properties are summarized in Table 4.1. The lowest unoccupied molecular orbital (LUMO) energy levels were estimated from reduction potentials by the reference energy level of ferrocene (4.8 eV below the vacuum level) according to the following equation:[56] $E^{LUMO} = [-(E^{onset} - 0.45) - 4.8]$ eV. However, the oxidation potentials of all metallo-polymers were not detectable, so the highest occupied molecular orbital (HOMO) energy levels can be estimated by the sums of LUMO energy levels and optical band gaps. All metallo-polymers exhibit reversible reduction peaks around -1.54 V in

cathodic scans (up to -2.5 V). These peaks are attributed to the reduction of terpyridyl-based moieties.[44,84] The absence of oxidation peaks in the anodic scans (up to 1 V) of these polymers, are due to the metal oxidation of d^{10} zinc( ) ion species being extremely difficult to be observed.[59-60] The optical band gaps were estimated from absorption spectra in DMF solutions by extrapolating the tails of the lowest energy peaks, and the optical band gaps of these polymers were ranged from 3.15 to 3.16 eV. Since metallo-polymers **P1-P4** possess similar backbone structures, there are no obvious differences in the optical band gaps. The electrochemical results indicate that the incorporation of 1,3,4-OXD pendant groups into the backbones of metallo-polymers will efficiently reduce the LUMO energy levels, and thus to reduce the electron injection barrier between the cathode and the emitters.[66,83]

4.4.5 UV-Visible and Photoluminescence Titration

To characterize the formation of metallo-hompolymer **P1** and complexes **5a-5b**, the UV-visible (UV-vis) and photoluminescence (PL) titration experiments are clear ways to investigate their stepwise changes. Figure 4.2 described that upon addition of Zn^{2+} ions to monomer **4a** (**M1**) reaching a ratio of Zn^{+2}:**4a** (**M1**) = 1:1, the spectra revealed clear shifts of three absorption bands at 364, 379, and 405 nm along with one isosbestic point, which suggests that an equilibrium occurred between a finite number of spectrorscopically distinct species.
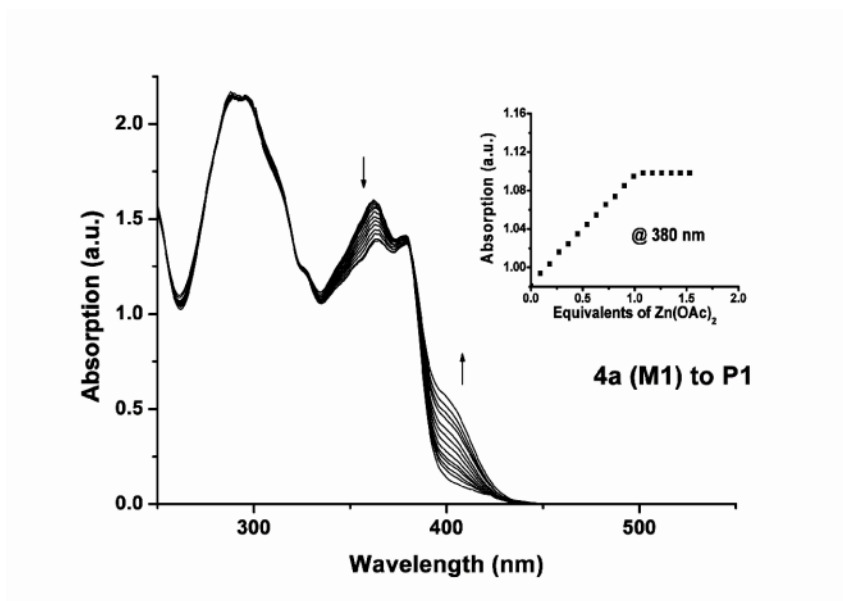
Figure 4.2 UV-vis spectra acquired in the process of **4a** (**M1**) to **P1** upon the titration of monomer **4a** (**M1**) in $CH_3CN/CHCl_3$ (2/8 in vol.) with $Zn(OAc)_2$. The spectra are shown at selected ranges of Zn^{+2}:**4a** (**M1**) = 0 to 1. The inset shows the normalized absorption at 380 nm as a function of Zn^{+2}:**4a** (**M1**) ratio.

The titration curve (in the inset of Figure 4.2) showed a linear increase and a sharp endpoint at the ratio of Zn^{+2}:**4a** (**M1**) = 1:1, indicating the formation of metallo-homopolymer **P1**. The syntheses and characterization of metallo-homopolymers by adding Zn^{2+} ions to monomers **4b** (**M2**) or **4c** (**M3**) to the ratio of Zn^{+2}:**4b** (**M2**) = 1:1 or Zn^{+2}: **4c** (**M3**) = 1:1 have also been investigated.[84] Beyond this point (Figures 4.3 and 4.4), the subsequent addition of Zn^{2+} ions induced new peaks at 279, 285, 348, and 394 nm for complex **5b** (332, 348, and 393 nm for **5c**) as well as new isosbestic points to form, which points out that an equilibration arose between spectroscopically distinct species.
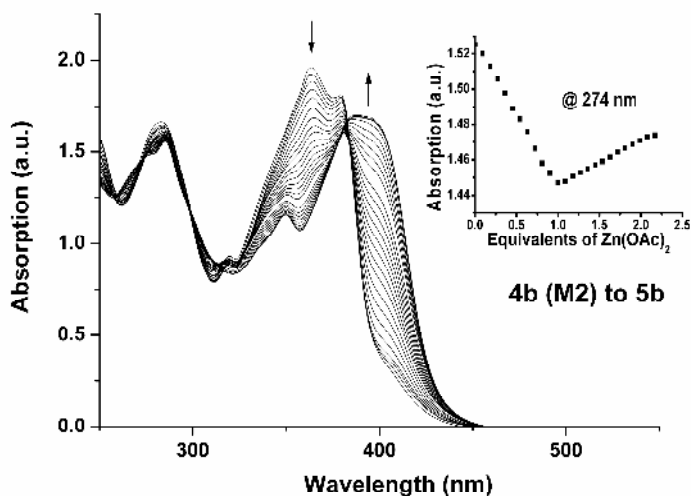
Figure 4.3 UV-vis spectra acquired (in the process of **4b** (**M2**) to **5b**) upon the titration of monomer **4b** (**M2**) in CH$_3$CN/CHCl$_3$ (2/8 in vol.) with Zn(OAc)$_2$. The spectra are shown at selected ranges of Zn^{+2}:**4b** (**M2**) = 0 to 2. The inset shows the normalized absorption at 274 nm as a function of Zn^{+2}:**4b** (**M2**) ratio.
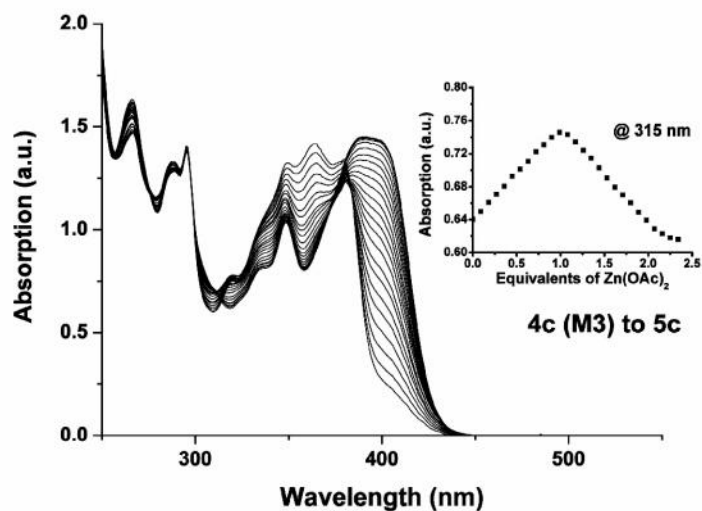
Figure 4.4 UV-vis spectra acquired (in the process of **4c** (**M3**) to **5c**) upon the titration of monomer **4c** (**M3**) in CH$_3$CN/CHCl$_3$ (2/8 in vol.) with Zn(OAc)$_2$. The spectra are shown at selected ranges of Zn^{+2}:**4c** (**M3**) = 0 to 2. The inset shows the normalized absorption at 315 nm as a function of Zn^{+2}:**4c** (**M3**) ratio.

Thus, Figures 4.3 and 4.4 depicted that the ratios of Zn^{2+} ions to monomers **4b** (**M2**) or **4c** (**M3**) are above 1:1, and the depolymerization is driven by the formation of

chain-terminating complexes **5b** or **5c**.[62,84] All of the UV-vis titration spectra showed the lowest absorption around λ_{Abs} = 394-404 nm, which corresponds to a charge transfer occurring between the electron-rich central fluorenyl components and the electron-deficient metal-coordinated terpyridyl moieties.[54c,62] In Figure 4.5, monomer **4a** (**M1**) showed an emission band around 429 nm. As the ratio of Zn^{2+}: **4a** (**M1**) reached 1:1, a new emission band at 456 nm was induced. The PL quantum yields of medium complexes, i.e. the ratio of Zn^{+2}: **4a** (**M1**) gradually approached 1:1 in the inset of Figure 4.5, were scarcely increased that followed by increasing molar ratio of Zn^{+2} ions.
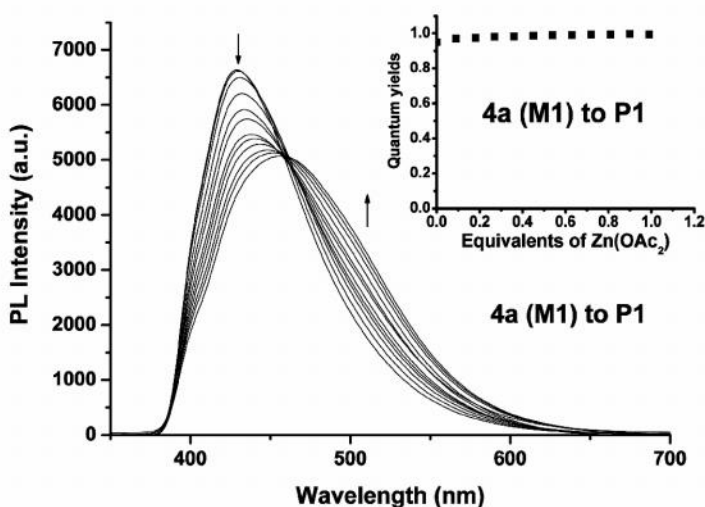
Figure 4.5 PL spectra acquired upon the titration of monomer **4a** (**M1**) in $CH_3CN/CHCl_3$ (2/8 in vol.) with $Zn(OAc)_2$. The spectra are shown at selected ranges of Zn^{+2}:**4a** (**M1**) = 0 to 1. The inset shows the quantum yields as a function of Zn^{+2}:**4a** (**M1**) ratio.

Therefore, the PL quantum yields of metallo-homopolymer **P1** can be marginally enhanced by attaching 1,3,4-OXD pendent groups to the polymer backbones. Furthermore, the monomer **4b** (**M2**) exhibited a similar PL result by the formation of metallo-homopolymer reaching the ratio of Zn^{2+}: **4b** (**M2**) = 1:1, except for the metallo-homopolymer synthesized from monomer **4c** (**M3**) with CAZ pendants possessing a much lower quantum yield (in solution) than its monomer **4c**.[84]

4.4.6 Photophyscial Properties

The photophycial measurements of monomers **4a**-**4c** (**M1-M3**) and metallo-polymers **P1-P4** were carried out by UV-vis absorption and photoluminescence (PL) experiments in both dilute DMF (*N,N*-dimethylformamide) solutions (with some solubility problems) and solid films, and their photophysical properties are presented in Table 4.2.

Table 4.2 Photophyscial Properties of Monomers **4a-4c** (**M1-M3**) and Metallo-Polymers

P1-P4

Compound	Abs.,sol (nm) [a]	max,PL,sol/ PL,sol (nm) [a,b,c]	Abs.,film (nm)	max,PL,film (nm)
4a (**M1**)	292,363,378	414/0.33	--	--
4b (**M2**)	285,319,363,373	415/0.20	--	--
4c (**M3**)	287,294,319, 347,364,374	414/0.25	--	--
P1	288,327,361,377	418/0.53	289,298,337, 399	500
P2	287,317,361,378	416/0.51	299,354,413	502
P3	287,294,318, 361,377	416/0.34	289,354,408	502 (472,533)
P4	288,295,316, 348,361,378	416 (401)/0.35	297,353,410	500 (473)

[a] Concentration of 1×10^{-6} M in DMF.

[b] Coumarin-1 in ethanol(ca. $5 * 10^{-6}$ M, quantum yield = 0.73) used as a reference to determine the quantum yields of PL in solutions.

[c] The PL emission shoulders are shown in the parentheses.

In Figure 4.6, similar absorption features of polymers **P1**-**P4** were observed at 286, 320, and 377 nm. In general, other absorption peaks can be assigned to pendent groups (i.e. $_{Abs}$ = 295 and 300 nm for CAZ and OXD pendants, respectively) and these absorption peaks attributed to pendent groups also can assist to confirm the metallo-copolymer structures.
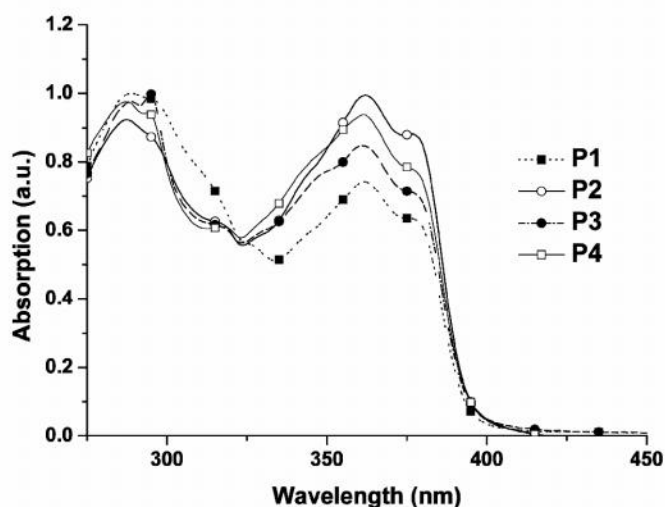
Figure 4.6 Normalized UV-vis spectra of metallo-polymers **P1-P4** in DMF solutions.

PL emissions of all monomers and polymers are assigned to intra-ligand (*-) fluorescence.

They showed purple-blue emission colors in DMF solutions, where the values of PL

emission peaks ($_{max,PL}$) were around 414 nm (in DMF) with quantum yields ( ) of 20

%-33% for monomers **4a**-**4c** (**M1-M3**) and $_{max,PL} \sim$ 417 nm (in DMF) with quantum yields

( ) of 34%-53 % for metallo-polymers **P1-P4**. The enhancement of the quantum yields in

metallo-polymer were attributed to the polymerization procedure and similar results were

reported in the literatures.[44,84,94] Nevertheless, PL emissions from the OXD pendants were

not observed, even when metallo-polymers were excited at the absorption peaks of the OXD

pendants. This indicates the existence of efficient energy transfer from the OXD pendants to

the polymer backbones.[56c] Comparing PL quantum yields of metallo-copolymers **P2-P4** with

the same molar ratio (50%) of OXD pendants, the order of PL quantum yields (in solutions)

is **P2** > **P4** > **P3**, which is reverse to the order of the molar ratio of CAZ pendants in

metallo-polymers **P2-P4**, i.e. **P2** (0% CAZ) < **P4** (25% CAZ) < **P3** (50% CAZ). It suggests

that of the metallo-polymers containing **M2** (with alkyl pendants) have larger PL quantum

yields than those containing **M3** (with CAZ pendants). This behavior fits well with the PL

quantum yield (53%) of metallo-homopolymer **P1** containing **M1** (with OXD pendants)

being larger than that $(23\%)^{84}$ of metallo-homopolymer containing **M2** (with alkyl pendants), and also larger than that $(11\%)^{84}$ of metallo-homopolymer containing **M3** (with CAZ pendants). Overall, in contrast to metallo-polymers containing alkyl pendants, the quantum yields were greatly enhanced by introducing 1,3,4-OXD pendants but reduced by carbazole (CAZ) pendants. Hence, PL quantum yields of metallo-polymers were truly affected by incorporating different monomer ligands into main-chain polymeric structures.

Regarding solid films of these metallo-polymers, they emitted blue to green colors with PL values of $_{max,PL}$ ranging at 509-520 nm (Figure 4.7). According to PL emissions of polymer films, all polymers showed large Stokes shifts (ca. 83-104 nm) in contrast to their PL emissions in solutions, which were attributed to the excimer formation resulting from - stacking of aromatic interaction in solid films.[63a,64a] When the bulky pedants (i.e. CAZ) were attached to the C-9 position of fluorene units, they were able to suppress the excimer formation as shown in our previous result.[44] However, metallo-copolymers **P3** and **P4** only showed small shoulders around 472 nm (see Figure 4.7), which correspond to the emissions of polymer backbones, and metallo-polymers **P1** and **P2** even with dominant excimer emissions around 500 nm. Nevertheless, compared with our previous result of metallo-homopolymers containing CAZ pendants, OXD pendants in all metallo-polymers **P1-P4** did not suppress the excimer formation efficiently, which might be due to more flexible pendent configurations (with lower Tg values) of metallo-polymers containing 1,3,4-OXD pendants in comparison with those containing CAZ pedants.
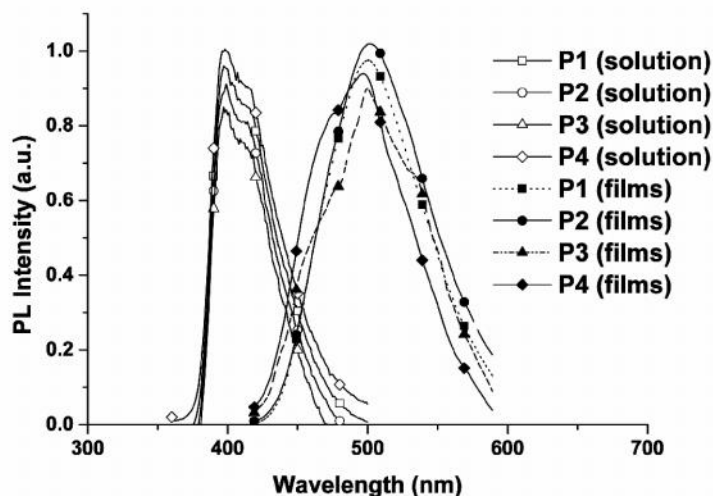
Figure 4.7 Normalized PL spectra of metallo-polymers **P1-P4** in solutions and solid films.

4.4.7 Electroluminescence (EL) Properties

Two device configurations were applied in the EL measurements, where the metallo-polymers were used as an emission layer and PEDOT: PSS was utilized as a hole transporting layer. Either TPBI or BCP/ALQ was used as an electron transporting layer, and the results are separately discussed as follows:

(a) ITO/PEDOT:PSS/Polymer(**P1-P2**)/TPBI/LiF/Al Devices. Good photoluminescence properties exhibited by solutions of metallo-polymers **P1** and **P2** suggest both polymers are suitable candidates for fabrication of PLED devices, and devices with configurations of ITO/PEDOT:PSS(40-55 nm)/Polymer(**P1**-**P2**) (50-65 nm)/TPBI (40 nm)/LiF (1 nm)/Al (150 nm) were fabricated.
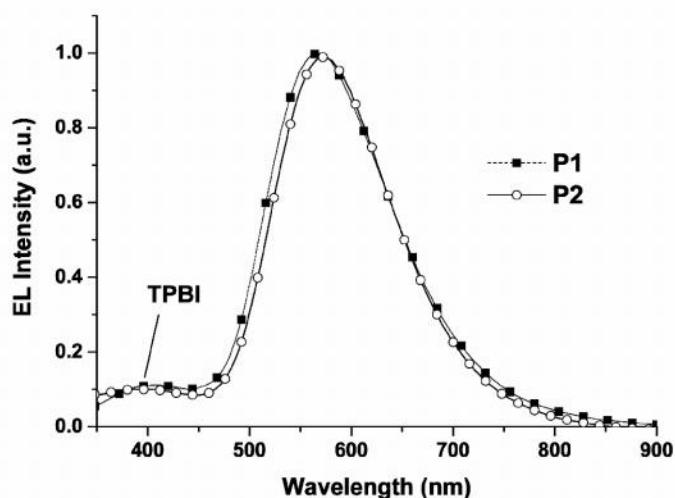
Figure 4.8 Normalized EL spectra of PLED devices with configurations of
ITO/PEDOT:PSS/Polymer (**P1**-**P2**)/TPBI/LiF/Al at 10 V.

Figure 4.8 shows normalized EL spectra of metallo-polymers **P1** and **P2**, and an emission band around 570 nm and a small shoulder around 400 nm originated from TPBI emissions were observed.[90,100] It is worthy of noting that the EL spectra of PLED devices do not resemble their corresponding PL spectra in solid films (as shown in Figure 4.7). This is presumably due to the EL and PL emissions originating from different excited states and/or ground states.[63c,84] In comparison with the HOMO values of polymers **P1** (-6.26 eV) and **P2** (-6.20 eV), TPBI (-6.20 eV) layer could not block holes from emitters sufficiently for polymers **P1** and **P2** in the PLED devices[90-100], so they exhibited very similar results to each other. Hence, no further investigation has been done in the other TBPI-based PLED devices regarding polymers **P3** and **P4**.

(b) ITO/PEDOT:PSS/Polymer/BCP/ALQ/LiF/Al Devices. Green EL emissions were obtained for all metallo-polymers with configurations of ITO/PEDOT:PSS (40-55 nm)/Polymer(**P1-P4**) (50-65 nm)/BCP (10 nm)/ALQ (30 nm)/LiF (1nm)/Al (150 nm), and the electroluminescence properties are listed in Table 4.3. Figure 4.9 illustrates the normalization EL spectra of metallo-polymers **P1-P4** with emission bands around 550 nm.

Similarly, the EL spectra of BCP/ALQ devices do not resemble their corresponding PL spectra in solid films due to the same reason as explained in the TPBI-based PLED devices. At a bias voltage of 10 V, all PLED devices in Figure 4.9 show green emissions with $_{max,EL}$ values around 550 nm and their EL intensities were enhanced by increasing the bias voltages.

Table 4.3 Electroluminescence (EL) Properties of PLED Devices[a] Containing a Layer of Emitting Metallo-Polymers **P1-P4**.

Polymer	$_{max,EL}$ (nm)	V_{on} (V)[b]	Max. Luminescence (cd/m^2) (V)	Power Efficiency (cd /A) [c]	CIE Coordinates (x and y)
P1	549	6.5	2913 (14.5)	1.12	(0.41,0.52)
P2	549	6.5	3550 (15)	1.35	(0.41,0.52)
P3	551	6.0	3320 (15)	1.25	(0.41,0.55)
P4	550	6.5	2313 (14.5)	1.05	(0.41,0.52)

[a] Device structure: ITO/PEDOT:PSS/Polymer(**P1-P4**)/BCP/ AlQ/LiF/Al, where the metallo-polymer (**P1-P4**) is an emitting layer.

[b] V_{on} is the turn-on voltage.

[c] Power efficiencies were obtained at 100 mA/cm^2.
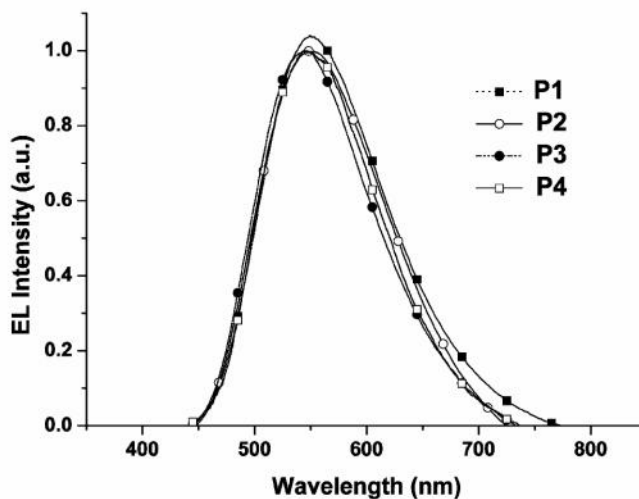
Figure 4.9 Normalized EL spectra of PLED devices with configurations of ITO/PEDOT:PSS/Polymer (**P1**-**P4**)/BCP/ALQ/LiF/Al at 10 V.

The turn-on voltages of all PLED devices based on BCP/ALQ were approximately 6.0-6.5 V. The power efficiency and maximum luminance of PLED devices for all polymers were

ranged from 1.05 to 1.35 cd A^{-1} (at 100 mA cm^{-2}) and 2313-3550 cd m^{-2} (at 14-15 V), respectively. The current density-voltage (*I-V*) and luminance-voltage (*L-V*) characteristic curves of PLED devices containing metallo-polymers **P1-P4** are shown in Figures 4.10 and 4.11, and similar turn-on voltages for both current density and luminance demonstrate that a matched balance of both injection and transportation in charges were achieved,[56c] which were much improved in contrast to TPBI-based PLED devices. The BCP layer (HOMO = -6.70 eV, LUMO = -3.20 eV) can offer a large hole barrier between BCP and the emitter but show no influence on electron-transporting behavior of ALQ (HOMO = -6.00 eV, LUMO = -3.30 eV).[101] As shown in Figure 4.11, it indicates that no ALQ emission band was observed. The EL spectra of BCP/ALQ-based devices (polymers **P1** and **P2**) revealed less Stocke shifts (ca. 20 nm) than those of TPBI-based devices. The different timing for the charge arriving at the emitter region may be related to different electron mobilities for these two transporting materials.[90,101] From this result, it can be concluded that the incorporation of electron-transporting (OXD) or hole-transporting (CAZ) pendants into polymer backbones can improve the EL performance of the PLED devices.[66]
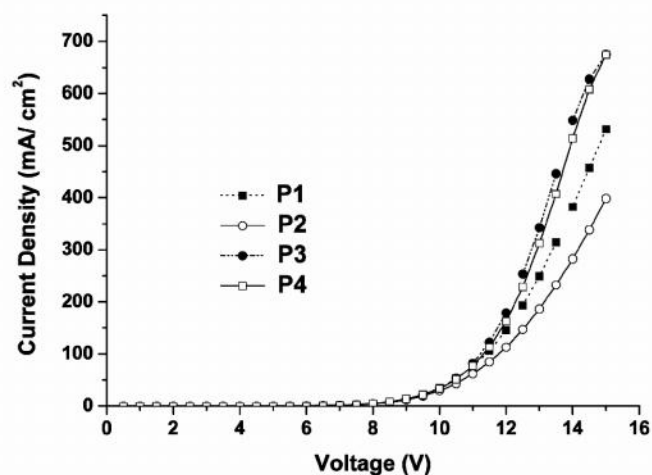
Figure 4.10 Current density-voltage (*I-V*) curves of PLED devices with configurations of ITO/PEDOT:PSS/Polymer (**P1**-**P4**)/BCP/ALQ/LiF/Al.
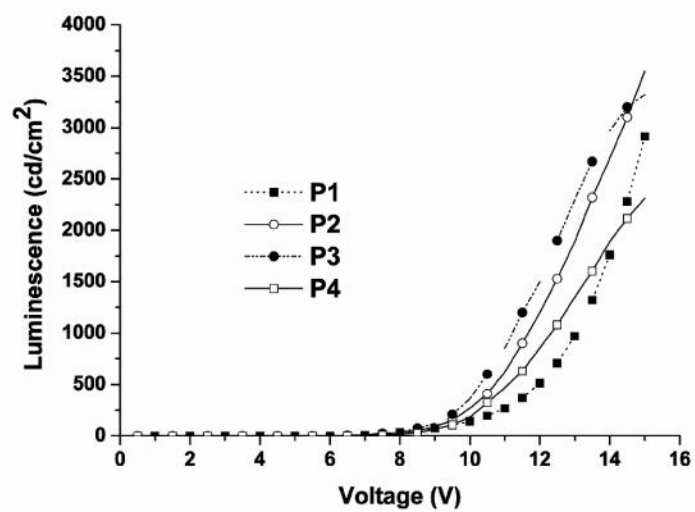
Figure 4.11 Luminance-Voltage (*L-V*) curves of PLED devices with configurations of ITO/PEDOT:PSS/Polymer (**P1**-**P4**)/BCP/ALQ/LiF/Al.

4.5 Conclusion

In summary, a series of novel poly(fluorene/ethynylene/(terpyridyl)zinc(II))-based metallo-polymers containing 1,3,4-OXD pedants were obtained by different stoichiometric ratios of complexes. Furthermore, the thermal, photophyscial, and electroluminescence properties are greatly affected by the nature of the pendent groups in the C-9 position of fluorene via long alkyl spacers. The incorporation of various pendants into polymer backbones will change the rigidities and the thermal stability (as well as the Td and Tg values) of the metallo-polymers. In comparison with metallo-polymers containing alkyl pendants, the quantum yields were greatly enhanced by introducing 1,3,4-OXD pendants but reduced by carbazole (CAZ) pendants. The enhancement of PL quantum yields by the introduction of 1,3,4-OXD pendants into metallo-polymers is due to the energy transfer happened between pedants and polymer backbones. By utilization of these metallo-polymers as emitting materials to fabricate PLED devices, green EL emissions and high EL performance can be obtained in the double-heterojunction device structures with PEDOT as the hole transporting material and either TPBI or BCP/ALQ as the electron transporting material.

Chapter 5

Synthesis and Characterization of Metallo-Polymers for Light-Emitting and Photovoltaic Applications: Facile Self-Assembly of Fluorene/Phenothiazine Building Blocks and Zn(II)/Ru(II) Metal Ions

5.1 Abstract

Various supramolecular structures of metallo-polymers **P1**-**P4** were produced by coordination of Zn^{2+} and Ru^{2+} metal ions with two ditopic receptor monomers **4a** and **4b**, which were composed of two terminal terpyridyl (tpy) units connected through ethynylene bridges with central fluorene and phenothiazine units, correspondingly. In order to verify the metallo-polymeric structures, UV-visible and photoluminescence (PL) spectral titration experiments were carried out by varying the coordination molar ratios of metal ions (Zn^{2+}/Ru^{2+}) to monomers. Enhancement of thermal stability (T_d) was introduced by the coordination polymerization which offered valuable properties for the applications of polymer light-emitting diodes (PLEDs) and polymer photovoltaic cells (PPVCs). The photophysical properties of polymers **P1** and **P2** exhibited blue PL emissions (around 398 and 450 nm, respectively) with quantum yields of 26-36 % (in DMF). However, due to metal-to-ligand charge transfer (MLCT) transitions in polymers **P3** and **P4**, no PL emissions were observed in solid films. Electroluminescent (EL) devices with polymers **P1** and **P2** as emitters showed green and red EL emissions (around 567 and 682 nm, respectively), with the maximum efficiencies of 0.29-0.32 cd/A (at 100 mA/cm^2), and the maximum luminances of 578-618 cd/m^2 (around 15 V), respectively. The active layers of PPVCs were made from composite films of polymers **P3** and **P4**, individually, blended with fullerene derivative

[6,6]-phenyl C_{61}-butyric acid methyl ester (PCBM) at the ratio of 1:3 (by wt. ratio). Under AM 1.5 solar simulator (at 100 mW/cm^2), the values of energy conversion efficiency (ECE) of PPVCs containing active polymer mixtures of PCBM and polymers **P3**-**P4** were 1.7×10^{-4} % and 2.5×10^{-4} %, respectively.

5.2 Introduction

In recent years, polymeric and organic materials have attracted increasing attention for the electro-optical applications of light-emitting diodes (PLED) and photovoltaic cells (PVCs).[102-103] Compared with inorganic materials, polymers have the benefits of easy process (spin-coating of thin films) and low cost of fabrication. However, solubility of conjugated polymers is often low and purification is always difficult after polymerization, and disruption of conjugation lengths by defective linkages cannot be avoided.

Metal-ligand coordination seems to open an alternative path to produce conjugated polymers,[47c,55a,93,104] and 2,2':6',2"-terpyridine (tpy) ligands are ideally suitable for the construction of coordination polymers.[105] Three chelating pyridyl units in a tpy ligand offer a supplementary increase of the binding constant, and the formation of octahedral 2:1 ligand-metal complexes does not give rise to enantiomers. In particular, by proper selections of metal-ligand combinations, it is possible to realize ideal conditions for self-assembly, i.e., formation of kinetically labile but nevertheless thermodynamically stable bonds. Additionally, the easy synthetic access of 4'-substituted tpy derivatives offers the possibility for the construction of perfectly linear rods or dendrimers in coordination polymers.[23,52] Constable et al. have developed the concept concerning the utilization of dipotic tpy ligands as building blocks of coordination oligomers and polymers.[51a]

In the past years, a large number of tpy complexes containing Zn^{2+} or Ru^{2+} metal ions as photoactive species, as well as coordination polymers built up from tpy ligands, have been introduced by several research groups.[59b,106] In our previous reports,[84] a series of terpyridyl-Zn(II) metallo-polymers containing polyfluorene backbones as emitters were fabricated into PLED devices with multilayer structures. It was found that metallo-polymers incorporating lateral pendant groups with the main-chains of terpyridyl-Zn(II) complexes showed the maximum luminescences and the power efficiencies ranged from 1704-2819 (cd/m^2) and 0.85-1.11 (cd/A), respectively. Recently, dye-sensitized solar cells based on

terpyridyl-Ru(II) complexes have also been fabricated, and the energy conversion efficiency (ECE) in excess of 10 % has been achieved as a liquid electrolyte is used.[106a] However, the presence of liquid electrolytes inside the cells seriously limits the industrial development of regarding technology due to the poor long-term stability of the liquid cells. Several strategies have been tested to replace the liquid electrolyte by another solid polymer electrolyte, i.e. inorganic and organic hole-transporting materials.[106b,106c] Recently, Chan and co-workers have reported that conjugated metallo-polymers (Ru-PPVs) containing terpyridyl-Ru(II) complexes were blended with sulfonated polyaniline (SPAN) for the fabrication of multilayer PVCs by a layer-by-layer deposition method., where the short-circuit currents were around 7.5–32.9 $\mu A/cm^2$ and the ECE values were ranged from 0.95×10^{-3} to 4.4×10^{-3} %.[106c]

In this text, a series of terpyridyl-Zn(II)/Ru(II) metallo-polymers, including fluorene and phenothiazine units as building blocks, were constructed by self-assembled reaction. In addition, the thermal, photophysical, and electrochemical properties were also investigated. Finally, terpyridyl-Zn(II) metallo-polymers were utilized in the applications of PLEDs due to the prominent photoluminescent (PL) and electroluminescent (EL) properties. Moreover, the PVC applications of terpyridyl-Ru(II) metallo-polymers blended with fullerene derivative [6,6]-phenyl C_{61}-butyric acid methyl ester (PCBM) were also studied.

5.3 Experiment

5.3.1 Measurements

^{1}H NMR spectra were recorded on a Varian Unity 300 MHz spectrometer using $CDCl_3$ and

DMSO-d_6 solvents. Elemental analyses were performed on a HERAEUS CHN-OS RAPID

elemental analyzer. Phase transition temperatures were determined by differential scanning

calorimetry (DSC, Model: Perkin Elmer Diamond) with a heating and cooling rate of 10

°C/min. Thermogravimetric analyses (TGA) were conducted on a Du Pont Thermal Analyst

2100 system with a TGA 2950 thermogravimetric analyzer at a heating rate of 10 °C/min

under nitrogen. Viscosity measurements were proceeded by 10 % weight of polymer

solutions (in NMP) in contrast to that proceeded by monomer solutions under the same

condition (with viscosity   = 6 cp) on a BROOKFILEL DV-III+ RHEOMETER system at 25

°C (100 RPM, Spindle number: 4). UV-visible (UV-vis) absorption spectra were recorded in

dilute DMF solutions (10^{-5} M) on a HP G1103A spectrophotometer, and fluorescence spectra

were obtained on a Hitachi F-4500 spectrophotometer. Fluorescence quantum yields were

determined by comparing the integrated photoluminescence (PL) density of coumarin-1 in

ethanol with a known quantum yield (ca. 5 x 10^{-6} M, quantum yield = 0.73). Cyclic

voltammetry (CV) was performed at a scanning rate of 100 mV/s on a BAS 100 B/W

electrochemical analyzer, which was equipped with a three-electrode cell. Pt wire was used

as a counter electrode, and an Ag/AgCl electrode was used as a reference electrode in the CV

measurements. The CV experiments were performed at a scanning rate of 100 mV/s by solid

samples immersed into electrochemical cells containing a 0.1 M tetrabutylammonium

hexafluorophosphate (Bu_4NPF_6) solutions (in DMF) at room temperature under nitrogen.

Polymer solid films were spin-coated on quartz substrates from DMF solutions with a

concentration of 10 mg/ml. UV-vis and PL titrations were preformed by that 1.0 x 10^{-5} M of

monomer solutions in the solvent of EtOH were titrated with 50 µl aliquots of 3.9 x 10^{-4} M

solutions containing metal salts $Zn(OAc)_2$ and $RuCl_3·3H_2O$ in the solvent of EtOH. The

addition was done stepwise and the formation of Zn(II)- and Ru(II)-coordination polymers was monitored by UV-vis spectroscopy, respectively.

Fabrication of PLED Devices. EL devices with the configuration of ITO/PEDOT:PSS(40-50 nm)/polymer (**P1-P2**) (50-70 nm)/BCP(10 nm)/AlQ(30 nm)/LiF(1 nm)/Al(150 nm) were made, where BCP (i.e., 2,9-dimethyl-4,7-diphenyl-1,10-phenanthroline) or AlQ (i.e., tris(8-hydroxyquinoline)aluminium) was used as an electron transporting layer. The ITO substrates were routinely cleaned by ultrasonic treatments in detergent solutions and diluted water, followed by rinsing with acetone and then ethanol. After drying, the ITO substrates were kept in oxygen plasma for 4 min before being loaded into the vacuum chamber. The solutions (10 mg/ml) of light-emitting materials in DMF were spin-coated on glass slides precoated with indium tin oxide (ITO) having a sheet resistance of ~20 /square and an effective individual device area of 3.14 mm^2. The spin coating rate was 6000 rpm for 60 s with PEDOT: PPS, 4000 rpm for 60 s with resulting polymers, and the thicknesses of PEDOT: PPS and polymers were measured by an Alfa Step 500 Surface Profiler (Tencor). BCP and AlQ layers were thermally deposited at a rate of 1-2 Å/s under a pressure of ~2 x 10^{-5} torr in an Ulvac Cryogenic deposition system. Under the same deposition systems and conditions, one layer of LiF was thermally deposited as a cathode at a rate of 0.1-0.2 Å/s, which was followed by capping with an aluminum layer. The *I-V* characteristics in the dark and under illumination were measured with Keithley 236 source meter.

Fabrication of PPVC Devices. Polymer photovaltic cell (PPVC) devices were made from composite films of polymers **P3** and **P4** blended with fullerene derivative [6,6]-phenyl C$_{61}$-butyric acid methyl ester (PCBM), respectively, at a ratio of 1:3 (by wt. ratio) as an active layer. PPVC devices with the configuration of ITO/PEDOT:PSS(40-50 nm)/polymer (**P3-P4**):PCBM(65-75 nm)/LiF(1 nm)/Al(150 nm) were fabricated, and the photocurrents were measured under a solar simulator with AM 1.5 illumination (at 100 mW/cm^2).

5.3.2 Materials.

Chemicals and solvents were reagent grades and purchased from Aldrich, ACROS, TCI, and Lancaster Chemical Co. Solvents were purified and dried according to standard procedures. Chromatography was performed with Merck silica gel (mesh 70-230) and basic aluminum oxide, which was deactivated with 4 wt% of water. Compounds **1a, 1b,** and 4'-[[(trifuroromethyl)sulfonyl]oxy]-2,2':6',6''-terpyridines were prepared and purified according to literature procedures.[54a,84,107] The synthetic routes of monomers and metallo-polymers are illustrated in Schemes 1-3.

Compound 2a. To a solution of compound **1a** (32 mmol) in 60 mL of THF/Et$_3$N (1/1), 3-methyl-1-butyn-3-ol (96 mmol) was added. After the solution was degassed with nitrogen for 30 min, Pd(PPh$_3$)$_2$Cl$_2$ (0.32 mol), PPh$_3$ (13 mol), and CuI (3.2 mmol) were added. The reaction was then refluxed at 70 °C under N$_2$ for 12 h. The solvent was removed under reduced pressure. The resulting solid was extracted with CH$_2$Cl$_2$/H$_2$O then dried over MgSO$_4$. The crude product was purified by column chromatography (silica gel, hexane/ethyl acetate = 4/1) to afford a white solid. mp 97-98 °C. ^{1}H NMR (300 MHz, CDCl$_3$): 7.59 (d, J = 8.4 Hz, 2H), 7.37-7.41 (m, 4H), 2.09 (s, 2H), 1.90-1.95 (m, 4H), 1.66 (s, 12H), 0.57-0.67 (m, 10H). Yield: 83%. FABMS: m/e 414; C$_{29}$H$_{34}$O$_6$ requires m/e 414.26.

Compound 2b. To a solution of compound **1b** (28 mmol) in 60 mL of THF/Et$_3$N (1/1), 3-methyl-1-butyn-3-ol (84 mmol) was added. After the solution was degassed with nitrogen for 30 min, Pd(PPh$_3$)$_2$Cl$_2$ (0.28 mmol), PPh$_3$ (11 mmol), and CuI (2.8 mmol) were added. The reaction was then refluxed at 70 °C under N$_2$ for 12 h. The solvent was removed under reduced pressure. The resulting solid was extracted with CH$_2$Cl$_2$/H$_2$O then dried over MgSO$_4$. The crude product was purified by column chromatography (silica gel, hexane/dichloromethane = 3/1) to afford a yellow solid. mp 82-83 °C. ^{1}H NMR (300 MHz, CDCl$_3$): 7.12-1.18 (m, 4H), 6.71 (d, J = 8.4 Hz, 2H), 3.77 (t, J = 6.6 Hz, 2H), 2.11 (br, 2H), 1.73-1.76 (m, 2H), 1.59 (s, 12H), 1.29-1.45 (m, 6H), 0.86 (t, J = 6.6 Hz, 3H). Yield: 82%.

FABMS: *m/e* 447; $C_{28}H_{33}NO_2S$ requires *m/e* 447.22.

Compound 3a. A mixture of compound **2a** (1.63 mmol) and KOH (6.5 mmol) in 60 mL of 2-propanol was refluxed under N_2 with a vigorous stirring for 3 h. The solvent was then removed and crude product was purified by column chromatography (silica gel, hexane) to afford a white solid. mp 147-148 °C. ^{1}H NMR (300 MHz, CDCl$_3$): 7.63 (d, *J* = 8.4 Hz, 2H), 7.47-7.49 (m, 4H), 3.16 (s, 2H), 1.90-1.96 (m, 4H), 0.59-0.69 (m, 10H). Yield: 76%. FABMS: *m/e* 298; $C_{13}H_{22}$ requires *m/e* 298.17.

Compound 3b. A mixture of compound **2b** (1.21 mmol) and KOH (4.9 mmol) in 50 mL of 2-propanol was heated to reflux under N_2 with a vigorous stirring for 3 h. The solvent was then removed and crude product was purified by column chromatography (silica gel, hexane) to afford a yellow solid. mp 109-110 ℃. 7.13-1.18 (m, 4H), 6.67 (d, *J* = 8.4 Hz, 2H), 3.79 (t, *J* = 6.7 Hz, 2H), 3.12 (s, 2H), 1.72-1.9 (m, 2H), 1.30-1.46 (m, 6H), 0.86 (t, *J* = 6.6 Hz, 3H). Yield: 74%. FABMS: *m/e* 331; $C_{22}H_{21}NS$ requires *m/e* 331.14.

Monomer 4a. Compound **3a** (0.5 mmol) and 4'-[[(trifuroromethyl)sulfonyl]oxy]-2,2':6',6''-terpyidine (1.1 mmol) were dissolved in nitrogen-degassed benzene, then [Pd^0(PPh$_3$)$_4$] (0.06 mmol) was added and followed by nitrogen-degassed ^{i}Pr$_2$NH. The solution was then heated to react at 70 °C. After complete consumption of starting materials, the solvent was evaporated and the product was purified by column chromatography (alumina, hexane/dichloromethane = 8/1 in vol.) to afford a yellow solid. mp 212-213 °C. ^{1}H NMR (300 MHz, CDCl$_3$): 8.73 (d, *J* = 4.2 Hz, 4H), 8.62-8.65 (m, 8H), 7.88 (t, *J* = 8.4 Hz, 4H), 7.72 (d, *J* = 7.8 Hz, 2H), 7.59-7.61 (m, 4H), 7.34-7.38 (m, 4H), 2.01-2.03 (m, 4H), 0.70 (br, 10H). Yield: 78%. FABMS: *m/e* 761; $C_{53}H_{40}N_6$ requires *m/e* 760.33. Anal. Calcd for $C_{53}H_{40}N_6$: C, 83.66; H, 5.30; N, 11.04. Found: C, 83.98; H, 5.77; N, 11.36.

Monomer 4b. Compound **3b** (1.1 mmol) and 4'-[[(trifuroromethyl)sulfonyl]oxy]-2,2':6',6''-terpyidine (2.1 mmol) were dissolved in

nitrogen-degassed benzene, then [Pd^0(PPh$_3$)$_4$] (0.12 mmol) was added and followed by nitrogen-degassed ^{i}Pr$_2$NH. The solution was then heated to react at 70 °C. After complete consumption of starting materials, the solvent was evaporated and the product was purified by column chromatography (alumina, hexane/dichloromethane = 12/1 in vol.) to afford a yellow solid. mp 189-190 °C. ^{1}H NMR (300 MHz, CDCl$_3$): 8.71 (d, J = 4.2 Hz, 4H), 8.55-8.61 (m, 8H), 7.86 (t, J = 7.8 Hz, 4H), 7.30-7.36 (m, 8H), 6.82 (d, J = 8.7 Hz, 2H), 3.85 (t, J = 6.9 Hz, 2H), 1.79-1.84 (m, 2H), 1.31-1.47 (m, 6H), 0.89 (br, 3H). Yield: 75%. FABMS: m/e 793; C$_{52}$H$_{39}$N$_7$S requires m/e 793.3. Anal. Calcd for C$_{52}$H$_{39}$N$_7$S : C, 78.66; H, 4.95; N, 12.35. Found: C, 79.07; H, 5.22; N, 12.78.

Synthetic Procedures of Metallo-Polymers (P-P4). P1. To a solution of monomer **4a** (0.52 mmol) in 30 ml of NMP, Zn(OAc)$_2$ (0.52 mmol) in NMP (10 ml) was dropwise added. The resulting solution was heated to react at 105 °C under a nitrogen atmosphere. After stirring for 24 h, excess KPF$_6$ was added into the hot solution. The resulting solution was poured into methanol and the precipitate obtained was purified by repeated precipitations using NMP and ether. The polymer was dried under vacuum at 60 °C for 24 h and collected as yellow solids. ^{1}H NMR (300 MHz, DMSO-d_6): 9.34 (br, 4H), 8.95 (br, 4H), 8.30 (br, 4H), 7.81-7.98 (m, 10H) 7.54 (br, 4H), 2.16-2.19 (m, 4H), 0.76 (br, 10H). Yield: 74-80 %.

P2. The procedure is analogous to that described for **P1.** Yields: 80-82 %. ^{1}H NMR (300 MHz, DMSO-d_6): 9.22 (br, 4H), 8.91 (br, 4H), 8.27 (br, 4H), 7.96 (br, 4H), 7.51-7.62 (m, 8H), 7.22 (br, 2H), 4.02 (br, 2H), 1.76 (br, 2H), 1.32-1.46 (m, 6H), 0.87 (br, 3H). Yield: 76-79%.

P3. To a suspension of RuCl$_3$·3H$_2$O (0.66 mmol) in ethanol (10ml) was added monomer **4a** (0.66 mmol) in NMP (30ml), and the suspension was heated 3 h under reflux at 105 °C under nitrogen atmosphere. Excess AgBF$_4$ (silver tetrafluoroborate) was added to the mixture together with acetone (5ml), and the reflux was continuted for 24 h. The resulting product was allowed to cool at room temperature, and the AgCl (silver chloride) was removed by

filitration. The block filtrate was concertrated, and after addition of saturated KPF$_6$ water solution than a block precipitate appeared. The precipitate obtained was purified by repeated precipitations using DMAc and ether. The polymer was dried under vacuum at 60 °C for 24 h and collected as a black solid. ^{1}H NMR (300 MHz, DMSO-d_6):   8.96 (br, 8H), 8.80 (br, 4H), 8.49 (br, 4H), 7.91-8.08 (m, 8H), 7.95 (br, 2H), 2.15 (br, 4H), 0.66 (br, 10H). Yield: 73-76 %.

P4. The procedure is analogous to that described for **P3.** ^{1}H NMR (300 MHz, DMSO-d_6): 8.91 (br, 8H), 8.74 (br, 4H), 8.42 (br, 4H), 8.03 (br, 2H), 7.85 (br, 4H), 7.61 (br, 4H), 4.43 (br, 2H), 1.73(br, 2H), 1.50 (br, 2H), 1.33 (br, 4H), 0.87 (br, 3H). Yield: 69-72 %.

5.4 Results and Discussion

5.4.1 Synthesis and Characterization.

The synthetic routes of monomers **4a-4b** and a series of metallo-polymers **P1-P4** are illustrated in Schemes 5.1-5.2. According to Scheme 5.1, monomers **4a** and **4b** were synthesized from compounds **1a-1b** reacted with propargylic alcohol via the Sonogashira coupling reaction, and further deprotected by refluxing 2-propanol in a basic condition. Then, a cross-coupling reaction between **3a-3b** and 4'-[[(trifluoromethyl)sulfonyl]-oxy]-2,2':6',2"-terpyridine in the presence of a catalytic amount of Pd(0) complexes under a basic condition to obtain monomers **4a-4b**.[56d]

Scheme 5.1 Synthetic Routes of Monomers **4a (M1)** and **4b (M2)**
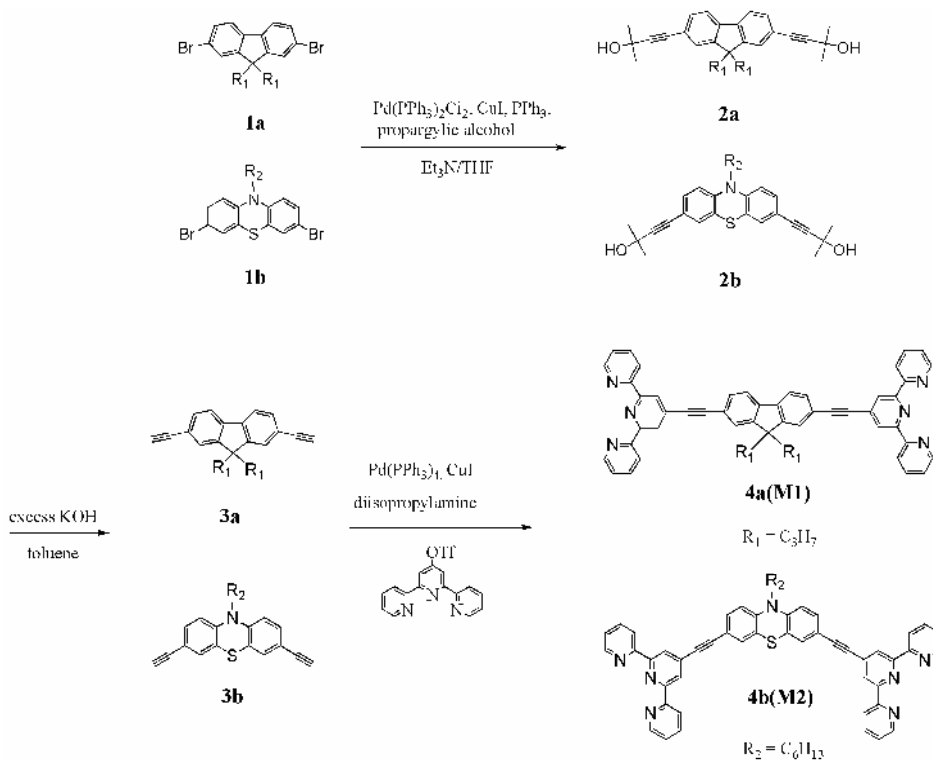
Polymers **P1-P2** were obtained by refluxing monomers **4a** and **4b** with $Zn(OAc)_2$, respectively, at a molar ratio of 1:1 in NMP solutions and followed by subsequent anion exchanges, where Zn^{2+} ions from $Zn(OAc)_2$ were used to prepare for the terpyridyl-Zn(II) metallo-polymers.[84] Furthermore, terpyridyl-Ru(II) metallo-polymers **P3-P4** were

synthesized according to the procedures similar to those of polymers **P1**-**P2**.[57b]

Scheme 5.2 Synthetic Routes of Metallo-Polymers **P1-P4**
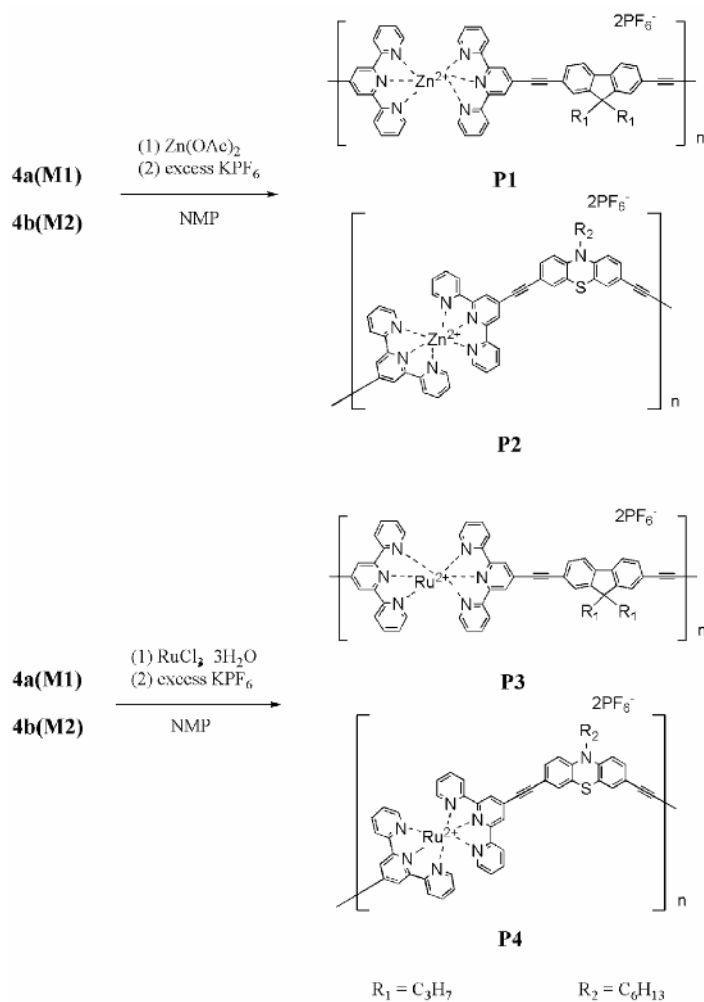
5.4.2 Thermal and Viscosity Properties.

The thermal and viscosity properties of monomers **4a**-**4b** and polymers **P1-P4** were studied by thermogravimertric analyses (TGA) and rheometer as summarized in Table 5.1. The decomposition temperatures (T_d) (5% weight loss measured by TGA) of these polymers under a nitrogen atmosphere were ranged from 291 to 353 °C. In contrast to monomers, polymers exhibited slightly enhanced thermal stability due to the increased rigidity of the main-chain structures.[55a] Moreover, polymers **P2** and **P4** showed lower T_d values than those

of the other linear polymers **P1** and **P3** due to the bent structures of backbones in **P2** and **P4**, which are originated from the bent configuration of the phenothiazine units and thus to reduce the rigidity of the polymers.[48c,55b]

To further confirm the structures of metallo-polymers, molecular weights of these metallo-polymers should be investigated. However, these polymers showed poor solubilities in THF, CH₃Cl, and alcoholic solvents, so standard measurements of molecular weights by GPC (gel permeation chromatography) could not be proceeded. Therefore, the relative viscosities of polymers to monomers were carried out to support the polymer structures. Solutions of monomers **4a**-**4b** (10 % wt. ratio) in NMP with viscosity   = 6 cp at 25 °C were used as references to compare with the viscosities of polymers. In comparison with the viscosity values of monomers **4a**-**4b**, polymers **P1**-**P4** exhibit increased viscosity values (viscosity   = 9-11 cp as shown in Table 5.1) by adding metal ions, and the relative viscosities of polymers to monomers were in the range of 1.50-1.66 cp. Similar phenomena were also reported in our previous study.[84]

5.4.3 Electrochemical Properties.

The electrochemical properties of polymers, as summarized in Table 5.1, were studied by cyclic voltammetry (CV), and the lowest unoccupied molecular level (LUMO) energy levels were estimated from reduction potentials by the reference energy level of ferrocene (4.8 eV below the vacuum level) according to the following equation:[58] $E^{LUMO} = [-(E^{onset} - 0.45) - 4.8]$ eV. The optical band gaps (ranged from 2.02 to 3.16 eV) were estimated from absorption spectra in DMF solutions by extrapolating the tails of the lowest energy peaks. Polymers **P1**-**P4** exhibited reversible reduction peaks in the range of -1.44 to -1.47 V in cathodic scans up to -3 V, and these peaks were attributed to the reduction of terpyrdiyl-based moieties.[84,105a] For example, the first reduction peak (-1.13 V) of polymer **P2** was assigned to the reduction of the central phenothiazine/enthylene groups, and the

second one was attributed to that of the tpy moieities. Interestingly, in contrast to **P1**, polymer **P3** exhibited additional less negative reduction peaks (around -0.24 and -1.07 V) by coordination with Ru^{2+} ions, which is in agreement with the different electron-withdrawing abilities of metal ions (Zn^{2+}/Ru^{2+}) and tpy ligands. Nevertheless, the first reduction peak (-1.16 V) of polymer **P4** occurs at almost the same potential as the first reduction peak of polymer **P2**. Moreover, in contrast to **P1** and **P3**, polymers **P2** and **P4** revealed lower optical band gaps due to the central phenothiazine components from their spectral responded near-infrared (NIR) regions.[105a,108]

Table 5.1 Physical Properties of Polymers P1-P4

Compound	T_d (°C) [a]	(cp) [b,c]	$E^{red/peak}$ (V) [d]	E^{LUMO} (eV) [e]	Band Gap (eV) [f]
P1	332	11	-1.45(r),-1.96(ir)	-2.97	3.16
P2	291	11	-1.13(ir),-1.46(r) -2.01(r)	-3.05	2.61
P3	353	10	-0.24(r),-1.07(ir) -1.47(r),-2.0(ir)	-4.19	2.16
P4	306	9	-1.18(r),-1.44(r)	-3.31	2.02

[a] The decomposition temperatures (T_d) (5% weight loss) were determined by TGA with a heating rate of 20 ℃/min under N_2 atmosphere. The T_d values are 312 °C for **4a** and 245 °C for **4b**.

[b] The viscosities of polymers (10 % in weight) in NMP solutions at 25 °C (100 RPM, Spindle number: 4) were determined by rheometer system.

[c] Solutions of monomers **4a**-**4b** (10 % wt.) in NMP (with viscosity = 6 cp, 25 °C) were used as references to determine the viscosity of polymers.

[d] Reduction peaks in N_2-purged DMF, r in parentheses means reversible.

[e] LUMO energy levels were calculated from the measured reduction potentials versus ferrocene/ferrocenium couple in DMF solutions.

[f] Optical band gaps were estimated from the absorption spectra in solutions by extrapolating the tails of the lower energy peaks.

5.4.4 UV-visible and Photoluminescence (PL) Titration.

To characterize the formation of metallo-polymers **P1-P4**, titration experiments by UV-visible and photoluminescence spectra are clear ways to investigate the stepwise change of supramolecular structures. Figure 5.1 depicted that upon addition of Zn^{2+} ions to monomer **4a** reaching a molar ratio of 1:1 (Zn^{+2}:**4a**), the UV-vis spectra revealed a set of three other absorption bands at 272, 350, and 399 nm along with two isosbestic points, which suggests that an equilibrium occurred between a finite number of spectroscopically distinct species.
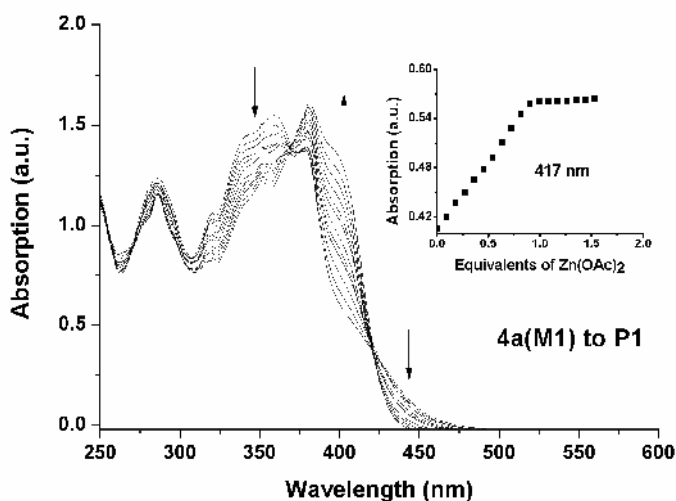
Figure 5.1 UV-vis spectra acquired (in the process of **4a** (**M1**) to **P1**) upon the titration of monomer **4a** in EtOH with solutions of $Zn(OAc)_2$. The spectra are shown at selected Zn^{+2}:**4a** (molar ratio) ranging from 0 to 1.5. The inset shows the normalized absorption at 417 nm as a function of Zn^{+2}:**4a** (molar ratio).

The titration curve (Figure 5.1, inset) showed a linear increase and an apparent saturation point at the molar ratio of 1:1 (Zn^{+2}:**4a**), indicating the formation of metallo-polymers. In the process of the formation of polymer **P2** by adding Zn^{2+} to monomer **4b** reaching a molar ratio of 1:1 (Zn^{+2}:**4b**) in Figure 5.2, the UV-vis spectra revealed a set of three other absorption bands at 272, 351, and 402 nm along with two isosbestic points, and the inset spectra also revealed the same result as the titration curves in Figure 5.1. As reported in the

previous study[84], new absorption peaks were raised due to the intra-ligand charge transfer (ILCT) in terpyridyl-Zn(II) polymers.[59b,109]
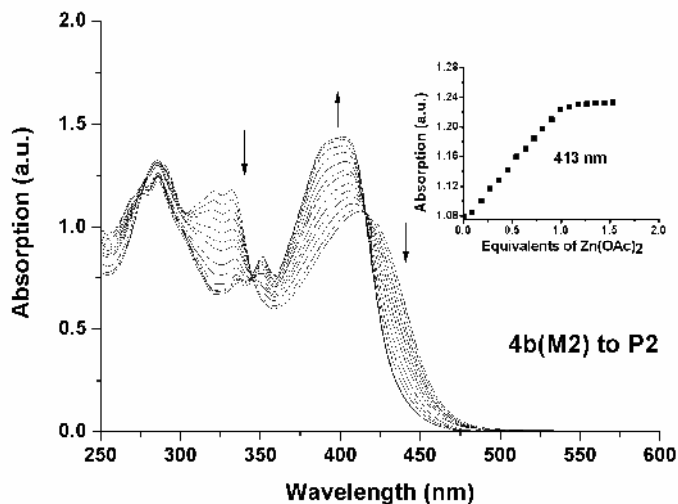
Figure 5.2 UV-vis spectra acquired (in the process of **4b** (**M2**) to **P2**) upon the titration of monomer **4b** in EtOH with solutions of Zn(OAc)$_2$. The spectra are shown at selected Zn^{+2}:**4b** (molar ratio) ranging from 0 to 1.5. The inset shows the normalized absorption at 417 nm as a function of Zn^{+2}:**4b** (molar ratio).

Moreover, the lowest absorption peaks of polymers **P1** and **P2** showed the opposite results (i.e. red-shifts for **P1** and blue-shifts for **P2**). The phenomena were attributed to the central fluorene and phenothiazine units possessing different electron push-pull effects within the terpyridyl-Zn(II) moieties, respectively.[110] Figure 5.3 depicted that upon addition of Ru^{3+} to monomer **4a** reaching a molar ratio of 1:1 (Ru^{+3}:**4a**), the UV-vis spectra revealed a small absorption shoulder at 470 nm and no isosbestic point was found, where the titration curve (Figure 5.3, inset) showed a linear increase but no sharp saturation point around a molar ratio of 1:1 (Ru^{+2}:**4a**).
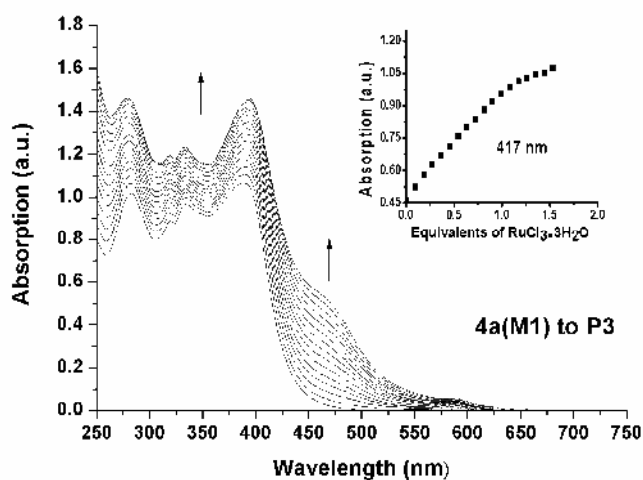
Figure 5.3 UV-vis spectra acquired (in the process of **4a** (**M1**) to **P3**) upon the titration of monomer **4a** in EtOH with solutions of $RuCl_3.3H_2O$. The spectra are shown at selected Ru^{+2}:**4b** (molar ratio) ranging from 0 to 1.5. The inset shows the normalized absorption at 417 nm as a function of Ru^{+2}:**4a** (molar ratio).

The UV-vis spectra of Figure 5.4 revealed the same results as Figure 5.3 upon addition of Ru^{3+} to monomer **4b** reaching a molar ratio of 1:1 (Ru^{+3}:**4b**). This result regarding no sharp saturation point suggested that the Ru^{3+} ion was not under going reduction process to become Ru^{2+} ion, hence, the coordination process was not observed in Uv-vis titration experiments.

Figure 5.4 UV-vis spectra acquired (in the process of **4b** (**M2**) to **P4**) upon the titration of monomer **4b** in EtOH with solutions of $RuCl_3.3H_2O$. The spectra are shown at selected Ru^{+2}:**4b** (molar ratio) ranging from 0 to 1.5. The inset shows the normalized absorption at 417 nm as a function of Ru^{+2}:**4b** (molar ratio).
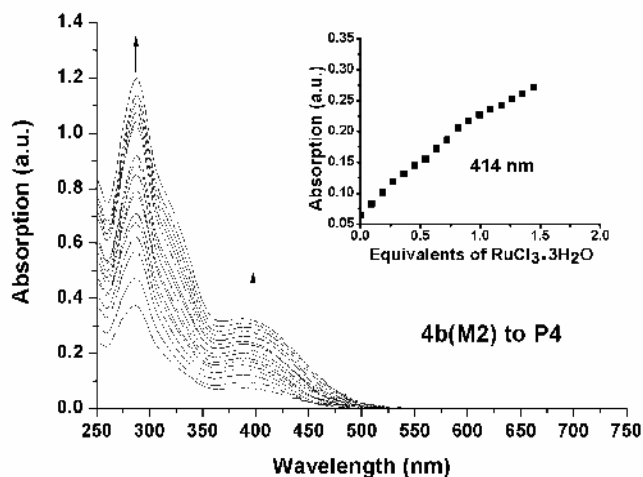
The complexation can also be followed by a photoluminescence (PL) titration experiment to further investigate PL properties of polymers **P1-P4**. In Figure 5.5, monomer **4a** showed three emission bands around 392, 418, and 447 nm. As the molar ratio of Zn^{+2}: **4a** approaching 1:1, a new emission band at 458 nm was induced. The PL quantum yields of medium complexes (the molar ratio of Zn^{+2}: **4a** gradually approaching 1:1 in the inset of Figure 5.5) were dramatically enhanced and followed by increasing the molar ratio of Zn^{+2} ions.
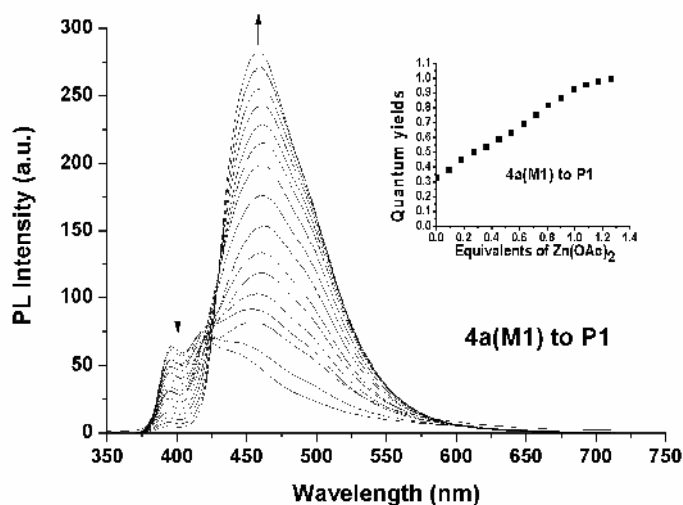
Figure 5.5 PL spectra acquired upon the titration of monomer **4a** (**M1**) in EtOH with solutions of $Zn(OAc)_2$. The spectra are shown at selected Zn^{+2}:**4a** (molar ratio) ranging from 0 to 1.3. The inset shows the quantum yields as a function of Zn^{+2}:**4a** (molar ratio).

Furthermore, the PL titration experiment of monomer **4b** showed an emission band at 558 nm in Figure 5.6. As an end point of titration was reached, polymer **P2** also displayed a significant increase in the PL quantum yield of the medium complex (the molar ratio of Zn^{+2}: **4b** gradually approaching 1:1 in the inset of Figure 5.6) and a new emission band was observed at 440 nm. In general, the results of PL titrations truly fit well to those of UV-vis titrations. On the other hand, both results of PL titration in forming terpyridyl-Ru(II) polymers **P3** and **P4** in Figures 5.7 and 5.8, respectively, revealed the same phenomena of Uv-vis titration experment, however the PL quantum yields decrease gradually as the molar

ratio of Ru^{+2}: **4a** (**4b**) gradually approaching 1:1 in the insets of Figures 5.7 and 5.8. Hence, the PL emission and quantum yields of metallo-polymers can be sufficiently controlled by coordination of different functional ligands with various metal ions.[84,111]
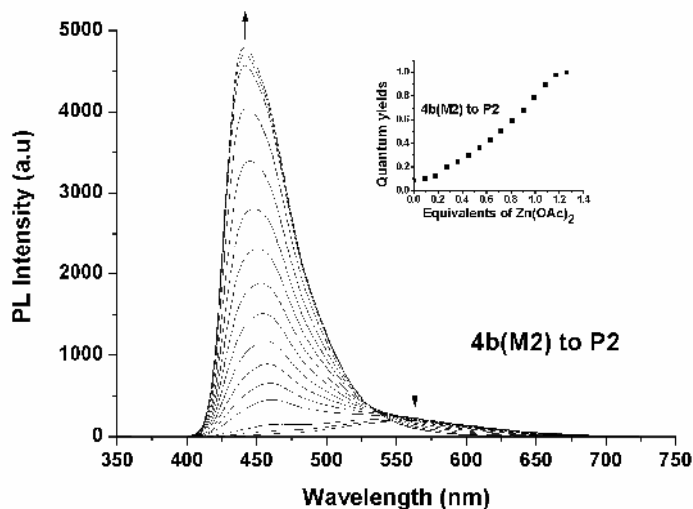
Figure 5.6 PL spectra acquired upon the titration of monomer **4b** (**M2**) in EtOH with solutions of Zn(OAc)$_2$. The spectra are shown at selected Zn^{+2}:**4b** (molar ratio) ranging from 0 to 1.3. The inset shows the quantum yields as a function of Zn^{+2}:**4b** (molar ratio).
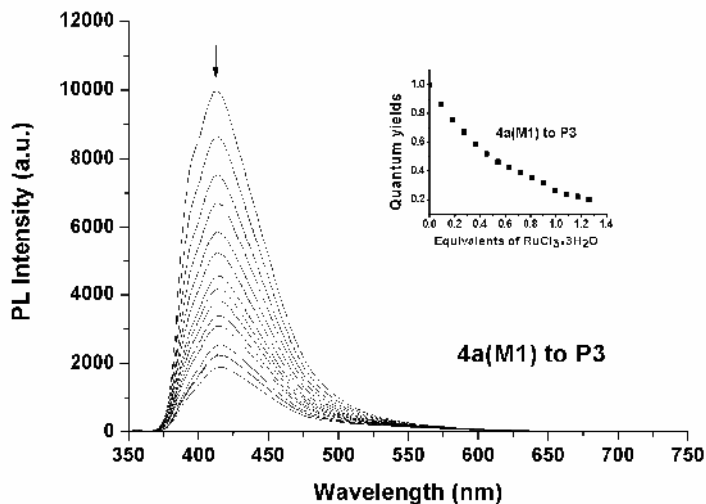
Figure 5.7 PL spectra acquired upon the titration of monomer **4a** (**M1**) in EtOH with solutions of RuCl$_3$.3H$_2$O. The spectra are shown at selected Ru^{+2}:**4a** (molar ratio) ranging from 0 to 1.3. The inset shows the quantum yields as a function of Ru^{+2}:**4a** (molar ratio).
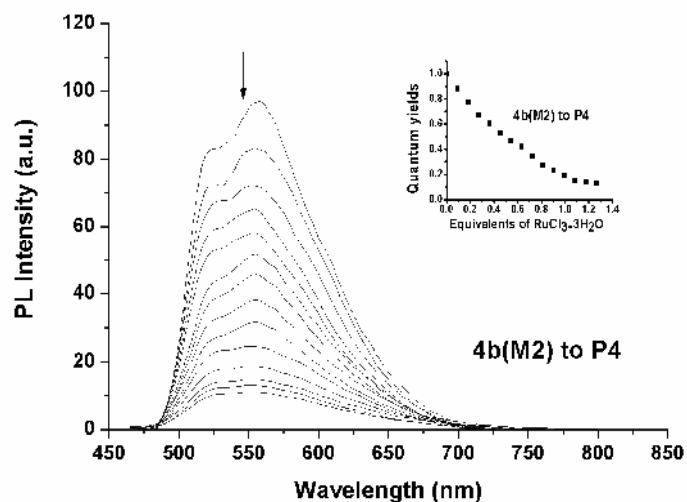
Figure 5.8 PL spectra acquired upon the titration of monomer **4b** (**M2**) in EtOH with solutions of RuCl$_3$.3H$_2$O. The spectra are shown at selected Ru^{+2}:**4b** (molar ratio) ranging from 0 to 1.3. The inset shows the quantum yields as a function of Ru^{+2}:**4b** (molar ratio).

5.4.5 Photophyscial Properties.

The photophycial characteristics of monomers **4a**-**4b** and polymers **P1-P4** were carried out by UV-vis absorption and PL emission in both dilute DMF (*N,N*-dimethylformamide) solutions (with solubility problem) and solid films, and their photophysical properties are demonstrated in Table 5.2. As shown in Figure 5.9, different absorption features of polymers **P1-P4** in DMF solutions were observed. For all polymers, they showed the ligand-centered π-π^* transitions between tpy moieties and central chromophores around 283 to 390 nm.[84,112] Both Ru^{+2} metallo-polymers **P3** and **P4** possessed the MLCT transitions, which were derived from the promotion of an electron from the metal (Ru^{+2})-centered d-orbital to unfilled ligand-centered π^* orbitals,[113] appeared at $\lambda_{Abs,sol}$ = 458, 505, and 583 nm for **P3**; $\lambda_{Abs,sol}$ = 421 and 511 nm for **P4.**

Table 5.2 Photophyscial Properties of Monomers 4a-4b and Polymers P1-P4

Compound	Abs.,sol (nm)[a]	λmax,PL,sol/ ΦPL,sol (nm)[a,b,c]	Abs.,film (nm)	λmax,PL,film (nm)
4a	284, 318, 361, 377	397(413)/0.27	--[d]	--[d]
4b	290, 400	414(396)/0.11	--[d]	--[d]
P1	286, 319, 359, 376	398(412)/0.36	242, 288, 343, 389	502
P2	291, 389	450(540)/0.26	238, 287, 344, 399	530(468)
P3	287, 329, 383, 458, 505, 583	396(412)/--[e]	290, 323, 414, 506	--[f]
P4	284, 321, 421, 511	398(413)/--[e]	292, 329, 500	--[f]

[a] Concentration of 1×10^{-6} M in DMF.

[b] Coumarin-1 in ethanol(ca. $5 * 10^{-6}$ M, quantum yield = 0.73) used as a reference to

determine the quantum yields of PL in solutions.

[c] The PL emission shoulders are shown in the parentheses.

[d] The UV-vis absorption for monomers **4a-4b** were not measured due to their poor film qualities.

[e] The quantum yields (Φ_{PL}) of PL in solutions were too small to be detected in polymers **P3** and **P4**.

[f] The PL emissions of polymers **P3** and **P4** in solid films were not detected due to their negligible emissions.

In the case of Zn^{+2}-based metallo-polymers **P1** and **P2**, the absorption bands originated from ILCT were observed without MLCT transition peaks; the MLCT of Ru^{+2} metal ions to tpy units can be excluded. As shown in Figure 5.10, the PL emissions of polymers **P1** and **P2** showed different spectra in DMF solutions, where the values of $\lambda_{max,PL}$ were 398 and 450 nm for **P1** and **P2,** respectively. They were assigned to fluorene/tpy- and phenothiazine/tpy-based fluorescence involving different π^*-π levels.
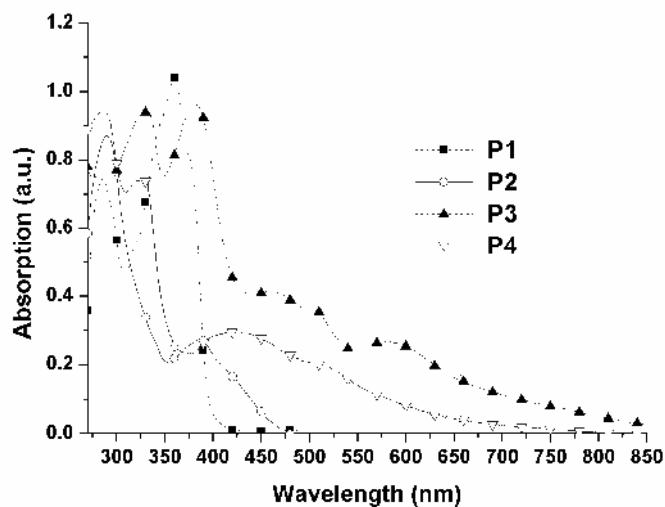
Figure 5.9 Normalized UV-vis spectra of polymers **P1-P4** in DMF solutions.
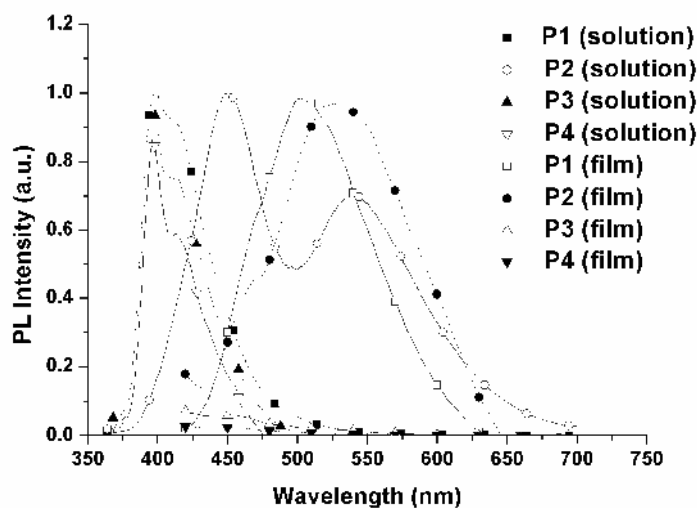
Figure 5.10 Normalized PL spectra of polymers **P1-P4** in solutions and solid films.

Especially, an obvious excimer emission was observed around 540 nm in polymer **P2**. In the case of Ru^{+2}-based metallo-polymers **P3** and **P4**, the state of Ru^{+2} ions complexed with terpyridyl units was quenched by a low-lying metal-centered (MC) state and room temperature emission was not observed.[114]

However, solutions of polymers **P3** and **P4** employing ligands composed of fluorene and phenothiazine moieties, where the ligands are well known materials for fluorescence,

showed weak emission peaks around 396-398 nm at room temperature. This phenomenon

may be due to the noncoordinating tpy units of the acceptor ligands. Moreover, Zn^{+2}-based

metallo-polymers **P1** and **P2** have larger PL quantum yields (= 0.36 and 0.26, respectively)

than their analogous monomers **4a** and **4b** (= 0.27 and 0.11, respectively); whereas,

Ru^{+2}-based metallo-polymers **P3** and **P4** showed negligible PL quantum yields (see Table

5.2). These trends fit well to their quantum yield changes of PL titration experiments (as

shown in the insets of Figures 5.7-5.8). Solid films of polymers **P1** and **P2** emitted green

lights with values of $_{max,PL}$ ranging at 502-530 nm (Figure 5.10). Comparing PL emissions

of all polymer films, polymer **P1** showed the largest Stokes shift (ca. 103 nm), which was

attributed to the excimer formation resulting from the - stacking of aromatic interactions

in the solid state.[84,91,92] While the nonlinear supramolecular structure of polymer **P2** was

generated by the complexation of bent monomer **4b** and Zn^{+2} ions, in which the steric

interactions of the polymer main-chains were enhanced, therefore, **P2** in solid state did not

show such a large Stokes shift of PL emission as that of polymer **P1**. Moreover, no PL

emissions were observed in solid films of both polymers **P3** and **P4**. Similar PL results of

polymers **P3** and **P4** in solutions allowed us to assign the emissions of **P3** and **P4** were

quenched by a low-lying metal(Ru^{+2})-centered (MC) state.

5.4.6 Electroluminescence (EL) Properties.

Multilayered PLED devices with a configuration of ITO/PEDOT:PSS(40-50 nm)/polymer

(**P1-P2**) (50-70 nm)/BCP(10 nm)/ALQ(30 nm)/LiF(1 nm)/Al(150 nm) were fabricated by

standard procedures of spin-coating and vacuum deposition, where polymers **P1-P2** were

used as the emitting layer and PEDOT: PSS as the hole transporting layer. Besides, BCP and

AlQ were used as electron transporting materials,[84,100,115] and their EL properties are listed in

Table 5.3.

Table 5.3 Electroluminescence (EL) Properties of PLED Devices[a] Containing an

Emitting Layer of Polymers P1-P2

Polymers	$_{max,EL}$ (nm)	V_{on} (V)[b]	Max. Luminescence (cd/m^2) (V)	Power Efficiency (cd /A)[c]	CIE Coordinates (x and y)
P1	567	6.5	578(15)	0.29	(0.37, 0.35)
P2	682	6.5	618(14)	0.32	(0.69, 0.31)

[a] Device structure: ITO/PEDOT:PSS/Polymer(**P1-P2**)/BCP/AlQ/LiF/Al, where the polymer (**P1** and **P2**) is an emitting layer.

[b] V_{on} is the turn-on voltage.

[c] Power efficiencies were obtained at 100 mA/cm^2.

Since PL properties of Ru^{+2}-based metallo-polymers **P3** and **P4** were very poor, the EL devices of **P3** and **P4** were not investigated. As shown in Figure 5.11, at a bias voltage of 10 V, PLED devices containing polymers **P1** and **P2** showed green and red emissions with $_{max,EL}$ around 567 and 682 nm, respectively, and their EL intensities were enhanced by increasing the bias voltage. The turn-on voltages of both PLED devices were about 6.5 V, and the maximum efficiencies and luminances were 0.29-0.32 cd/A (at 100 mA/cm^2) and 578-618 cdm^{-2} (at 14~15 V), respectively. It is worthy noting that the EL spectra of these devices did not resemble their corresponding PL spectra in solid films, which is presumably due to the EL and PL emissions originated from different excited states and/or ground states.[63c,84] Figure 5.12 depicts the current density-voltage-luminance (*I-L-V*) characteristic curves of polymers **P1** and **P2**, and similar turn-on voltages for both current density and luminance illustrated that a matched balance of injection and transportation in both charges was achieved.[66a-b]
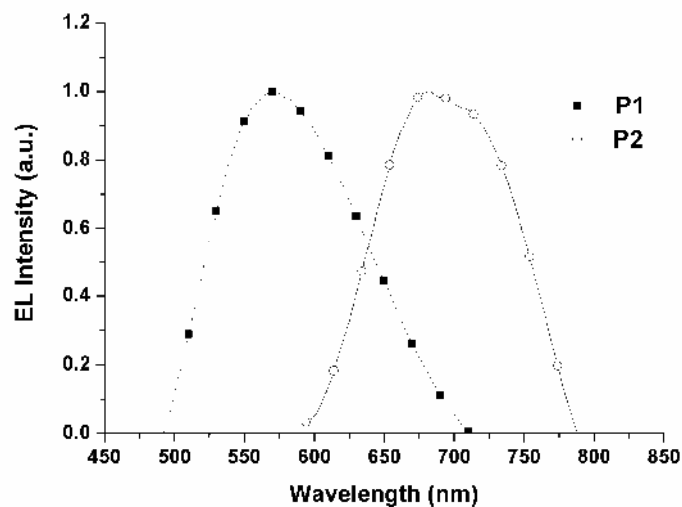
Figure 5.11 Normalized EL spectra of PLED devices with the configuration of ITO/PEDOT:PSS/Polymer (**P1**-**P2**)/BCP/AlQ//LiF/Al at 10 V.
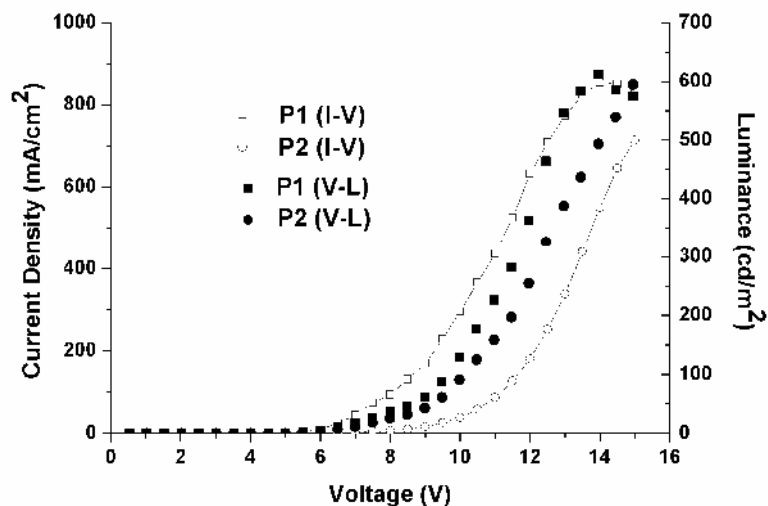
Figure 5.12 Current density-voltage-luminance (*I-V-L*) curves of PLED devices with the configuration of ITO/PEDOT:PSS/Polymer (**P1**-**P2**)/BCP/AlQ/LiF/Al.

5.4.7 Photovoltaic Properties.

In order to make use of Ru^{+2}-based metallo-polymers **P3** and **P4** in the application of photovoltaic cells, polymer photovaltic cell (PPVC) devices were made from composite films of polymers **P3** and **P4**, respectively, blended with fullerene derivative [6,6]-phenyl C_{61}-butyric acid methyl ester (PCBM) at the ratio of 1:3 (by wt. ratio) as an active layer,

where PCBM was utilized as a typical electron acceptor.[116] PPVC devices with the configuration of ITO/PEDOT:PSS(40-50 nm)/polymer (**P3-P4**):PCBM(65-75 nm)/LiF(1 nm)/Al(150 nm) were produced and the *I-V* curves were measured according to procedures similar to those of PLED devices.

Table 5.4 Photovoltaic Properties of PPVC Devices[a] Containing an Active Layer of

Polymers P3-P4 Blended with PCBM

Active layer (by wt. ratio)	V_{oc} (V)[b]	I_{sc} (mA/cm^2)[c]	FF (%)[d]	ECE (%)[e]
P3:PCBM = 1:3	0.68	4.7×10^{-2}	53.3	1.7×10^{-4}
P4:PCBM = 1:3	0.67	7.0×10^{-2}	55.1	2.5×10^{-4}

[a] Device structure: ITO/PEDOT:PSS/Polymer(**P3-P4**):PCBM/LiF/Al, where the polymer (**P3-P4**) : PCBM is an active layer.

[b] V_{oc} is the open-circuit voltage.

[c] I_{sc} is the short-circuit current.

[d] FF is the fill factor.

[e] ECE is the energy conversion efficiency.

Furthermore, the values of energy conversion efficiency (ECE) and fill factor (FF) were calculated according to the following equation:[117] ECE = (FF)$I_{sc}V_{oc}$/ P_{in}; FF = I_mV_m/ $I_{sc}V_{oc}$, where P_{in}, I_{sc}, V_{oc}, I_m, and V_m are the incident radiation flux (mW/cm^2), short-circuit current (mA/cm^2), open-circuit voltage (V), current and voltage at the maximum power output, respectively. ECE values were measured under AM 1.5 solar simulator at 100 mW/cm^2, and the photovoltaic performance data of these PPVC devices are summarized in Table 5.4. The *I-V* characteristics of PPVC devices with mixtures of polymer **P3** (or **P4**): PCBM = 1: 3 (by wt. ratio) as an active layer are shown in Figure 5.13. The values of I_{sc}, V_{oc}, and ECE for PVC devices bearing polymer **P3** under illumination were 4.7×10^{-2} mA/cm^2, 0.68 V, and 1.7×10^{-4} %, respectively, while the corresponding values of PPVC devices containing polymer **P4** were 7.0×10^{-2} mA/cm^2, 0.67 V, and 2.5×10^{-4} %, respectively. Comparing the performance of these devices, both polymers **P3** and **P4** showed poor PPVC properties even blended with PCBM. However, the metallo-polymers containing Ru^{+2} ions open a new

avenue for the application of PPVC devices, and many efforts to optimize the device performance are in progress.
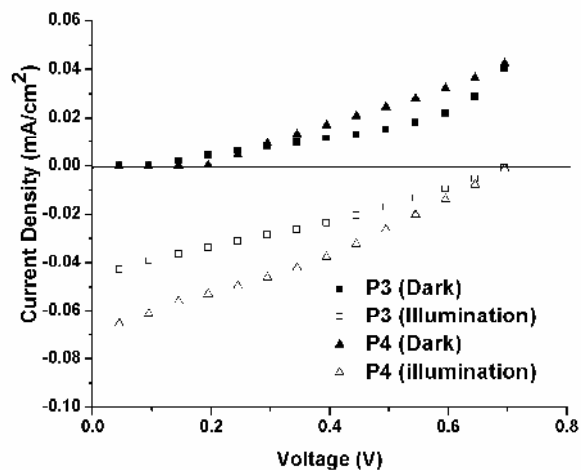
Figure 5.13 Current density-voltage (*I-V*) curves of polymer photovaltic cell (PPVC) devices with the configuration of ITO/PEDOT:PSS/ Polymer(**P3-P4**):PCBM/LiF/Al in dark and under white light illumination

5.5 Conclusion

In summary, a series of Zn^{+2}- and Ru^{+2}-based metallo-polymers **P1**-**P4** containing fluorene and phenothiazine building blocks were obtained by exact stoichiometric ratio of complexes. Furthermore, the thermal, photophyscial, and electrochemical properties were greatly affected by the nature of different monomer ligand structures as well as the Zn^{2+} and Ru^{2+} metal ions. The incorporation of terpyridyl-Zn(II) complexes into polymer backbones will induce ILCT transition and increase PL quantum yields. On the other hand, by the introduction of terpyridyl-Ru(II) complexes to metallo-polymer backbones, the PL quenching happened within polymer backbones of Ru^{+2}-based metallo-polymers **P3** and **P4** due to MLCT transition. Using Zn^{+2}-based metallo-polymers **P1** and **P2** as emitting materials to fabricate PLED devices, they showed green and red EL emissions with the efficiencies of 0.29-0.32 cd/A (at 100 mA/cm^2), respectively. As Ru^{+2}-based metallo-polymers **P3** and **P4** were blended with PCBM at the ratio of 1: 3 (by wt. ratio), the energy conversion efficiencies of $1.7\text{-}2.5\times10^{-4}$ % (at 100 mA/cm^2) were achieved under an AM 1.5 simulated solar light. Finally, by facile self-assembled reactions of coordination chemistry, more novel polymer LED (PLED) and photovoltaic cell (PPVC) materials can be further developed.

Chapter 6

Conclusion

A logical synthetic protocol for the synthesis of poly(fluorene/ethynylene/(terpyridyl)zinc(II))-based metallo-polymers is presented, including metallo-homopolymers and metallo-*alternating*-copolymer were developed with proper stoichiometric ratios of monomer ligands and ions (monomer/Zn^{2+}= 1/1) by self-assembled reactions. Furthermore, the photophysical and electroluminescent properties are greatly affected by the nature of the pendent groups of the coordination polymers. Moreover, the incorporation of various pendants into polymer backbones will change the rigidities and the thermal stability (as well as the Td and Tg values) of the metallo-polymers. i.e. The incorporation of rigid carbazole (CAZ) pendants into polymer side-chains reveals that the formation of excimers was suppressed and both PL and EL properties were enhanced. In comparison with these metallo-polymers, the quantum yields were greatly enhanced by introducing 1,3,4-Oxadiazole (OXD) pendants due to the energy transfer happened between pedants and polymer backbones, but reduced by carbazole (CAZ) pendants. By utilization of these metallo-polymers as emitting materials to fabricate PLED devices, green EL emissions and high EL performance can be obtained in the double-heterojunction device structures with PEDOT as the hole transporting material and BCP/ALQ as the electron transporting material.

A series of poly(fluorene/phenylene/ethynylene/(terpyridyl)zinc(II))-based supramolecular polymers containing various lateral substituents were obtained by self-assembled process. Besides, the experiments of ^{1}H-NMR and UV-vis titration over the ratio of Zn^{2+}/monomer = 1/1 confirmed the exact stoichiometric ratio of these metallo-supramolecular polymers. Various lateral substituents, such as methoxy (OMe), methyl (Me), and fluorine (F) units, were attached to the conjugated bis-terpyridine ligands, and thus to control the thermal

properties and energy band gaps of the resulting metallo-polymers. Compared with the monomer counterparts, the film quality and the quantum yields of PL and EL were enhanced by the metallo-supramolecular design via introducing zinc(II) ions. These metallo-polymers gave green to yellow PL emissions (with good PL quantum yields) in solid films, and showed yellow to orange EL emissions.

A series of Zn(II)- and Ru(II)-based metallo-polymers containing fluorene and phenothiazine building blocks were obtained by exact stoichiometric ratio of complexes. The incorporation of terpyridyl-Zn(II) complexes into polymer backbones will induce ILCT transition and increase PL quantum yields. On the other hand, by the introduction of terpyridyl-Ru(II) complexes to metallo-polymer backbones, the PL quenching happened within polymer backbones of Ru(II)-based metallo-polymers due to MLCT transition. Using Zn(II)-based metallo-polymers as emitting materials to fabricate PLED devices, they showed green and red EL emissions. As Ru(II)-based metallo-polymers were blended with PCBM for polymer photovoltaic cells (PPCV), the energy conversion efficiencies were measured under an AM 1.5 simulated solar light. Finally, by facile self-assembled reactions of coordination chemistry, more novel polymer LED (PLED) and photovoltaic cell (PPVC) materials can be further developed.

In general, the incorporation of suitable substituents or polymer backbones into metallo-polymers reveals that the thermal and photophysical properties can be easily adjusted. Hence, with finely tuned structures integrated with coordination chemistry, metallo-polymers can provide a new protocol for the development of novel PLED and PPVC materials.

References

(1) Lehn, J.-M. *Supramolecular Chemistry, Comcepts and Prespectives,* **1995**.

(2) Philp, D.; Stoddart, F. J. *Angew. Chem. Int. Ed.* **1996**, *35*, 1154.

(3) Darmell, J.; Lodish, H.; Baltimore, B.; *Molecular Cell Biology, Scientific American Books,* New York, **1990**.

(4) Schubert, U. S. in *Tailored Polymers & Applications,* eds. Yagic, M. K. M. Y.; NuyKen, O.; Ito, K.; Wenk, G.. VSP Publishers, Utrecht, **2000**, pp. 63.

(5) Balzani, V.; Credi, F.; Raymo, F. M.; Stoddart, J. F. *Angew. Chem. Int. Ed.* **2000**, 39, 3348.

(6) Schubert, U. S.; Eschbaumer, C. *Angew. Chem. Int. Ed.* **2002**, *41*, 2892.

(7) For a general review of supramolecular polymer, see Brunsveld, L.; Folmer, B.J. B.; Meijer, E. W.; Sijbesma, R. P. *Chem. Rev.* **2001**, *101*, 4071

(8) ten Cate; A. T.; Sijbesma, R. P. *Macromol. Rapid Commun.* **2002**, *23*, 1094.

(9) Yao, S.; Beginn, U.; Gress, T.; Lysetska, M.; Würthner, F. *J. Am. Chem. Soc.* **2004**, *126*, 8336.

(10) For an extensive review of supramolecular metal–ligand systems, see Swiegers, G. F.; Malefetse, T. J. *Chem. Rev.* **2000**, *100*, 3463.

(11) Janiak, C. *J. Chem. Soc. Dalton. Trans.* **2003**, 2781.

(12) Kitagawa, S.; Kitaura, R.; Noro, S. *Angew. Chem. Int. Ed.* **2004**, *43*, 2334.

(13) Rehahn, M. *Acta. Polym.* **1998**, *49*, 201.

(14) Ciferri, A. *Macromol. Rapid Commun.* **2002**, *23*, 511. For supporting Information, see Würthner, F.; Thalacker, C.; Sautter, A.;Schärtl, W.; Ibach, W.; Hollricher, O. *Chem. Eur. J.* **2000**, *6*, 3871.

(15) Yount, W. C.; Juwarker, H.; Craig, S. L. *J. Am. Chem. Soc.* **2003**, *125*, 15302.

(16) The overall binding constant ( ) is defined as the product of individual bing constamts (K) $_n$ = $K_1 \times K_2 \times ..... \times K_n$.

(17) Huheey, J. E.; Keiter, E. A.; Keiter, R. L. *Inorganic Chemistry: Principles of structures and Reactivity, 4th ed.*; Harper Collins: New York, **1993**; pp 547.

(18) Yamasaki, K.; Yasuda, M. *J. Am. Chem. Soc.* **1956**, *78*, 1324.

(19) Anderegg, G. *Helv. Chim. Acta.* **1963**, *315*, 2813.

(20) Benniston, A. C.; Harriman, A.; Lawrie, D. J.; Mayeux, A.; Rafferty, K.; Russell, O. D. *J. Chem. Soc. Dalton Trans.* **2003**, 4762.

(21) Vögtle, F. *Supramolecular Chemistry: An Introduction,* New York, **1995**.

(22) Constable, E. C. *Adv. Inorg. Chem. Radiochem.* **1986**, *30*, 69.

(23) Sauvage, J. P.; Collin, J. P.; Chambron, J. C.; Guillerez, S.; Coudret, C.; Balzani, V.; Barigelletti, F.; De, Cola., L.; Flamigni, L. *Chem. Rev.* **1994**, *94*, 993.

(24) Daniher, A. T.; Bashkin, J. K. *Chem. Commun.* **1998**, 1077.

(25) Spatz, J. P. *Angew. Chem. Int. Ed.* **2002**, *41*, 3359.

(26) Newkome, G. R.; He, E. *J. Mater. Chem.* **1997**, 7, 1237.

(27) Armspach, D.; Constable, E. C.; Housecroft, C. E.; Neuberger, M.; Znhnder, M. *J. Organomet. Chem.* **1998**, *550*, 193.

(28) Constable, E. C. *Macromol. Symp.* **1995**, *98*, 503.

(29) Heller, M.; Schubert, U. S. *Macromol. Rapid Commun.* **2001**, *22*, 1358.

(30) El-Ghayoury, A.; Schenning, A. P. H. J.; Meijer, E. W.; *J. Polym. Sci. Part A: Polym. Chem.* **2002**, *23*, 957.

(31) McMillin, D. R.; Moore, J. J. *Coord. Chem. Rev.* **2002**, *229*, 113.

(32) Schubert, U. S.; Schmaloch, S. *Polym. Prepr. (Am. Chem. Soc. Div. Polym. Chem.)* **2001**, *42*, 295

(33) Schmatloch, S.; van den Berg, A.; Fijten, M. W. M.; Schubert, U. S. *Macromol. Rapid Commun.* **2003**, *87*, 237.

(34) Lohmeijer, B. G. G.; Schubert, U. S. *Macromol. Chem. Phys.* **2003**, *204*, 1072.

(35) Lohmeijer, B. G. G.; Schubert, U. S. *Angew. Chem. Int. Ed.* **2002**, *41*, 3825.

(36) Schmatloch, S.; Schubert, U. S.; Precup, A. A. *Des. Monomer Polym.* **2002**, *5*, 211.

(37) Calzia, K. J; Tew, G. N. *Macromolecules* **2002**, *35*, 6090.

(38) Heller, M.; Schubert, U. S. *Macromol. Rapid Commun.* **2002**, *43*, 211.

(39) Cho, Y. S.; Lee, H. K.; Lee, J. S. *Macromol. Chem. Phys.* **2002**, *203*, 2495.

(40) Salditt, T.; Schubert, U. S.; *Rev. Mol. Biotechnol.* **2002**, *90*, 55.

(41) Diaz, D. J.; Storrier, G. D.; Bernhard, S.; Takada, K; Abruña, H. D. *Langmuir* **1999**, *15*, 7351.

(42) Collin, J. P.; Deronzier, A.; Essakalli, M. *J. Phys. Chem.* **1991**, *95*, 5906

(43) Bloom, C. J.; Elliott, C. M.; Schorder, P. G.; France, C. B.; Parkinson, B. A. *J. Phys. Chem. B* **2003**, *107*, 2933.

(44) Yu, S. C.; Kwok, C. C.; Chan, W. K.; Che, C. M. *Adv. Mater.* **2003**, *15*, 1643.

(45) (a) Lehn, J. M. *Angew. Chem.* **1988**, *100*, 91.; *Angew. Chem. Int. Ed.* **1988**, *27*. 89. (b) Blau, F.; *Ber. Dtch. Chem. Ges.* **1888**, *21*. 1077. (c) Kalyanasundaram, K. *Coord. Chem. Rev.* **1982**, *46*, 159.

(46) (a) Morgan, S. G.; Burstall, F. H. *J. Chem. Soc.* **1931**, 20. (b) Morgan, S. G.; Burstall, F. H. *J. Chem. Soc.* **1937**, 1649. (c) Newkome, G. R.; He, E.; moorefield, C. N.; *Chem. Rev.* **1999**, *99*, 1689.

(47) (a) Wong, C. T.; Chan, W. K.; *Adv. Mater.* **1999**, 11, 455. (b) Antonietti, M.; Lohmann, S.; Eisenbach, C. D.; Schubert, U. S. *Macrol. Rapid. Commun.* **1995**, *16*, 283. (c) Yu, S. C.; Gong, X.; Chan. W. K. *Macromolecules,* **1998**, *31*, 5639.

(48) (a) Kelch, S.; Rehahn, M; *Macromolecules,* **1997**, *30*, 6185. (b) Andres, P. R.; Schubert, U. S. *Adv. Mater.* **2004**, 16, 1043. (c) Knapton, D.; Iyer, P. K.; Rowan, S. J.; Weder, C. *Macromolecules,* **2006**, 31, 5639.

(49) (a) Dobrawa, R. and Würthner, F. *J. Polym. Sci. Part A: Polym. Chem.* **2005**. 43. 4981.

(b) Hofmeier, H.; Schubert, U. S. *Chem. Commun.* **2005**, 2423.

(50) (a) Archer, R. D. *Coord. Chem. Re*v. **1993**, 93, 49. (b) Manners, I. *Science* **2001**, 294, 1664.

(51) (a) Constable, E. C.; Cargill Thompson, A. M. W. *J. Chem. Soc. Dalton. Trans.* **1992**, 3467. (b) Schütte, M.; Kurth, D. G.; Linford, M. R.; Cölfin, H.; Möhwald, H. *Angew. Chem. Int. Ed.* **1998**, *37*, 2891

(52) Barigelletti, F.; Flamigni, L. *Chem. Soc, Rev.* **2000**, *29*, 1.

(53) (a) Ng, W. Y.; Gong, X.; Chan. W. K.; *Chem. Mater.* **1999**, *11*, 1165. (b) Hofmeier, H.; Schubert, U. S. *Chem. Soc, Rev.* **2004**, *33*, 373. (c) Chu, Q.; Pang, Y. *J. Polym. Sci. Part A: Polym. Chem.* **2006**. *44*. 2338.

(54) (a) Dobrawa, R. and Würthner, F. *Chem. Commun.* **2002**, 319. (b) Dobrwa, R.; Lysetska, M.; Ballester, P.; Grüne, M.; Würthner, F. *Macromolecules* **2005**, *38*, 1315. (c) Wang, X. Y.; Guzreo, A. D.; Schmehl, R. H. *Chem. Commun.*, **2002**, 2344. (d) Goodall, W.; Williams, J. A. G. *Chem. Commun.* **2001**, 2514.

(55) (a) Yu, S. C.; Hou, S.; Chan, W. K. *Macromolecules* **2000**, *33*, 3259. (b) Huang, F.; Wu, H.; Wang, D.; Wang, W.; Cao, Y. *Chem. Mater.* **2004,** *16*, 708.

(56) (a) Sung, H. H.; Lin, H. C. *Macromolecules* **2004**, *37*, 7945. (b) Potts, K. T.; Konwar, D. *J. Org. Chem.* **1991**, *56*. 4851. (c) Sung, H. H.; Lin, H. C. *J. Polym. Sci. Part A: Polym. Chem.* **2005**. *43*. 2700. (d) Ziessel, R.; Khatyr, A. *J. Org. Chem.* **2000.** *65*. 3126.

(57) (a) Kelch, S.; Rehahn, M; *Macromolecules,* **1999**, *32*, 5818. (b) Schmelz, O.; Rehahn,. M. *e-Polymers* **2002**, no. 047.

(58) Janitetz, S.; Bradley, D. D.C.; Grelly, M.; Giebeler, C.; Inbasekaran, M.; Woo, E. P. *Appl. Phys. Lett.* **1998**, *73*, 2453.

(59) (a)Loiseau, F; Pietro, C. D.; Serroni, S.; Campagna, S.; Licciardello, A.; Manfredi, A.; Pozzi, G.; Quici, S. *Inorg. Chem.* **2001**, *40*, 4901. (b) Hwang, S. H.; Wang, P.;

Moorefield, C. N.; Godinez, L.A.; Manriquez, J.; Bustos, E.; Newkome, G. R. *Chem. Commun.* **2005**, 4672.

(60) (a) Thomas, K. R. J.; Chang, C. P.; Chuen, C. H.; Chenu, C. C.; Lin, *J. T. J. C. C. S.* **2002**, *49*, 833. (b) Newkome, G. R.; Cho, T. J.; Moorefield, C. N.; Cush, R.; Russo P. S.; Godinez, L. A.; Saunder, M. J.; Mohapatra, P. P. *Chem. Eur. J.* **2002**, *8*, 2946.   (c) Newkome, G. R.; Cho, T. J.; Moorefield, C. N.; Mohapatra, P. P.; Godinez, L. A. *Chem. Eur. J.* **2004**, *10*, 1493..

(61) Hu, B.; Fuchs, A.; Huseyl, S.; Gordaninejad, F. *J. Appl.. Polym. Sc*i. **2006**. *100*. 2464.

(62) Iyer, P. K.; Beck, J. B.; Weder, C.; Rowan, S. J. *Chem. Commun.* **2005**, 319.

(63) (a) Desiraju, G. R.; Gavezotti, A.; *J. Chem. Soc. Chem. Commun.* **1989**, 621. (b) Desiraju, G. R. *Chem. Commun.* **1997**, 1475. (c) Kwok, C. C.; Yu, S. C.; Sham, S. T.; Che, C. M. *Chem. Commun.* **2004**, 2758.

(64) (a) Alcock, N. W.; Barker, P. R.; Haider, J. M.; Hannon, M. J.; Painting, C. L.; Pikramenou, Z.; Plummer, E. A.; Rissanen, K.; Saarenketo, P. *J. Chem. Soc. Dalton Trans.* **2000**, 1447. (b) Ishow, E.; Gourdon, A.; Launay, J. P. *Chem. Commun.* **1998**, 1909.

(65) (a) Lee, Y. Z.; Chen, X.; Chen, S. A.; Wei, P. K.; Fann, W. S. *J. Am. Chem. Soc.* **2001**, 123, 2296. (b) Wu, F. I.; Reddy, S.; Shu, C. F.; Liu, M. S.; Jen, A. K. Y. *Chem. Mater*. **2003**, *15*, 269.

(66) (a) Burn, P. L.; Grice, A. W. Tajbkhsh, A. Bradley, D. D. C.; Thomas, A. C. *Adv. Mater.* **1997**, *9*, 1171. (b) Jin, Y.; Kim, J. Y.; Park, S. H.; Kim, J.; Lee, S.; Lee. K.; Shu, H. *Polymer* **2005**, *46*, 12158.

(67) (a) Wu, C. W.; Lin, H. C. *Macromolecules*, **2006**, in Press. (b) Shu, C. F.; Dodda, R.; Wu, F. I.; Liu, M. S.; Jen, A. K. Y. *Macromolecules*, **2003**, *36*, 6698.

(68) Maruyama, T.; Kubota, K.; Yamamoto, T. *Macromolecules* **1993**, *26*, 4057.

(69) Zhang, K.; Kumar, G. S.; Necker, D. C.; *J. Polym. Sci. Polym. Chem. Ed.* **1985**, *23*, 1253.

(70) Barigelletti, F.; Flamigni, L.; Calogero, G.; Harmmarstrom, L.; Sauvage, J. P.; Collin, J. P. *Chem. Commun.* **1998**, *7*, 2333.

(71) Ng, W. Y.; Chan, W. K.; *Adv. Mater.* **1997**, *9*, 716.

(72) Nguyen, P.; Gomez-Elipe, P.; Manners, I. *Chem. Rev.* **1999**, *99*, 1515.

(73) Khlobystov, A. N.; Blake, A. J.; Champness, N. R.; Lemenkovsmii, D. A.; Majouga, A. G.; Zyk, N. V.; Schröder, M. *Coord. Chem. Rev.* **2001**, *222*, 155.

(74) Würthner, F.; Sautter, A.; Thalacker, C., *Angew. Chem. Int. Ed.* **2000**, *39*, 1243.

(75) Velten, U.; Lahn, B.; Rehahn, M.; *Macromol. Chem. Phys.* **1997**, *198*, 2798.

(76) Vogel, V.; Gohy, J. F.; Lohmeijer, B, G. G.; Broek, J. A. V. D.; Haase, W.; Schubert, U. S.; Schubert, D. *J. Polym. Sci. Part A: Polym. Chem.* **2003**, *41*, 3159.

(77) Holder, E.; Marin, V.; Alexeev, A.; Schubert, U.S. *J Polym Sci Part A: Polym Chem* **2005**, *43*, 2765.

(78) Shunmugam, R.; Tew, G, N.; *J. Polym. Sci. Part A: Polym. Chem.* **2005**, *43*, 5831.

(79) Tzanetos, N. P.; Andreopoulou, A. K.; Kallitsis J. K.; *J. Polym. Sci. Part A: Polym. Chem.* **2005**, *43*, 4838.

(80) Lehn, J. M. Supramolecular Chemistry, Concepts and Perspective, VHC, Weinheim, Germany 1995.

(81) Chang, S. C.; Bharathan, J.; Yang, Y.; Helgeson, R.; Reynolds, J. R. *Appl. Phys. Lett.* **1998**, *72*, 2561.

(82) Bliznyyuk, V. N.; Cater, S. A.; Sott, J. C.; Klarner, G.; Miller R. D.; Miller, D. C. *Macromolecules* **1999**, *32*, 361.

(83) Xia, C.; Advincula, R. C. *Macromolecules* **2001**, *34*, 5854.

(84) Chen, Y. Y.; Tao, Y. T.; Lin, H. C. *Macromolecules* **2006**, *39*, 8559.

(85) Lee, S. H.; Nakamura, T.; Tsutsui, T. *Org. Lett.* **2001**, *33*, 478.

(86) Bao, Z.; Chen, Y.; Cai, R.; Yu, L. *Macromolecules* **1993**, *26*, 5281.

(87) Ziener, U.; Godt, A. *J. Org. Chem.* **1997**, *62*, 6137.

(88) Kimura, M.; Horai, T.; HanaBusa, K.; Shirai, H. *Adv. Mater.* **1998**, *10*, 459.

(89) Heck, R. F. *Org. React.* **1982**, *27*, 354.

(90) Balasubramaniam E.; Tao, Y. T.; Danel, A.; Tomasik, P. *Chem. Mater.* **2000**, *12*, 2788.

(91) Baldo, M. A.; O'brien, D. F.; Thompson, M. E.; Forrest, S. R. *Phys. Rev. B* **1999**, *60*, 14422.

(92) Lu, W.; Mi, B. X.; Chan, M. C. W.; Hui, Z.; Zhu, N. Y.; Lee, S. T.; Che, C. M. *Chem. Commun.* **2002**, 206.

(93) Yu, S. C.; Hou, S.; Chan, W. K. Macromolecules, **1999**, *32*, 5251.

(94) Chen, Y. Y.; Lin, C. H. *J. Polym. Sci. Part A; Polym. Chem.* **2007**, Accepted.

(95) Wang, C. S.; Jung, G. Y.; Hua, Y.; Pearson, C.; Bryce, M. R.; Petty, M. C.; Batsanov, A. S.; Goeta, A. E.; Howard. J. A. K. *Chem. Mater.* **2003**, *13*, 1167.

(96) Kraft, A.; Grimsdale, A. C.; Holmes, A. B. *Angew. Chem., Int. Ed. Engl.* **1998**, 37, 402.

(97) Segura, J. L. *Acta. Polym.* **1998**, *49*, 319.

(98) Thelakkat, M.; Schmidt, H.-W. *Polym. Adv. Technol.* **1998**, *9*, 429.

(99) Mitschke, U.; Bauerle, P. *J. Mater. Chem .***2000**, *10*, 1471.

(100) Tao, Y. T.; Chuen, C. H.; Ko, C. W. Peng, J. W. *Chem. Mater.* **2004**, *14*, 4256.

(101) Yao, Y. S.; Xiao, J.; Wang, X. S.; Deng, Z. B.; Zhang, B. W. *Adv. Funct. Mater.* **2006**, *16*, 709.

(102) (a) Bernius, M. T.; Inbasekaran, M.; O'Brien, I. J.; Wu, W. *Adv. Mater.* **2000**, *12*. 1737. (b) Frind, R. H. P*ure App. Chem.* **2001**, *73*, 425 and references therein. (c) Kulkarni, A. P.; Tonzola, C. J.; Babel, A.; Jenekhe, A. A. *Chem. Mater.* **2004**, *16*, 4556. (d) Bracbe, C. J.; Saricific, N. S.; Hummelen, J. C. *Adv. Funct. Mater.* **2001**, *11*. 15. (e) Bustos, E.; Maníquez, J.; Echegoyen, L.; Godínez, L. A. *Chem. Commun.* **2005**, 1613. (f) Yang, R.; Tian, R.; Yong, Z.; Yang, J, Hou, Q.; Yang, W.; Zhang, C.; Cao, Y. *Macromolecules,*

2005, *38,* 244.

(103) (a) Kulkarni, A. P.; Kong, X.; Jenekhe, S. *Macromolecules,* **2006,** *39,* 8699. (b) Wu, F. I.; Shin, P. I., Shu, C. F. *Macromolecules,* **2006,** *38,* 9028.

(104) Constable E. C. *Chem. Soc. Rev*., **2007,** *36*, 246.

(105) (a) Hwang, S. H.; Wang. P.; Moorefield, C. N.; Jung, J. C.; Kim, J. Y.; Lee, S. W.; Newkome, G. R. *Macromol. Rapid commun.* **2006**, *27,* 1809. (b) Sato, K.; Sadamitsu, Y.; Araib, S.; Yamagishi, T. *Tetrahedron Lett.* **2007,** *48,* 1493. (c) Peng, X.; Xu, Y.; Sun, S.; Wu Y.; Fan, J. *Org. Biomol. Chem.* **2007,** *5,* 226.

(106) (a) Gratzel, M. Nature **2002**, 414, 338. (b) Duprez, V.; Biancardo, M.; Spanggaard, H.; Krebs, F. C. *Macromolecules*, **2005**, *38*, 10436. (c) Man, K. K.Y.; Ling, M. H.; W. K. Chan. *Langmuir* **2006**, *22*, 3368.

(107) Kim, G. O.; Cho, M. J. Yu, Y. J.; Kim, Z. H.; Jin, J. T.; Kim, D. Y.; Choi, D. H.; *Chem. Mater*. **2007,** *19.* 42.

(108) (a) Fabre, M.; Bonvoisin, J. *J. Am. Chem. Soc.* **2007,** 1*29,* 1434. (b) Wolpher, H.; Sinha, S.; Pan, J.; Johansson, A.; Lundqvist, M. J.; Persson, P.; Lomoth, R.; Bergquist, J.; Sun, L.; Sundstrolm, V.; kermark, B.; Polívka, T. *Inorg. Chem.* **2007,** *46,* 638.

(109) (a) Wang, X. Y.; Guerzo, A. D.; Schmehl, R. H. *Chem. Commun.* **2002,** 2344. (b) Hofmeier, H.; El-ghayoury, A.; Shenning, A. P. H. J.; Schubert, U. S. *Chem. Commun.* **2004,** 318.

(110) (a) Cheng, L. T.; Tam, W.; Meredith, G. R.; Marder, S. R. *Mol. Cryst. Lid. Cryst.* **1990,** *189,* 137. (b) Coe, B. J.; Jones, L. A.; Harris, J. A.; Brunschwing, B. S.; Asslberghs, I.; Clays, K.; Persoons, A.; Garìn, J.; Ordina, J. *J. Am. Chem. Soc.* **2004,** 1*26,* 3880. (c) Tessore, F.; Roberto, D.; Ugo, R.;Pizzotti, M. I*norg. Chem.* **2005,** *44,* 8967.

(111) Zhao, Y.; Lin, Z.; Ou, S.; Duan, C.; Liao, H.; Bai, Z. *Inorg. Chem. Commun.* **2006,** *9,* 802.

(112) Liu, Y.; Li, J.; Cao, H.; Qu. B; Chen, Z.; Gong, Q.; Xu, S.; Cao, S. *Polym. Adv. Technol.* **2006,** *17,* 468.

(113) Beley, M.; Collin, J. P.; Sauvage, J. P.; Heisel, F.; Miech, A. *J. Chem. Soc., Dalton Trans.* **1991**, 3157.

(114) Juris, A.; Balzani, V.; Barigelletti, F.; Campagna, S.; Belser, P.; von Zelewsky, A. *Coord. Chem.. Rev.* **1988,** *84,* 85.

(115) Tao, Y. T.; Balasubramaniam, E.; Danel, A.; Tomasik,. P. *Appl. Phys. Lett.* **2000**, *77,* 933.

(116) Bhattacharyya, S.; Kymakys, E.; Amaratunga, G. A. J.; *Chem. Mater.* **2004**, 4816.

(117) (a) Sariciftic, N.; Smilowitz, L.; Heggeer, A. J.; Wudl, F.; *Science* **1992**, *258*, 1474. (b) Coakely, K. M.; McGehee, M.; *Chem. Mater.* **2004**, 4533.